

DELFT UNIVERSITY OF TECHNOLOGY

Temperature Modeling for Nodal Analysis

M.Sc. Thesis



Picture from Trans-Alaska-Pipeline

Temperature Modeling for Nodal Analysis

By

Rezvan Sharifian
4410610

To obtain the degree of Master of Science in Applied Earth Sciences
Faculty of Civil Engineering & Geosciences
At Delft University of Technology
To be defended publicly on Thursday July 28, 2016.

Supervisor: Prof. Dr. Ir. J.D. Jansen

Thesis committee: Prof. Dr. Ir. J.D. Jansen,
Prof. Dr. W. R. Rossen,
Dr. A. Twerda.

Abstract

Predicting accurate temperature profiles in flowing wells can greatly improve the design of production facilities in petroleum and geothermal engineering. Temperature profiles help to calculate accurate two-phase-flow pressure drop predictions, which, in turn, can improve an artificial-lift system design. Existing temperature correlations are usually limited to a specific range of data, and do not always give accurate results because they do not consider the effects of different fluids in the annulus and the cooling and heating of the fluid resulting from phase change. The primary objective of this study is to develop a non-isothermal wellbore simulator to model steady-state fluid flow (such as production from, or injection to, a reservoir) and the associated heat flow. Starting from an existing numerical well bore flow model in MATLAB, this work aims at implementing a coupled flow-heat transfer well bore model. To solve the governing differential equations in each interval of the well, a fourth-order Runge-Kutta method is used with a standard MATLAB function that integrates the pressure and temperature gradient equations simultaneously. The surrounding formation temperature and the flowing fluids thermodynamic properties are updated in each well depth intervals to account for changes in heat-transfer rate between the wellbore fluid and the formation. Model validation has been performed by running four field examples. In all cases, the model results are in good agreement with the field data.

Acknowledgments

With this report, I present my master thesis with the title “Temperature Modelling for Nodal Analysis”. This report marks the end of my study at the Faculty of Civil Engineering and Geosciences at the Delft University of Technology, and serves as closure of my MSc in Applied Earth Sciences with a specialization in Petroleum Engineering and Geosciences.

I am grateful to have been able to spend the last two years at Delft University of Technology within the Petroleum Engineering section. This project would not have been possible without the help and support of so many people. I would like to express this gratitude to some of them in particular. First of all I would like to thank TU Delft for awarding me the TU Delft excellence scholarship, from the Delft Energy Initiative. This award has been an honor to me, and without its financial help, which covered all costs for two years of my master degree, I would not have been able to participate in this program and gain such a wonderful experience.

I would like to sincerely thank my thesis supervisor; Professor Jan-Dirk Jansen for his continuous support throughout my M.Sc. Thesis. I greatly appreciate his guiding advice, the constructive discussions that we had, and his careful review of the thesis. I would also like to express my appreciation to the other members of my committee.

Finally, I would like to thank my parents and my lovely sister for always believing in me, supporting me, and encouraging me to achieve my dreams. Without their help I would never be able to be where I am now. Also I would like to thank the Dooper family for their admirable personal support during the many ups and downs I had during my stay in the Netherland, for their kindness and their love.

Rezvan Sharifian

07/28/2016, Delft

Table of Contents

LIST OF FIGURES.....	7
LIST OF TABLES.....	10
1 INTRODUCTION AND LITERATURE REVIEW.....	11
1.1 Introduction	11
1.2 Literature Review	11
1.2.1 Analytical Temperature Modelling.....	12
1.2.2 Numerical Temperature Modelling.....	13
1.3 Objectives.....	14
1.4 Thesis Organization.....	15
2 MODEL FORMULATION	16
2.1 Modelling Approach.....	16
2.2 Pressure Gradient Calculation in the Wellbore	16
2.2.1 Governing Equations	16
2.2.1.1 Conservation of Mass	16
2.2.1.2 Conservation of Momentum	17
2.2.2 Single Phase Flow Pressure Drop	19
2.2.3 Multiphase-Flow model.....	20
2.2.3.1 Liquid Holdup and Pressure Drop	20
2.2.3.2 Flow Patterns	22
2.2.3.3 Mukherjee & Brill.....	23
2.3 Wellbore Fluid Temperature Distribution	23
2.3.1 Steady-State Heat Transfer	24
2.3.1.1 Heat Transfer by Conduction	24
2.3.1.2 Heat Transfer by Convection	25
2.3.1.3 Heat Transfer by Radiation	25
2.3.2 Formation Temperature Distribution	26
2.3.3 Conservation of Energy for Wellbore Fluid	27
2.3.4 The Overall Heat Transfer Coefficient	29
2.3.5 Temperature Profile	33
2.3.6 Joule-Thomson effect.....	34
2.3.6.1 Joule-Thomson Coefficient for Liquids	35
2.3.6.2 Joule-Thomson Coefficient for a Real Gas	35
2.3.6.3 Joule-Thomson Coefficient for Multiphase Flow	36
2.4 Assumptions Summary.....	37
3 ANALYSIS AND INTERPRETATION.....	38

3.1 Solution Procedure	38
3.1.1 Single-phase Oil Flow (oil_dpTds.m)	38
3.1.2 Single-phase Gas Flow (gas_dpTds.m)	39
3.1.3 Multi-phase Gas-Oil-Water (Muk_Brill_dpTds).....	39
3.2 Well Applications.....	39
3.2.1 Case Study 1: Oil/Gas/Water Producer, Vertical Well.....	39
3.2.2 Case Study 2: Oil/Gas/Water Producer, Deviated Well.....	44
3.2.3 Case Study 3: Oil Producer, Vertical Well.....	48
3.2.4 Case Study 4: Oil/Gas Producer, Vertical Well	50
3.3 Sensitivity Analysis.....	53
3.3.1 Effect of Tubing Diameter	53
3.3.2 Effect of Gas-Liquid Ratio	55
3.3.3 Effect of Water-Oil Ratio	57
3.3.4 Effect of Formation Thermal Conductivity	59
3.3.5 Effect of Production Time.....	60
4 SUMMARY, CONCLUSION, AND FUTURE WORK	61
4.1 Summary and Conclusion	61
4.2 Future Work	62
NOMENCLATURE	63
REFERENCES	66
APPENDIX A	70
Hold-up and Friction Correlations	70
Mukherjee and Brill	70
Pressure drop analysis.....	72
APPENDIX B.....	73
Case Study 1: Oil/Gas/Water Producer, Vertical Well.....	73
Case Study 2: Oil/Gas/Water Producer, Deviated Well.....	75
Case Study 3: Oil Producer, Vertical Well.....	77
Case Study 4: Oil/Gas Producer, Vertical Well	79
APPENDIX C.....	81
APPENDIX D	83
Joule-Thomson derivation	83
Oil Heat Capacity	83
Water Heat Capacity.....	83
Gas Heat Capacity	83

List of Figures

Figure 2-1.	Segment of an inclined pipe.....	17
Figure 2-2.	Segment of a deviated well, showing well inclination.....	18
Figure 2-3.	Schematic of multiphase flow patterns in a vertical tube.....	23
Figure 2-4.	Schematic view of conduction heat transfer mechanism.....	24
Figure 2-5.	Heat transfer from a hot surface to the adjacent fluid by convection.....	25
Figure 2-6.	Heat flow through a series of resistances.....	30
Figure 2-7.	Iterative procedure for calculating annulus heat transfer rate.....	32
Figure 2-8.	Gas Joule-Thomson coefficient sign change vs. temperature and pressure....	36
Figure 3-1.	Comparison between computed fluid temperatures vs. along-hole depth, earth geothermal gradient, and field data. (Case study 1).....	41
Figure 3-2.	Temperature distribution prediction using linear interpolation, earth geothermal gradient, and field data (Case study 1).....	42
Figure 3-3.	Overall heat transfer coefficient (U_{to}) vs. depth. (Case study 1).....	42
Figure 3-4.	Radial heat loss rate per unit length of the well vs. along-hole depth with and without considering convective heat transfer in the annulus. (Case study 1).....	43
Figure 3-5.	Temperature gradient different components; heat loss to formation, acceleration, gravity, and Joule-Thomson effect (pressure effect). (Case study 1)....	43
Figure 3-6.	Pressure gradient different components; pressure loss due to gravity, friction, and acceleration forces. (Case study 1).....	44
Figure 3-7.	Well schematic for Case study 2.....	45
Figure 3-8.	Temperature-traverse computation with bottom-up approach done by original writers, together with real field data, picture from (Hasan,Kabir, and Wang, 2009). (Case study 2).....	46

Figure 3-9. Computed fluid temperature vs. along-hole depth, and earth geothermal gradient using bottom-up integration, using <i>example_traverse_thermal.m</i> (Case study 2).....	46
Figure 3-10. Comparison of pressure-traverse calculations between <i>Hassan_kabir</i> method, and the real field data. (Case study 2).....	47
Figure 3-11. Pressure gradient equation components. (Case study 2.).....	47
Figure 3-12. Computed fluid temperatures vs. along-hole depth, and earth geothermal gradient (Case study 3).....	48
Figure 3-13. Temperature gradient equation components. (Case study 3).....	49
Figure 3-14. Computed pressure profile vs. real field data. (Case study 4).....	50
Figure 3-15. Joule-Thomson coefficient vs. depth and flow regime, $\eta_{JT} \in [-1.5E-7 \text{ to } -3.5E-7]$. (Case study 4).....	51
Figure 3-16. Computed temperature profile (Case study 4).....	51
Figure 3-17. Temperature profile components, flow regime changes around 2678 ft and this results in a change in the slope of this graph at that depth (Case study 4).....	52
Figure 3-18. Computed pressure profile (Case study 4).....	52
Figure 3-19. Effect of tubing diameter on temperature profile in the wellbore.....	53
Figure 3-20. Effect of tubing diameter on wellbore heat-loss to the formation.....	54
Figure 3-21. Effect of tubing diameter on pressure profile.....	54
Figure 3-22. Effect of GOR on pressure profile.....	55
Figure 3-23. Effect of GOR on temperature gradient components.....	56
Figure 3-24. Effect of GOR on temperature gradient.....	56
Figure 3-25. Effect of water fraction on temperature profile in the wellbore.....	57
Figure 3-26. Effect of water fraction on temperature gradient components.....	58
Figure 3-27. Effect of water fraction on pressure profile in the wellbore.....	58

Figure 3-28. Effect of the earth thermal conductivity on temperature profile.....	59
Figure 3-29. Effect of production time on temperature profile.....	60
Figure B-1. Comparison between computed fluid temperatures bottom-up and top down using <i>example_traverse_thermal.m</i> , for a vertical oil producer well, Case study 3.....	78
Figure B-2. Pressure gradient equation components, Vertical oil producer well, Case study 3.....	78
Figure C-1. Effect of GOR on pressure profile components in the wellbore (A 5355 ft vertical well produces 600 STB/D oil, 0 water).....	83

List of Tables

Table A.1.	Summary of the boundaries recognition between different flow regimes, using Mukherjee and Brill numerical expressions.....	71
Table A.2.	Coefficients C_1 to C_6 used to calculated liquid hold-up in Mukherjee and Brill single hold-up correlation Eq. (A.14).....	72
Table B.1.	Input data for Vertical oil/gas/water producer well, Case study 1.....	73
Table B.2.	Thermal properties input data for Vertical oil/gas/water producer well, Case study 1.....	73
Table B.3.	Measured field temperature data, Vertical oil/gas/water producer well, Case study 1,	74
Table B.4.	Calculated fluid temperature, pressure and surrounding formation temperature, Vertical oil/gas/water producer well, Case study 1.....	74
Table B.5.	Input data for partially deviated oil/gas/water producer well, Case study 2...75	
Table B.6.	Input data for partially deviated oil/gas/water producer well, Case study 2....75	
Table B.7.	Calculated fluid temperature, pressure and surrounding formation temperature using <i>example_traverse_thermal.m</i> , for a partially deviated oil/gas/water producer well, Case study2.....	77
Table B-8.	Comparison between bottom-up and top down calculation results, using <i>example_traverse_thermal.m</i> , for a vertical oil producer well, Case study 3.....	79
Table B-9.	Input data file for a vertical oil/gas producer well, Case study 4.....	79
Table B-10.	Measured filed data and Hasan & Kabir results, for a vertical oil/gas producer well, Case study 4.....	80
Table B.11.	Calculated fluid temperature and pressure temperature, using <i>example_traverse_thermal.m</i> , for a vertical oil/gas producer well, Case study 4.....	80

1 INTRODUCTION AND LITERATURE REVIEW

1.1 Introduction

When a fluid flows in a pipe, properties of the fluid will be affected by many factors such as the pressure, temperature, rate of the flow, pipe diameter, pipe roughness, and pipe inclination. Temperature calculations of the well flow are of great importance, both in petroleum and geothermal engineering. When designing production equipment, it is also important to know the temperature of the well flow to be able to maximize the performance. Besides the fluid properties, there are various parameters to be considered when it comes to temperature modelling. For instance, the temperature loss due to fluid acceleration can be ignored in most cases, whereas ignoring the Joule-Thomson effect, formation heat properties, or the detailed well configuration (i.e. casings and cement layers) can lead to significant errors in the results. In this work, a steady-state computational method was developed using MATLAB programming software for calculating the fluid temperature at the end of a pipeline, when the temperature of the fluid at the inlet of the pipe is known. (In a well, calculations can be done *bottom-up* or *top-down* depending on the available input data). The method has been adapted to be used in an environment with a changing ambient temperature. The changing temperature is calculated stepwise in this method.

Due to its importance, temperature distribution predictions in flowing wells and pipelines have been the scope of many researches. In the following, some of the main literature contributions will be reviewed.

1.2 Literature Review

A rigorous prediction of the flowing temperature distribution in a pipe requires the simultaneous solution of mass, momentum, and energy conservation equations. The thermal interaction between the wellbore and the environment complicates this solution. Due to these complications, an *exact* analytical solution is usually impossible. However, predictions can be obtained using either *numerical* algorithms or *approximate analytical* solutions.

The numerical algorithms apply a double iterative procedure on both temperature and pressure for solving the three conservation equations simultaneously and require knowledge of the thermodynamic behavior of the flowing fluid, usually in the form of a table of enthalpy values for different pressures and temperatures.

Approximate analytical solutions for temperature prediction have been proposed by various investigators. By making some assumptions about the pipeline geometry, the heat transfer to the environment, and the thermodynamic behavior of the flowing fluid, these investigators could obtain explicit expressions for the flowing temperature distribution. A brief literature survey of the most well-known analytical and numerical temperature modelling approaches is presented in the following sections.

1.2.1 Analytical Temperature Modelling

One of the earliest works on predicting temperature profiles in a flowing well was presented by Kirkpatrick (Kirkpatrick, 1959) who presented a simple flowing-temperature-gradient chart that could be used to predict gas-lift valve temperatures at the injection depth. In spite of the simplicity, this chart lacked generality and accuracy. The inaccuracy of Kirkpatrick's method and thermal stress failure of casings in steam injection wells emphasized the importance of proper understanding of wellbore heat transfer and accurate estimation of flowing fluid temperature. Lesem (Lesem et al, 1957), and Moss and White (Moss and White, 1959) were the first to suggest procedures for estimating wellbore fluid temperatures. However, Ramey (Ramey, 1962) and Edwardson (Edwardson et al., 1962) were the first who presented a theoretical model for estimating fluid temperature as a function of well depth and producing time. Both works, however, neglect the effect of kinetic energy and friction and are applicable only to the flow of either a single-phase incompressible liquid or a single-phase ideal gas flowing in wells. Ramey (1962) presented a simple analytical equation to predict the temperature profile in an injection well. He modeled the wellbore as a line source and the surrounding earth as an infinite sink. In his work, he assumed that heat diffusion in the vertical direction is negligible compared to that in the horizontal plane, and that the heat transfer in the wellbore was steady-state whereas the heat transfer in formation is governed by transient radial conduction. The transient thermal behavior of the reservoir in Ramey's method is determined by solution of the problem of radial heat conduction in an infinite cylinder. The resistances to heat flow in the wellbore, caused by the presence of the tubing wall, tubing insulation, fluid in the casing/tubing annulus, casing wall, and cement are incorporated in an overall heat-transfer coefficient. Hagoort (Hagoort, 2004) studied Ramey's method and tried to establish criteria for its applicability. He claimed that Ramey's method is an excellent approximation except for the early transient period in which the calculated temperatures are significantly overestimated. Willhite (Willhite, 1967) deduced a computational methods to determine this overall heat transfer coefficient in the presence of natural convection in an annulus. His paper presents a comparison of calculated and measured casing temperatures during steam injection. Satter (Satter et al, 1965) extended Ramey's model to include two-phase flow by incorporating the influence of gas phase variations in steam injection wells. Sagar (Sagar et al., 1991) expanded Ramey's model for two-phase flow systems, and added the effects of kinetic energy and Joule Thompson cooling. Sagar's method is suitable for hand calculations and is based on field data. He assumed that the Joule-Thomson and the kinetic-energy terms are usually smaller than the other terms. Thus, he argued that it is reasonable to combine these two terms into a single term called F_c , and develop a correlation for F_c as a function of known physical properties (independent variables such as specific gravities, mass flow rate, wellhead pressure, and gas-oil ratio (GOR) specific to an interval. A data base of 392 wells was used as a basis for the development of the F_c correlation. According to Alves (Alves et al., 1992) all these methods include critical assumptions related to the thermodynamic behavior of the flowing fluid and thus are applicable only for a limited set of operational conditions. (Alves et al., 1992) present a general and unified equation for flowing temperature prediction that is applicable for the entire range of inclination angles. The equation degenerates to Ramey's equations for the case of injection wells and to the Coulter and Bardon method (Coulter and Bardon, 1979) for the

case of horizontal pipelines. His work also proposes an approximation method for determining the two-phase heat capacity and the Joule-Thomson coefficient. The approximations are useful when the generation of enthalpy tables is impossible or inconvenient. Hasan and Kabir (Hasan & Kabir, 1994) developed a formation temperature distribution model to account for the transient heat transfer in the formation with an appropriate inner boundary condition (finite wellbore). Previous researchers such as (Shiu and Beggs, 1980) generally assumed that heat transfer in the annulus was caused by conduction alone. However, (Hasan & Kabir, 1994) considered a natural convective heat transfer mechanism for the fluid in the annulus in order to calculate the overall heat transfer coefficient based on the tubing's outside surface area (U_{to}), and obtained more accurate U_{to} values which are a function of well depth.

1.2.2 Numerical Temperature Modelling

As mentioned previously, the numerical algorithms apply a double iterative procedure on both temperature and pressure for solving the three conservation equations (mass, momentum, energy) simultaneously and require knowledge of the thermodynamic behavior of the flowing fluid, usually in the form of a table of enthalpy values for different pressures and temperatures. The numerical integration of the enthalpy-gradient equation involves a trial-and-error solution for T_{i+1} for a guessed value of p_{i+1} (where T_i and p_i are known temperature and pressure at segment i in the wellbore), it also involves calculation of an average enthalpy gradient, and determination of the enthalpy of each phase and the mixture enthalpy at the end of the increment, (Brill and Mukherjee, 1999).

Based on the treatment of fluid PVT properties, numerical models can be categorized as black-oil models or compositional models. More specifically, in a black-oil model, the fluid PVT properties are treated as a single function of pressure and temperature, which means the PVT properties are interpolated from empirical relationships. A compositional model is more general, and it computes PVT properties from a function of in-situ composition, which is dependent on pressure and temperature. Fully coupled numerical formulations have been developed both for black-oil models (Stone et al. 1989) & (Livescu et al. 2010), and compositional models (Stone et al. 2002), (Pourafshary et al, 2008), and (Livescu et al., 2009). These simulators have incorporated various treatments for wellbore flow, including models with no slip between phases [Stone et al. (2002) for non-isothermal simulation], drift-flux models [Stone et al. (2002) for isothermal simulation; Livescu et al. (2010)] and mechanistic models (Stone et al. 1989). Most of the example cases presented in these papers involved only vertical wells, though Livescu et al. (2010) and Semenova et al. (2010) did present results for deviated and multilateral wells. A brief literature survey on some of the mentioned works is presented here.

Stone et al., (1989), describe a fully implicit, three dimensional thermal numerical model for simulating flow through a porous media and through a wellbore. Darcy's law together with conservation of energy and mass is used to model flow in the porous media. The wellbore simulator is a time dependent, thermal, three-phase, one dimensional model which conserves energy, momentum of all phases and mass. Wellbore grid blocks are embedded in reservoir grid blocks. Variables in the reservoir and wellbore are solved for simultaneously. This model is targeted mainly at horizontal wells. In (Stone et al. 2002) the authors extend their previously

reported well model, [(Stone et al. 1989)], to a compositional and thermal application, by focusing on thermal, heavy-oil applications. In the later work, the equation of state (EOS) or thermal K-value treatment of the fluid pressure/volume/temperature (PVT) is extended to the wellbore flow. Phase volumes are computed in each segment and are then used to calculate the multiphase pressure drop. Furthermore, an enhancement allows the definition of heat transfer coefficients. Another enhancement allows individual segments to inject or produce fluids, which permits the direct modeling of gas lift, downhole water pumps, or circulating wells, available in any mode.

(Pourafshary et al, 2008) presented a compositional-wellbore model coupled with a reservoir simulator to compute pressure and temperature distribution. The compositions of liquid and gaseous phases in the wellbore are determined by three-phase equilibrium flash calculations and by considering the slip between phases. Although the input requirements and computing expenses are higher for compositional calculations than for black-oil, Pourafshary et al. show that in some cases, such as those involving highly-volatile oil and retrograde condensate gas, ignoring compositional effects may lead to errors in pressure profile prediction for the wellbore.

(Shirdel and Sepehrnoori, 2011) present an implementation of a pseudo-compositional, thermal, fully implicit, transient two-fluid model for two-phase flow in wellbores. They solve gas/liquid mass balance, gas/liquid momentum balance, and two-phase energy balance equations to obtain five primary variables: liquid velocity, gas velocity, pressure, holdup, and temperature. They consider stratified, bubbly, intermittent and annular flow regimes using appropriate closure relations for inter-phase and wall shear stress terms in the momentum equations. In their research, they found that the inter-phase and wall shear stress terms for different flow regimes can significantly affect the model's results. In addition, the inter-phase momentum transfer terms mainly influence the holdup value.

1.3 Objectives

The main objective of this work is to develop a finite-difference steady-state wellbore temperature model for computing wellbore fluid temperature and pressure profiles in flowing wells which can be applied to pipelines or production and injection wells, under single phase, two-phase and three-phase flow conditions.

As part of the course AES1360 “Production Optimization” a large set of MATLAB routines is available to simulate and optimize the flow in oil and gas production systems with the aid of ‘nodal analysis’ (Jansen, 2016). However, these simulations are restricted to isothermal conditions in which it is assumed that the temperature profile along the production system is known a-priori. A more advance simulation of thermal effects requires the solution of an additional differential equation for the enthalpy drop in the wellbore. This thesis aims at programming a coupled pressure-temperature simulator starting from the existing MATLAB code.

Thus, to summarize, the primary objectives of this study are:

- To perform a literature search and become familiar with numerical simulation of temperature profiles in a production system.
- To develop algorithms to enable the simulation of steady-state pressure and temperature profiles in a production system. This will involve the use of an energy equation in terms of enthalpy.
- To update the existing wellbore simulator (AES1360 MATLAB programs) to model pressure and temperature.
- To verify and validate the developed model against field data.
- To investigate the effects of production parameters and wellbore geometry on the temperature distribution in wellbores.

1.4 Thesis Organization

The dissertation is organized in keeping with the objectives stated above. The thesis is organized into four chapters. Chapter 1 presents the introduction, literature review, objectives, and the thesis organization. Chapter 2 provides the theoretical background of the subject. The utilized modelling approach together with important thermodynamic and wellbore parameters are discussed. A black-oil model is presented to model steady-state pressure, phase fraction, phase velocity and temperature profiles in wellbores during production from vertical or inclined wells. The governing mass, momentum and energy equations for the wellbore fluid, and the numerical procedure used for solving the coupled pressure/temperature equations are also presented. In Chapter 3, different case studies are discussed and compared to field data to show the validity of the model. Also, a sensitivity analysis is performed. In Chapter 4, summary, conclusions and recommendations for future work are presented. More details on formula derivation together with program output data for field applications are explained in the Appendices.

2 MODEL FORMULATION

2.1 Modelling Approach

The semi analytic heat-transfer equation used in this study was initially presented by (Alves et al., 1992), and thereafter modified by (Hassan and Kabir, 2002) to account for transient heat transfer in the formation. In other similar works the Joule-Thomson and the kinetic-energy terms are usually combined into ϕ^* term, and are estimated using approximate empirical correlations. The drawback of those approaches is that applications are limited to specific ranges of input variables, e.g. GOR or fluid production rates. However, in this work, the Joule-Thomson effect and the kinetic energy term are being considered and calculated at each depth intervals. Furthermore, instead of assuming constants in integrating the temperature differential equation, the integration is done using a fourth-order Runge-Kutta method with MATLAB "ode45" function at each depth interval, simultaneously with pressure gradient equation. Thus, there is no need to assume constant U , C_p , η_{JT} , g_G , $alpha$, and dp/ds along the wellbore. At the beginning of this chapter, using mass and momentum balance equations for the fluid in the wellbore, pressure gradient equations for single-phase and then multiphase fluid flow are derived. Later on multiphase flow basic parameters and flow patterns are discussed. Finally, by writing the energy balance for the wellbore fluid, a temperature distribution model is presented. At the end of the chapter, a brief description of the MATLAB program functions used for single-phase gas, single-phase oil, and multiphase flow is given.

2.2 Pressure Gradient Calculation in the Wellbore

Pressure profile, phase fraction profiles and temperature distribution in the wellbore are the main parameters that affect the wellbore and reservoir relation. To obtain the pressure profile for a single-phase flow system, three governing equations are needed; a mass balance, a momentum balance, and an equation of state (EOS). In case of multiphase flow, mass and momentum balances are derived for the gas-liquid mixture (instead of modeling the dynamics of the two phases individually), and two additional closure equations are specified for the relationships between the mixture velocity and the phase velocities, and the mixture density and the phase densities, respectively. The latter two equations are usually empirical or semi-empirical.

2.2.1 Governing Equations

The text in this section is largely following Jansen (2016).

2.2.1.1 Conservation of Mass

For a given control volume, such as a segment of pipe, conservation of mass simply implies that the mass in, minus the mass out, must equal the mass accumulation (Knudsen and Katz,

* Also called F_c : $\phi = F_c = \mu \frac{dp}{ds} - v \frac{dv}{c_{pm}}$, for more information see (Sagar et al., 1991).

1958). Consider a section of an inclined pipeline with constant cross-sectional area; see Figure 2.1. One can write the mass balance per unit time for the section as:

$$A\rho v - A\left(\rho + \frac{\partial\rho}{\partial s}ds\right)\left(v + \frac{\partial v}{\partial s}ds\right) = A\frac{\partial\rho}{\partial t}ds, \quad (2.1)$$

where

A is the cross-sectional area of the pipe, m^2 ,

ρ is the fluid density, kg m^{-3} ,

v is the fluid velocity averaged over the cross-section[†], m s^{-1} ,

s is the coordinate along the pipe, m , and

t is time, s .

For the case of steady-state flow, no mass accumulation can occur. Assuming a constant cross sectional area (A) Eq. 2.1 then becomes

$$\frac{\partial(\rho v)}{\partial s} = 0. \quad (2.2)$$

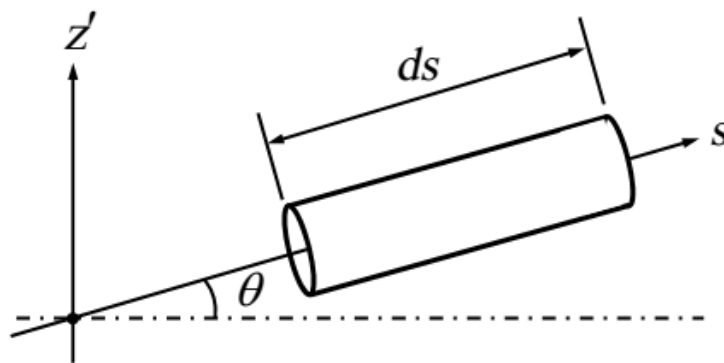


Figure 2-1. Segment of an inclined pipe (Jansen, 2016).

2.2.1.2 Conservation of Momentum

Application of Newton's first law to fluid flow in pipes requires that the rate of momentum out, minus the rate of momentum in, plus the rate of momentum accumulation in a given pipe segment must equal the sum of all forces on the fluid (Knudsen and Katz, 1958). Figure 2.1 defines the control volume and partial variables. Conservation of linear momentum can be expressed as

$$\begin{aligned} A\rho v^2 - A\left(\rho + \frac{\partial\rho}{\partial s}ds\right)\left(v + \frac{\partial v}{\partial s}ds\right)^2 + Ap - A\left(p + \frac{\partial p}{\partial s}ds\right) + F_g(\rho, s)ds \\ + F_f(\rho, \mu, v)ds = A\frac{\partial(\rho v)}{\partial t}ds, \end{aligned} \quad (2.3)$$

where

p is the pressure, Pa ,

[†] In reality the velocity will change over the cross-section of the pipe. It is zero at the wall and reaches its maximum value at the center. However, the use of an averaged velocity is accurate enough for our purpose.

$F_g(\rho, s)$ is the gravity force per unit length, N m^{-1} ,

$F_f(\rho, \mu, v)$ is the friction force per unit length, N m^{-1} , and

μ is the dynamic viscosity, Pa s .

The gravity force acting at a pipe element is defined as

$$F_g(\rho, s) = -\rho g \sin \theta(s) A ds, \quad (2.4)$$

where

g is the acceleration of gravity, m s^{-2} , and

$\theta(s)$ is the pipeline *inclination*, rad.

In pipeline engineering, the inclination θ is defined as the angle of the pipeline axis with respect to the horizontal plane. The term $\sin \theta$ is therefore a measure of the change in *elevation* (z') of the pipeline axis per unit length of *measured distance* (s). However, in well engineering it is common practice to define the wellbore geometry with a slightly different set of parameters; see Figure 2.2. The inclination α of the well is defined as the angle between the wellbore axis and the vertical direction. The term $\cos \alpha$ is therefore a measure of the change in *true vertical depth* (z), which is measured downwards, per unit length of s , which is now known as *along-hole depth* (AHD), or *measured depth*, and naturally is also positive in downward direction (Jansen, 2016).

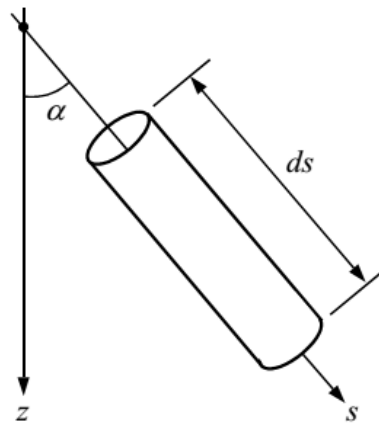


Figure 2-2. Segment of a deviated well showing well inclination (Jansen, 2016).

As a result of the different definition of the inclination, and because s is positive going downwards, the gravity force follows as

$$F_g(\rho, s) = \rho g \cos \alpha(s) A ds. \quad (2.5)$$

The frictional loss for single-phase flow in pipes with a circular cross section can be expressed as

$$\frac{F_f(\rho, v, s)}{A} = -\frac{\rho}{2d} f(\mu, \rho, v) \times v|v|, \quad (2.6)$$

where

d is the inside diameter of the pipe, m,

f is the dimensionless Moody (1944) friction factor.

The friction factor f is a function of μ , ρ and v through its dependence on the Reynolds number which is defined as

$$N_{Re} = \frac{\rho d |v|}{\mu} = \frac{\rho d |q|}{A \mu} = \frac{4 \rho |q|}{\pi \mu d}, \quad (2.7)$$

where μ is a known function of $p(s)$ and $T(s)$. The friction factor is also a function of the dimensionless pipe roughness ε , defined as

$$\varepsilon = \frac{e}{d}, \quad (2.8)$$

where e is the pipe roughness expressed in m, which we assume to be a constant. For Reynolds numbers lower than 2000 the flow is laminar, and f is given explicitly by

$$f = \frac{64}{N_{Re}}, \quad (2.9)$$

while for Reynolds numbers larger than 3000 the flow is turbulent, and f is given implicitly by the (Colebrook, 1939) equation:

$$\frac{1}{\sqrt{f}} - 1.74 - 2 \log_{10} \left(2\varepsilon + \frac{18.7}{N_{Re} \sqrt{f}} \right) = 0. \quad (2.10)$$

2.2.2 Single Phase Flow Pressure Drop

Combining Eq. (2.1), Eq. (2.2), and Eq. (2.3), and eliminating the time-dependent terms (assuming steady state condition) gives the pressure gradient equation for steady state conditions as

$$\frac{dp}{ds} = -\frac{\rho}{2d} f \times v |v| + \rho g \cos \alpha - \rho v \frac{dv}{ds}. \quad (2.11)$$

Here the possibility of negative fluid velocities (which, according to our sign convention correspond to production) has been taken into account through the use of the absolute value of the velocity $|v|$. Eq. (2.11) shows that the steady-state pressure gradient equation is made up of three components; friction, elevation and acceleration:

$$\left(\frac{dp}{ds} \right)_t = \left(\frac{dp}{ds} \right)_f + \left(\frac{dp}{ds} \right)_{el} + \left(\frac{dp}{ds} \right)_{acc}. \quad (2.12)$$

- The *frictional loss* is caused by the dissipation of energy by viscous forces in the fluid. This term depends strongly on the fluid properties, the flow regime (laminar or turbulent) and the fluid velocity. It is usually the most important component in pipelines. Friction losses normally represent 5 to 20% of the total pressure drop in wells (Brill and Mukherjee, 1999).

- The head loss or gravity loss is the static change in pressure caused by the change in the pipe's elevation. In near-horizontal pipelines this component is negligible, but it is usually the most important component in a well. The pressure between surface and bottom hole changes greatly, simply due to the weight of the column of fluid in the well, even if it is not flowing. It usually contributes from 80 to 95% of the pressure gradient in the wells (Brill and Mukherjee, 1999).
- The acceleration loss[‡] is caused by the change in momentum when the fluid is accelerated in the well due to expansion. Generally this term is less important and can be neglected in some cases. However, it can become of significance for very high rate gas wells (Jansen, 2016).

2.2.3 Multiphase-Flow model

Multiphase flow is complicated because at each section of the wellbore multiple phases are simultaneously competing for the available cross-sectional area. Computing each phase fraction is very important for determining the pressure gradient in multiphase-flow.

2.2.3.1 Liquid Holdup and Pressure Drop

The pressure gradient in a steady state system for multiphase-flow can be written as

$$\frac{dp}{ds} = -\rho_m g \sin\theta - \frac{\rho_m}{2d} f v_m |v_m| - \rho_m v_m \frac{dv_m}{ds}, \quad (2.13)$$

$$\frac{dp}{ds} = \left(\frac{dp}{ds}\right)_{el} + \left(\frac{dp}{ds}\right)_f + \left(\frac{dp}{ds}\right)_{acc}. \quad (2.14)$$

where v_m , ρ_m , and f_m represent mixture properties for velocity, density, and friction factor. Several slightly different formulations have been presented by various authors, but they all contain a head loss, frictional loss and acceleration loss component same as shown in Eq. (2.14). Mixture parameters depend directly on in-situ volume fractions of the phases. The pressure drop caused by elevation change depends on the density of the two-phase mixture and is usually calculated using a liquid holdup value. Friction losses require evaluation of a two-phase friction factor. Acceleration is often negligible and is usually calculated only for high flow velocities. The in-situ fraction of a phase is generally different from its input fraction. The main reason for this is the differences between gas and liquid velocities caused by their density differences. Thus, a major effort in modeling multiphase-flow is the correct estimation of in-situ phase volume fraction. In case of assuming slip between phases (which is usually the case), 'mixture, slip' density and velocity can be expressed in terms of the gas and liquid densities (ρ_g, ρ_l) as follow

$$\rho_{ms} = H_g \rho_g + H_l \rho_l, \quad (2.15)$$

[‡] Sometimes referred to as the *kinetic loss*.

$$v_{ms} = H_g v_g + H_l v_l, \quad (2.16)$$

where the subscript *ms* indicates ‘mixture, slip’. (ρ_g, ρ_l) and (v_g, v_l) are gas and liquid *local* densities and velocities (*in-situ* condition). ρ_l can be expressed in terms of water and oil volume fractions (f_w, f_o) and *local* densities (ρ_w, ρ_o) as

$$\rho_l = f_o \rho_o + f_w \rho_w, \quad (2.17)$$

where assuming that the liquids flow with equal velocities, the local oil and water *fractions* are defined as

$$f_o = \frac{q_o}{q_l} = \frac{q_o}{q_o + q_w}, f_w = \frac{q_w}{q_l} = \frac{q_w}{q_o + q_w}. \quad (2.18, 2.19)$$

The *local* or *in-situ* or *true* phase velocities are defined as

$$v_g = \frac{q_g}{A_g} = \frac{q_g}{H_g A} = \frac{q_g}{(1 - H_l) A}, v_l = \frac{q_l}{A_l} = \frac{q_l}{H_l A}, \quad (2.20, 2.21)$$

where q_g and q_l are the gas and liquid phase production rates, A_g and A_l are the parts of the pipe’s cross sectional area occupied by the gas and the liquid respectively, and $A = A_g + A_l$ is the total cross-sectional area. Being able to assign an averaged value for the liquid phase properties is beneficial, because in the case of three-phase gas/oil/water flow, treating the two liquid phases as one effectively reduces the system to a two-phase flow situation and has been generally found to yield acceptable predictive accuracy (Wang, 1996). In Eq. (2.20, 2.21), H_g and H_l are the gas and liquid hold-ups, and are (semi-) empirical functions of a large number of parameters such as inclination, pipe diameter, phase flow rates, and densities, viscosities and surface tensions. The expression “hold-up” is also often used in the oil industry to indicate the volume fractions occupied by gas and liquid, although in upward flow the gas is not actually held up, but to the contrary is speeded up. The gas and liquid hold-ups H_g and H_l are defined as

$$H_g = \frac{V_g}{V} = \frac{A_g}{A}, H_l = \frac{V_l}{V} = \frac{A_l}{A}, \quad (2.22, 2.23)$$

where V_g and V_l are the fractions of a reference volume of pipe that are being occupied by gas and liquid and $V = V_g + V_l$ is the total reference volume. Note that volumes and areas should be interpreted as quantities averaged over a length that is sufficiently large to suppress the effect of small scale flow features. The sum of phase hold-ups is equal to one.

Other fluid properties can also be defined using the same approach, Eq. (2.24) shows the mixture ‘slip’ averaged viscosity

$$\mu_{ms} = H_g \mu_g + H_l \mu_l. \quad (2.24)$$

Mixture properties can also be calculated by assuming that there is no slip between the phases; in that case instead of *ms*, subscript *mn* will be used, and it indicates ‘mixture, no-slip’, while instead of gas and liquid hold ups, phase volume fractions (λ_g, λ_l) will be used. For instance, the no- slip mixture density can be expressed as

$$\rho_{mn} = \lambda_g \rho_g + \lambda_l \rho_l . \quad (2.25)$$

The gas volume fraction and the liquid volume fraction are defined as

$$\lambda_g = \frac{q_g}{q_m} = \frac{q_g}{q_g + q_l}, \lambda_l = \frac{q_l}{q_m} = \frac{q_l}{q_g + q_l}, \quad (2.26, 2.27)$$

where the quantity $q_m = q_g + q_l = q_g + q_o + q_w$ is known as the *mixture* flow rate or *total* flow rate.

2.2.3.2 Flow Patterns

The empirical correlation or mechanistic model used to predict flow behavior varies with flow pattern. Because of many parameters such as phase velocity, geometry, wellbore orientation and fluid densities, the flowing phases take up a number of distinct configurations, called flow patterns or flow regimes. In vertical and near vertical systems, four major flow patterns are recognized: bubbly flow, slug flow, churn flow and annular flow. These flow patterns are clearly distinguishable and are generally recognized by all researchers. A schematic of different flow regimes in a vertical wellbore is shown in Figure 2.3.

- **Bubbly flow:** At low gas velocity, the liquid phase is the continuous phase and gas or vapor phase flows as bubbles in it. When the gas velocity is low, especially in vertical flow, the bubbles are uniformly distributed.
- **Slug flow:** As gas velocity increases, the bubbles coalesce and make larger bubbles. These large bubbles sometimes have almost the same diameter as the wellbore. Hence, as shown in Figure 2.3, the slug flow consists of two parts: large bubbles (Taylor bubbles) and continuous liquid phase containing small bubbles.
- **Churn flow:** This flow regime forms by the breakdown of slug flow Taylor bubbles because of high mixture velocity. The gas phase flows in a chaotic manner through the liquid phase and it is relatively unstable, hence the multiphase flow parameters such as holdup vary with time at each section when churn flow exists in the tubing.
- **Annular flow:** As the flow rate and fraction of the gas phase increases, this phase starts to flow through the center of the wellbore as a continuous core with some liquid droplets. The liquid phase forms a layer along the pipe wall and flows as an annulus.

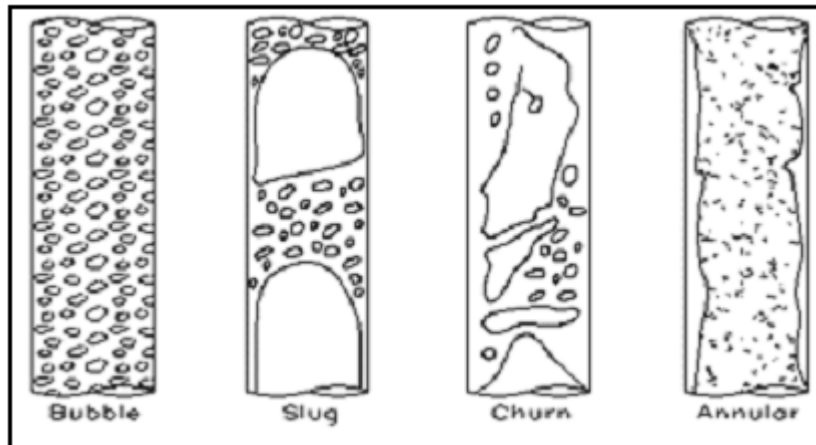


Figure 2-3. Schematic multiphase flow patterns in a vertical tube (From left to right: bubble flow, slug flow, churn flow and annular flow), picture from (Brill and Mukherjee, 1999).

2.2.3.3 Mukherjee & Brill

In this work, the Mukherjee and Brill method has been used to model the multi-phase flow system behavior. Mukherjee and Brill (1983, 1985a, 1985b) studied the behavior of flow in upward and downward directions over all possible inclinations by performing a large number of tests in a 1.5 inch diameter flow loop with a U shaped inclined section that could be raised from horizontal to vertical. They used air as the gas phase and kerosene or lube oil as the liquid phase. Both legs of the U contained a 32-feet transparent section to observe flow regimes, and a capacitance measurement device to measure hold-ups. Through curve fitting of a large number of measurements they developed a set of numerical expressions for the flow pattern boundaries, (Jansen, 2016). These numerical expressions are explained in more detail in Appendix A.

2.3 Wellbore Fluid Temperature Distribution

Modeling heat transfer in any system requires an energy balance for the wellbore fluids. Heat loss (or gain) to the surroundings by the wellbore fluid depends on various factors such as formation temperature distribution in the presence of a heat source/sink (the wellbore), temperature differences, and resistances to heat transfer within the elements of the wellbore. During the production from a formation, the hot reservoir fluids enter a wellbore and as they flow towards the surface, they begin losing heat to the cooler surrounding rock. As a result of this heat exchange between the wellbore fluid and the formation, the surrounding rock gradually heats up, reducing the temperature difference and the heat transfer between the fluids and the rock. Eventually, for a constant mass flow rate, the surrounding formation reaches a steady state temperature distribution. Prediction of fluid temperatures in the wellbore as a function of depth and time is necessary to determine the fluid's physical properties and calculate pressure gradient (Brill and Mukherjee, 1999).

2.3.1 Steady-State Heat Transfer

Because of high thermal conductivity and relatively small radial distance between the flowing fluids and the borehole wall, heat transfer in this region normally can be considered steady-state. Heat transfer in the wellbore is relatively rapid compared to the formation, since all heat lost by the fluids instantaneously flows through the wellbore and in to the surrounding rock (Brill and Mukherjee, 1999). However, heat transfer in the formation never reaches true steady-state due to the large thermal mass of the rock. The unsteady radial conduction in the formation is incorporated into the steady-state wellbore model by means of a log-linear time function which is derived from classic transient solutions for line or cylindrical sources in an infinite medium. Later on either an analytic or a numerical wellbore model can be coupled with the transient formation model for rapid computations of pressure, temperature, and velocity. A transient temperature model introduced by (Hasan & Kabir, 1994) is used in this model, and further information is provided under the ‘*Formation Temperature Distribution*’ section. In this section the main heat transfer mechanisms in the reservoir/wellbore system during production (or injection) are reviewed, including conduction, convection, and radiation heat transfer.

2.3.1.1 Heat Transfer by Conduction

Heat conduction, also called diffusion, is the transfer of energy from the more energetic particles of a substance to the adjacent, less energetic ones as a result of interaction between particles:

$$\dot{Q}_{cond} = kA \frac{T_1 - T_2}{\Delta x}, \quad (2.28)$$

where \dot{Q} is rate of heat transfer (heat transferred per unit time), k is the thermal conductivity of the material (Figure 2.4). In the limiting case $\Delta x \rightarrow 0$ the equation above reduces to the differential form that is called Fourier’s law of heat conduction after J. Fourier and becomes

$$\dot{Q}_{cond} = -kA \frac{dT}{dx}. \quad (2.29)$$

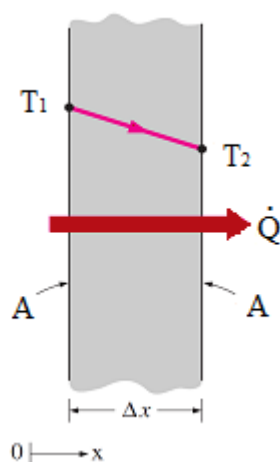


Figure 2-4. Schematic view of conduction heat transfer mechanism, picture from (Fidan, 2011).

2.3.1.2 Heat Transfer by Convection

Convective heat transfer can occur between a solid surface and the adjacent liquid or gas that is in motion. Convection is called forced convection if the fluid is forced to flow over the surface by external means such as fan, pump, or the wind. In contrast, convection is called natural (or free) convection if the fluid motion caused by buoyancy forces that are induced by density differences due to the variation of temperature in the fluid (Figure 2.5). The rate of convection heat transfer is expressed by Newton's law of cooling as

$$\dot{Q}_{conv} = hA_s(T_s - T_f), \quad (2.30)$$

where T_s is the temperature of the object's surface, T_∞ is the temperature of the environment (adjacent fluid); i.e. the temperature suitably far from the surface, h is the heat transfer coefficient, and A is the heat transfer surface area.

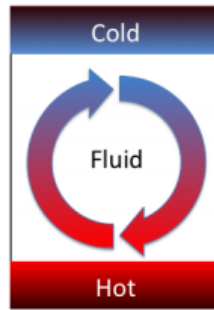


Figure 2-5. Heat transfer from a hot surface to the adjacent fluid by convection, picture from (Fidan, 2011)

2.3.1.3 Heat Transfer by Radiation

While both conduction and convection require matter to transfer heat, radiation is a method of heat transfer that does not rely upon any contact between the heat source and the heated object. Radiation is the energy emitted by matter in the form of electromagnetic waves as a result of changes in the electronic configurations of the atoms or molecules. The radiation energy per unit time from a blackbody is proportional to the fourth power of absolute temperature and can be described by Stefan-Boltzmann law as

$$\dot{Q}_{emit,max} = \sigma A_s T_s^4, \quad (2.31)$$

where $\sigma = 5.6703 \times 10^{-8} \text{ (W/m}^2\text{K}^4\text{)}$ is the Stefan-Boltzmann constant. For calculation of temperature distributions in this work, conductive and convective heat transfer mechanisms have been considered, but for simplicity reasons radiative heat transfer is neglected. For more information see (Hassan and Kabir, 2002).

2.3.2 Formation Temperature Distribution

To model heat flow in the formation, one can assume the formation to behave as a homogeneous solid. The three-dimensional (3D) problem can be simplified to a one-dimensional (1D) problem by assuming symmetry around the well, and by ignoring heat diffusion in vertical direction in the earth around the wellbore (due to small vertical temperature gradients). This approach has been adapted by (Hasan & Kabir, 1994) and others, and introduces very little error and allows an analytical solution for the formation diffusivity problem. The general one-dimensional radial heat diffusion equation is

$$\frac{\partial^2 T_e}{\partial r^2} + \frac{1}{r} \frac{\partial T_e}{\partial r} = \frac{c_e \rho_e}{k_e} \frac{\partial T_e}{\partial t}, \quad (2.32)$$

where T_e is the formation temperature at any arbitrary depth at time t , and r is the radial distance measured from the center of the wellbore. At the right hand side c_e, ρ_e, k_e are heat capacity, density and thermal conductivity of the formation, respectively. The thermal diffusivity equation is analogous to the one used in pressure diffusion while solving pressure-transient problems. The initial formation temperature is known (T_{ei}). In this work it is assumed that at $t = 0$ the formation temperature profile is linear based on the local geothermal gradient. The second boundary condition is the assumption of constant temperature at the outer boundary of the formation. Finally, at the wellbore/formation interface heat conduction is assumed to be constant. The heat flow rate at the wellbore/formation interface is governed by Fourier's law of heat conduction. The three boundary conditions can be written as follow

$$\lim_{t \rightarrow 0} T_e = T_{ei}, \quad (2.33)$$

$$\lim_{r \rightarrow \infty} \frac{\partial T_e}{\partial r} = 0, \quad (2.34)$$

$$Q = -2\pi k_e \left(\frac{r \partial T_e}{\partial r} \right)_{r=r_w}, \quad (2.35)$$

where Q is the heat flow rate from the well to the formation per unit length of the well (W/m). As production continues, heat transfer from the wellbore causes a gradual rise in the surrounding formation temperature, which in turn, causes a slow decrease in the heat flow rate. (Ameen, 1992) used the superposition principle to account for changing heat flux using a numerical approach. His solution showed that the assumption of constant heat flux introduced very little inaccuracy.

Using the Laplace transformation, an equation for the temperature distribution as a function of distance and time can be presented. The general solution is a combination of Bessel functions, which can be found in the literature (Dake, 1978) and (Hasan & Kabir, 1994). An approximation to this analytical solution can be written as follows:

$$T_D = \left[0.4063 + \frac{1}{2} \ln t_D \right] \left[1 + \frac{0.6}{t_D} \right], \quad \text{if } t_D > 1.5, \quad (2.36)$$

$$T_D = 1.1281\sqrt{t_D} (1 - 0.3\sqrt{t_D}), \quad \text{if } t_D \leq 1.5, \quad (2.37)$$

where T_D, t_D are the dimensionless temperature and time, respectively:

$$t_D = \frac{k_e t}{\rho_e c_e r_w^2}, \quad (2.38)$$

$$T_D = \frac{2\pi k_e}{Q} (T_w - T_e). \quad (2.39)$$

T_D is always positive, and it relates heat flow rate (Q) to the temperature-difference driving force ($T_w - T_e$). In the case of fluid production, T_w is greater than T_e , meaning that the wellbore fluid loses heat to its surroundings. However, T_w is unknown, and should be replaced by wellbore fluid temperature. This substitution is accomplished by using an energy balance for the wellbore fluid.

2.3.3 Conservation of Energy for Wellbore Fluid

In addition to the mass and momentum conservation law, one can write the energy balance per unit time for the desired section. Application of energy conservation to fluid flow in pipes requires that in a given segment the energy in, minus the energy out, plus the heat energy transferred to or from the surroundings must equal the rate of energy accumulation (Bird, Stewart, and Lightfoot, 1960):

$$\frac{\partial(\rho e)}{\partial t} = \frac{\partial}{\partial s} \left[\rho v \left(e + \frac{p}{\rho} \right) \right] + \frac{Q'' \pi d}{A}, \quad (2.40)$$

where e is the intrinsic specific energy, $\text{m}^2 \text{s}^{-2} = \text{J kg}^{-1}$,

$$e = g S \sin\theta + \frac{1}{2} v^2 + u, \quad (2.41)$$

u is specific internal energy, J kg^{-1} , and Q'' is the heat flux, $\text{J m}^{-2} \text{s}^{-1}$

$$Q'' = U (T_f - T_e), \quad (2.42)$$

U is the overall heat-transfer coefficient, $\text{J m}^{-2} \text{s}^{-1} \text{°C}^{-1}$, T_e is the external (formation) temperature, and T_f is the fluid temperature inside the tubing, expressed in °C . Detailed expressions for U can be obtained by considering conduction and convection in the configuration of tubing and casing strings that make up the well.

For a deviated well with constant inclination α and flowing bottom-hole temperature T_{wf} , the external temperature is given by

$$T_e(s) = T_{wf} - g_G(s_{tot} - s) \cos \alpha, \quad (2.43)$$

where g_G is the geothermal gradient, expressed in °C/m. In case of different values of g_G , the program needs to be run separately for each depth interval (Case Study 2, in well application section shows this).

For steady-state flow Eq. (2.40) reduces to

$$\frac{d}{ds} \left[\rho v \left(e + \frac{p}{\rho} \right) \right] = - \frac{Q'' \pi d}{A}. \quad (2.44)$$

Expanding the left side of Eq. (2.44) yields

$$\rho v \frac{d}{ds} \left(e + \frac{p}{\rho} \right) + \left(e + \frac{p}{\rho} \right) \frac{d(\rho v)}{ds} = - \frac{Q'' \pi d}{A}, \quad (2.45)$$

Combining Eq. (2.41) and Eq. (2.1), for a steady-state flow condition yields

$$\rho v \frac{d}{ds} \left(g s \sin \theta + \frac{1}{2} v^2 + u + \frac{p}{\rho} \right) = - \frac{Q'' \pi d}{A}. \quad (2.46)$$

Using definition of specific enthalpy

$$h = u + \frac{p}{\rho}, \quad (2.47)$$

Eq. (2.46) can be expressed as

$$\rho v g s \sin \theta + \rho v^2 \frac{dv}{ds} + \rho v \frac{dh}{ds} = - \frac{Q'' \pi d}{A}, \quad (2.48)$$

where we assumed that θ (s) is changing so slowly that

$$\frac{\partial(s \sin \theta)}{\partial s} = \sin \theta + s \frac{\partial \sin \theta}{\partial s} \approx \sin \theta. \quad (2.49)$$

Finally, solving for enthalpy gradient

$$\frac{dh}{ds} = - \frac{Q'' \pi d}{\rho v A} - g s \sin \theta - v \frac{dv}{ds}, \quad (2.50)$$

$$\left(\frac{dh}{ds} \right)_t = \left(\frac{dh}{ds} \right)_{HT} + \left(\frac{dh}{ds} \right)_{el} + \left(\frac{dh}{ds} \right)_{acc}. \quad (2.51)$$

recall that

$$\left(\frac{dh}{ds} \right)_{HT} = - \frac{Q'' \pi d}{\rho v A} = - \frac{U \pi d (T_f - T_e)}{w}, \quad (2.52)$$

Just like in Eq. (2.13) and Eq. (2.14) for the pressure drop, the acceleration loss in Eq. (2.51) can usually be disregarded. Eq. (2.51) can be numerically integrated along the wellbore.

2.3.4 The Overall Heat Transfer Coefficient

Heat transfer within the tubing and in a fluid filled annulus is primarily a result of convection, whereas heat transfer through tubing and casing walls and through a cemented-filled annulus between the casing and borehole wall primarily results from conduction. Conduction heat transfer can be described by Fourier's equation in radial coordinates as follow:

$$q = -2\pi r \Delta L k \frac{\partial T}{\partial r}, \quad (2.53)$$

where q (W) is heat flow rate. In other word, q is the amount of heat flowing radially through a solid with thermal conductivity, k ($\text{W m}^{-1} \text{ } ^\circ\text{C}^{-1}$), ΔL is the depth interval, and r is the radial distance between T_1 and T_2 .

Integrating Eq. (2.53) gives:

$$q = 2\pi \Delta L k_{1-2} \frac{(T_2 - T_1)}{\ln(r_1/r_2)}. \quad (2.54)$$

Heat transfer resulting from convection can be described by

$$q = 2\pi r \Delta L h \Delta T, \quad (2.55)$$

where h is local convective-film coefficient ($\text{W m}^{-2} \text{ } ^\circ\text{C}^{-1}$).

Under steady state heat transfer in the wellbore assumption, q is constant. Expressions for temperature change through the wellbore can be developed from Eq. (2.54) and Eq. (2.55) as follow:

- For convection inside the tubing,

$$T_f - T_{ti} = \frac{q}{2\pi \Delta L} \frac{1}{r_{ti} h_f}, \quad (2.56)$$

where the subscripts ti and f indicate tubing inside and the flowing fluid, respectively.

- For conduction through the tubing wall,

$$T_{ti} - T_{to} = \frac{q}{2\pi \Delta L} \frac{\ln\left(\frac{r_{to}}{r_{ti}}\right)}{k_t}, \quad (2.57)$$

where r_{to} and T_{to} are the tubing outer radius and temperature, respectively, and k_t is the tubing wall thermal conductivity.

- For convection through the casing/tubing annulus,

$$T_{to} - T_{ci} = \frac{q}{2\pi \Delta L} \frac{1}{r_{ci} h_{ann}}, \quad (2.58)$$

where r_{ci} and T_{ci} are the casing inside radius and temperature, respectively, and h_{ann} is the annulus fluid local convective-film coefficient.

- For conduction through the casing,

$$T_{ci} - T_{co} = \frac{q}{2\pi\Delta L} \frac{\ln\left(\frac{r_{co}}{r_{ci}}\right)}{k_c}, \quad (2.59)$$

where r_{co} and T_{co} are the casing outer radius and temperature, respectively, and k_c is the casing wall thermal conductivity.

- For conduction through the cement in the casing/borehole annulus,

$$T_{co} - T_w = \frac{q}{2\pi\Delta L} \frac{\ln\left(\frac{r_w}{r_{co}}\right)}{k_{cem}}, \quad (2.60)$$

where r_w and T_w are wellbore radius and wellbore temperature at wellbore/formation interface, respectively, and k_{cem} is the cement thermal conductivity.

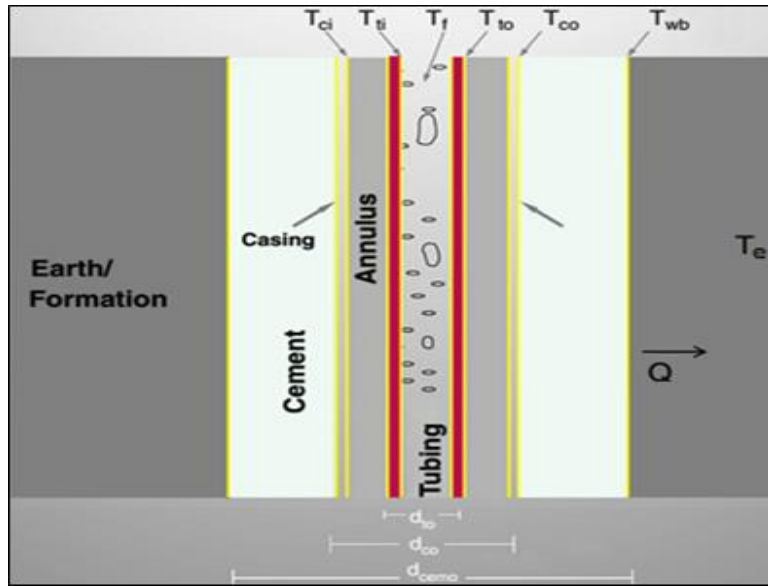


Figure 2-6. Heat flow through a series of resistances, picture from (Hasan and Kabir, 2006).

Combining Eq. (2.56) to Eq. (2.60) and Eq. (2.39) determines the total temperature change between the fluids and the undisturbed geothermal temperature of the surrounding rock:

$$T_f - T_e = (T_f - T_{ti}) + (T_{ti} - T_{to}) + (T_{to} - T_{ci}) + (T_{ci} - T_{co}) + (T_{co} - T_w) + (T_w - T_e), \quad (2.61)$$

$$T_f - T_e = \frac{q}{2\pi\Delta L} \left[\frac{1}{r_{ti}h_f} + \frac{\ln\left(\frac{r_{to}}{r_{ti}}\right)}{k_t} + \frac{1}{r_{ci}h_{ann}} + \frac{\ln\left(\frac{r_{co}}{r_{ci}}\right)}{K_c} + \frac{\ln\left(\frac{r_w}{r_{co}}\right)}{K_{cem}} + \frac{T_D}{K_e} \right]. \quad (2.62)$$

From Newton's law of cooling a simple equation for the total heat loss from the fluids in the tubing can be estimated,

$$q = 2\pi r_{to} \Delta L U_{to} \Delta T, \quad (2.63)$$

where ΔL (also referred to as Δs) is the interval along the hole. Comparing Eq. (2.62) and Eq. (2.63), it is evident that overall heat transfer coefficient (U) is equal to:

$$\frac{1}{U_{to}} = r_{to} \cdot \left[\frac{1}{r_{ti} h_f} + \frac{\ln\left(\frac{r_{to}}{r_{ti}}\right)}{k_t} + \frac{1}{r_{ci} h_{ann}} + \frac{\ln\left(\frac{r_{co}}{r_{ci}}\right)}{K_c} + \frac{\ln\left(\frac{r_w}{r_{co}}\right)}{K_{cem}} + \frac{T_D}{K_e} \right]. \quad (2.64)$$

U_{to} is overall heat transfer coefficient calculated based on tubing outside radius, r_{to} . Similarly U_{co} , U_{ci} , and U_{wb} can be calculated by using r_{co} , r_{ci} , and r_{wb} instead of r_{to} in Eq. (2.64). For a typical well one may assume that the fluid heat transfer coefficient is so high that T_f may be assumed equal to T_{ti} . Thus first term of Eq. (2.64) can be neglected. The resistance to heat transfer offered by annulus, $(1/h_{ann})$, may involve radiative (h_r) and natural-convective (h_c) heat transfer mechanisms:

$$\frac{1}{U_{to}} = r_{to} \left[\frac{\ln\left(\frac{r_{to}}{r_{ti}}\right)}{k_t} + \frac{1}{r_{ci} (h_r + h_c)} + \frac{\ln\left(\frac{r_{co}}{r_{ci}}\right)}{K_c} + \frac{\ln\left(\frac{r_w}{r_{co}}\right)}{K_{cem}} + \frac{T_D}{K_e} \right]. \quad (2.65)$$

In most cases of oil production, the temperature difference across the annulus is small and one needs to consider convective heat transfer only. When a fluid at a given temperature is in contact with a surface at a different temperature, heat transfer takes place via conduction as well as natural convection. Density of a fluid depends on its temperature; the temperature difference and thus the density difference between the bulk fluid and the fluid close to the surface causes fluid circulation, which in return enhances heat transfer. Unfortunately, very little work on natural convection in a vertical annular geometry is reported in the literature. (Hassan and Kabir, 2002) adapt the correlation proposed by (Dropkin and Somerscales, 1965) for the heat transfer coefficient for natural convection in fluid between two vertical plates. Dropkin and Somerscales correlation for natural convection is

$$h_{ann} = \frac{0.049(N_{Gr} N_{Pr})^{1/3} N_{Pr}^{0.074} k_{ann}}{r_{to} \ln\left(\frac{r_{ci}}{r_{to}}\right)}, \quad (2.66)$$

where N_{Pr} is Prandtl number and it is a measure of the interaction between the hydrodynamic boundary layer and the thermal boundary layer and is given by

$$N_{pr} = \frac{C_{p,ann} \mu_{ann}}{k_{ann}}. \quad (2.67)$$

The Grashof number N_{Gr} reflects the extent of motion of the annulus fluid resulting from natural convection

$$N_{Gr} = \frac{(r_{ci} - r_{to})^3 \rho_{ann}^2 \beta g (T_{to} - T_{ci})}{\mu_{ann}^2}, \quad (2.68)$$

where β is annulus fluid thermal expansion coefficient, $^{\circ}\text{C}^{-1}$.

An iterative solution procedure becomes necessary because the casing inside temperature (T_{ci}) and tubing outside temperature (T_{to}) are unknown. The iterative calculation procedure starts

with assuming the temperature drop across the annulus. Using the assumed temperature drop, the Grashof number, heat transfer coefficient for natural convection, and finally the overall heat transfer coefficient can be calculated. Once the overall heat transfer coefficient is calculated the fluid temperature can be estimated by employing the analytic temperature model explained in the previous section. The amount of heat loss to the formation can be calculated assuming steady state heat flow through the resistances between tubing fluid and formation. The temperature drop across the annulus fluid can be updated by Fourier's law of heat conduction. The iterative procedure continues until the desired convergence criterion is reached.

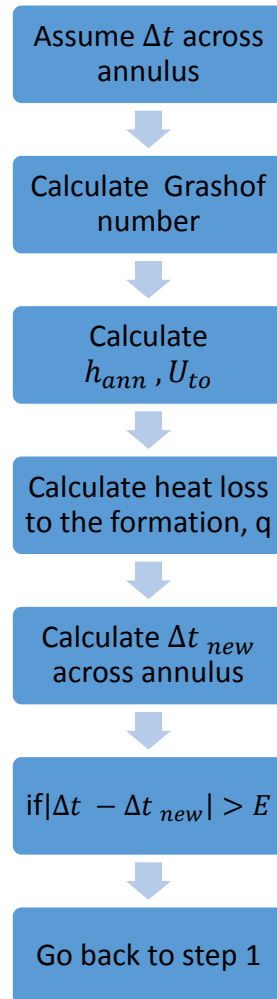


Figure 2-7. The iterative procedure for calculating annulus heat transfer rate.

Hassan and Kabir suggested using Eq. (2.66) to calculate the annular fluid convective heat transfer coefficient (h_{ann}). However, they believe that this correlation often leads to significant underestimation of wellbore fluid temperature, and they have found a value of $0.25 * h_{ann}$ to mimic field data, better. In case of a turbulent flow in pipes and wells the forced convective heat transfer takes place, and the annular fluid convective heat transfer coefficient (h_{ann}) can be estimated by an empirical correlation suggested by Sieder-Tate

$$Nu = \frac{hd}{k} = 0.023 N_{Re}^{0.8} N_{Pr}^{0.33} \left(\frac{\mu}{\mu_{wall}} \right)^{0.14}, \quad (2.69)$$

where all values represent those of the bulk fluid, and μ_{wall} is the fluid viscosity at the well temperature. The term (μ/μ_{wall}) is often neglected but becomes more important for highly viscous fluids.

The overall heat transfer coefficient U_{to} , is much smaller at the bottom of the well than at the wellhead. This variation in the U_{to} values with depth is a direct result of the contribution of the natural convective heat transfer coefficient of annular fluid (h_{ann}) to the overall heat transfer coefficient. The temperature difference between the tubing fluid and the earth is smaller near the bottom hole, and so is Δt across the annulus ($T_{to} - T_{ci}$), leading to smaller values of N_{Gr} and h_{ann} . This low h_{ann} value leads to smaller values of U_{to} . At the wellhead however, the reverse is true, resulting in larger U_{to} values. The other reason for the dependency of U_{to} on depth is due to well-completion design factors such as the number of casings. In MATLAB file `Overall_heat_transfer_coeff.m`, the well is assumed to produce fluids through a single tubing. The fluid inside the tubing/casing annulus is assumed to be NaCl 20%, and the annulus is assumed to be filled all the way from the bottom of the well to the surface. However, in reality the annulus is not usually filled with liquid up to the wellhead; quite often, gas occupies most of the annulus. In such cases, computations must be done in segments, allowing for variable h_{ann} with well depth, thereby honoring fluid composition in the annulus.

2.3.5 Temperature Profile

The temperature at a certain point s along the pipe can be computed when the enthalpy of the mixture is computed, e.g. with the aid of an equation of state. The numerical integration of the enthalpy-gradient equation involves a trial and error solution, and also involves calculation of an average enthalpy gradient, and determination of enthalpy of each phase and the mixture enthalpy at the end of increment. Approximate analytical solutions for integrating the enthalpy-gradient equation normally are adequate and simplify the calculations significantly. This is why in this work the analytical approach introduced by (Alves et al., 1992) is used for enthalpy calculation, both in case of single and multiphase flow (Brill and Mukherjee, 1999).

For a single phase fluid with no phase changes, enthalpy is a function of pressure and temperature. Thus, a change in enthalpy can be calculated by considering effects of temperature and pressure separately,

$$dh = \left(\frac{\partial h}{\partial T} \right)_p dT + \left(\frac{\partial h}{\partial p} \right)_T dp = C_p dT + \left(\frac{\partial h}{\partial p} \right)_T dp, \quad (2.70)$$

where C_p is the average specific heat capacity for the flowing fluid at constant pressure in the wellbore, $J \text{ kg}^{-1} \text{ } ^\circ\text{C}^{-1}$. At *isenthalpic conditions*, i.e. for $dh = 0$, equation reduces to

$$C_p dT + \left(\frac{\partial h}{\partial p} \right)_T dp = 0, \quad (2.71)$$

from which it follows that

$$\left(\frac{\partial h}{\partial p} \right)_T = -C_p \left(\frac{dT}{dp} \right)_h = -C_p \eta_{JT}, \quad (2.72)$$

where η_{JT} is the *Joule-Thomson coefficient* which is a measure of the amount of isenthalpic cooling or heating of a fluid per unit change of pressure. Assuming that the change in enthalpy along the pipe is small, it is justified to use Eq. (2.71) and Eq. (2.72) to rewrite Eq. (2.70) as

$$\frac{dh}{ds} = C_p \frac{dT}{ds} - C_p \eta_{JT} \frac{dp}{ds}. \quad (2.73)$$

Pressure and temperature are sufficient to compute any state variable, including enthalpy, provided there is a *single* chemical component and a *single* phase (gas only or liquid only or solid only, i.e. no boiling, melting, etc.) system. However, if there are more than one component or more than one phase, the chemical and/or phase make-up of the system needs to be specified to obtain the enthalpy. To avoid complications, (Alves et al., 1992) suggested the following analytical approximation for the Black Oil model to calculate the enthalpy of a multiphase flow. (Note that for compositional models, tables of enthalpy can be generated to give values for C_p and η_{JT}). By using the Alves et al. approach the generated/absorbed heat due to the phase changes in the system (latent heat) does not need to be calculated separately. Thus, for a multiphase flow (Hasan, Kabir, and Wang, 2009)

$$\begin{aligned} \frac{dh}{ds} &= x \frac{dh_g}{ds} + (1-x) \frac{dh_l}{ds} \\ &= [xC_{pg} + (1-x)C_{pl}] \frac{dT}{ds} \\ &\quad - [x C_{pg} \eta_{JT,g} + (1-x) C_{pl} \eta_{JT,l}] \frac{dp}{ds}. \end{aligned} \quad (2.74)$$

where x is the gas mass fraction (known also as the quality of the gas-liquid mixture),

$$x = \frac{\dot{m}_g}{\dot{m}_g + \dot{m}_l} = \frac{q_g \rho_g}{q_g \rho_g + q_l \rho_l} = \frac{q_g \rho_g}{q_g \rho_g + q_o \rho_o + q_w \rho_w}, \quad (2.75)$$

and \dot{m}_g, \dot{m}_l are the gas and liquid mass flow rates. Rearranging Eq. (2.73) and combining it with the energy-balance equation, Eq. (2.50), the fluid temperature gradient can be written as

$$\frac{dT}{ds} = \eta_{JT} \frac{dp}{ds} + \frac{1}{C_p} \left(-\frac{U\pi d (T_f - T_e)}{w} + g \cos \alpha - v \frac{dv}{ds} \right). \quad (2.76)$$

2.3.6 Joule-Thomson effect

The temperature change resulting from expansion is referred to as a *Joule-Thomson effect*. Thermodynamically, the Joule–Thomson coefficient (η_{JT}) is defined as the isenthalpic change in temperature in a fluid caused by pressure changes,

$$\eta_{JT} = \left(\frac{\partial T}{\partial p} \right)_h. \quad (2.77)$$

During a throttling ($h = \text{constant}$) process:

- If $\eta_{JT} > 0$ temperature decreases: Joule-Thomson cooling effect
- If $\eta_{JT} = 0$ temperature is constant

- If $\eta_{JT} < 0$ temperature increases, Joule-Thomson heating effect

The wellbore fluid can be a single-phase gas, a single-phase liquid, or a multiphase mixture of gas and liquid. In all cases, the general expression for the Joule-Thomson coefficient can be written as

$$\eta_{JT} = -\frac{1}{C_p} \left[V - T \left(\frac{dV}{dT} \right)_p \right]. \quad (2.78)$$

C_p values used for single gas, liquid, and multiphase are explained more in Appendix D.

2.3.6.1 Joule-Thomson Coefficient for Liquids

By definition, fluid thermal expansion coefficient, β , is given by

$$\begin{aligned} \beta &= \frac{1}{V} \left(\frac{\partial V}{\partial T} \right)_p \\ &= \frac{-1}{\rho_L} \left(\frac{\partial \rho_L}{\partial T} \right)_p, \end{aligned} \quad (2.79)$$

where V is liquid specific volume, $\text{m}^3 \text{kg}^{-1}$.

$$\eta_{JT} = \frac{1}{C_p} \left[T \left(\frac{dV}{dT} \right)_p - V \right] = \frac{V}{C_p} [T\beta - 1] = -\frac{1}{\rho_L C_p} \left[\frac{T}{\rho_L} \left(\frac{d\rho_L}{dT} \right)_p + 1 \right]. \quad (2.80)$$

Therefore, estimating the Joule-Thomson coefficient for liquids requires calculating the liquid density at two temperatures at constant pressure.

2.3.6.2 Joule-Thomson Coefficient for a Real Gas

Using the real-gas law:

$$V = \frac{RTZ}{Mp}, \quad (2.81)$$

where

V is gas specific density, $\text{m}^3 \text{kg}^{-1}$

R is the universal gas constant, $8.314 \text{ J mol}^{-1} \text{K}^{-1}$

T is absolute temperature, K

Z is the compression factor, -

M is real gas mixture molar mass, kg mol^{-1} .

From Eq. (2.81), it can be seen that

$$\begin{aligned} \left(\frac{dV}{dT} \right)_p &= \frac{R}{Mp} \left(\frac{d(TZ)}{dT} \right)_p = \frac{R}{Mp} \left(Z + T \left(\frac{dZ}{dT} \right)_p \right) = \frac{RTZ}{Mp} \left(\frac{1}{T} + \frac{1}{Z} \left(\frac{dZ}{dT} \right)_p \right) \\ &= V \left(\frac{1}{T} + \frac{1}{Z} \left(\frac{dZ}{dT} \right)_p \right). \end{aligned} \quad (2.82)$$

$$\begin{aligned}\eta_{JT} &= \frac{1}{C_p} \left[T \left(\frac{dV}{dT} \right)_p - V \right] = \frac{1}{C_p} \left[T \left[V \left(\frac{1}{T} + \frac{1}{Z} \left(\frac{dZ}{dT} \right)_p \right) \right] - V \right] \\ &= \frac{1}{\rho_g C_p} \left[\frac{T}{Z} \left(\frac{dZ}{dT} \right)_p \right].\end{aligned}\quad (2.83)$$

Therefore, estimating the Joule-Thomson coefficient for real gases requires calculating the gas compressibility factor at two temperatures at constant pressure. Eq. (2.83) can also be written as

$$\eta_{JT} = \frac{RT^2}{MC_p p} \left(\frac{dZ}{dT} \right)_p. \quad (2.84)$$

Eq. (2.84) clearly shows that η_{JT} is a function of pressure and temperature. Depending on the sign of $\left(\frac{dZ}{dT} \right)$, η_{JT} can be positive (gas cools as pressure decreases) or negative (gas warms on expansion). Transition between positive and negative values of η_{JT} happens at the Joule-Thomson inversion temperature, and may occur in the wellbore path, depending on temperature and pressure of the flowing fluid. The inversion temperature of a gas depends on its composition and differs from one gas to another. Gases have two different inversion temperatures (upper inversion temperature, and lower inversion temperature), Figure 2.8 shows the possible sign change of a gas η_{JT} depending on its temperature and pressure.

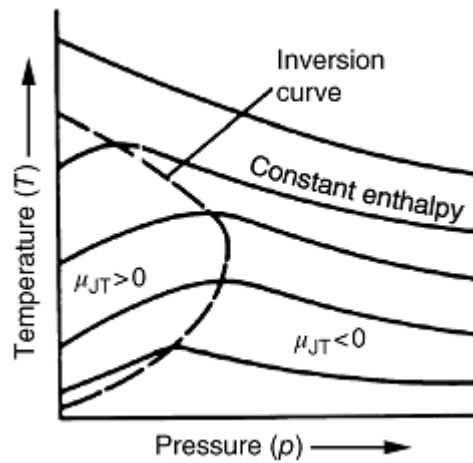


Figure 2-8. Gas Joule-Thomson coefficient sign change vs. temperature and pressure, picture from (Ullmann's Encyclopedia of Industrial Chemistry, 2002).

For more information on the natural gas Joule-Thomson effect, we refer to (Maric, 2005).

2.3.6.3 Joule-Thomson Coefficient for Multiphase Flow

In a multiphase system, it is possible to use the empirical correlation presented by (Sagar et al., 1991), or the theoretical approach developed by (Alves et al., 1992) to estimate the Joule-Thomson coefficient. Alves's equation can be expressed in terms of gas and liquid holdups (instead of gas mass fraction) as follow (Pourafshary et al, 2008)

$$\eta_{JT} = - \frac{1}{\rho_m C_p} \left[H_g \left(- \frac{T}{Z} \left(\frac{dZ}{dT} \right)_p \right) + H_l \left(\frac{T}{\rho_L} \left(\frac{d\rho_L}{dT} \right)_p + 1 \right) \right], \quad (2.85)$$

where

ρ_m is the mixture density, kg m^{-3}

H_g is gas hold-up, -

H_l is liquid hold-up, -.

The average specific heat capacity also can be calculated for multiphase-flow using gas and liquid holdups (Pourafshary et al, 2008):

$$C_p = C_{pg} H_g \frac{\rho_g}{\rho_m} + C_{pl} H_l \frac{\rho_l}{\rho_m}, \quad (2.86)$$

where subscripts g , l , and m refer to gas, liquid, and mixture properties.

2.4 Assumptions Summary

Some of the main assumptions used in this work are as follow:

- The section area of pipeline (A) is constant.
- The well is vertical or deviated with a fixed inclination.
- Fluid flow in the tubing is ID , vertical, and steady with constant mass flow rate.
- The formation is homogenous and isotropic with constant thermal conductivity.
- The fluid temperature is the same as the formation temperature on the wellbore surface.
- Radial heat flow between the wellbore and the formation is steady-state.
- In the surrounding earth, the initial geothermal gradient is a known function of depth.
- The vertical heat conduction in the formation can be ignored compared with the horizontal heat flow.
- The fluid flow process is assumed to be isenthalpic; $dh = 0$
- To determine fluid thermodynamic properties such as Joule-Thomson coefficient and specific heat capacity, an analytical approximation proposed by (Alves et al., 1992) is used.
- Tubing insulation is absent.
- Due to the small value of the tubing diameter, the fluid temperature is equal to the temperature at the inner side of the tubing. Thus: $T_f = T_{ti}$.
- Both the tubing and casing are made of metals like steel with high conductivities.
- The heat radiation term in the annulus is negligible.
- The flow process is steady-state (pressure change with time is zero).
- The temperature of fluid at the pipe intake is equal to the environmental temperature at the pipe intake.

3 ANALYSIS AND INTERPRETATION

3.1 Solution Procedure

MATLAB m-file `example_traverse_thermal.m`, solves the temperature and pressure gradients simultaneously to compute pressure, temperature, and phase fraction. Different boundary conditions can be considered to solve these equations, for example:

1. Constant and known flow rates and densities at the surface (q_{sc} , ρ_{sc}).
2. Constant bottom-hole pressure p_{wf} .
3. Constant bottom-hole temperature T_{wf} .

The wellbore is divided into segments and continuity, momentum balance equation, and energy balance equation are solved in each segment according to the following procedure:

For each depth interval (from s_{in} to s_{out}), the function `pipe_thermal.m` computes the pressure p_{out} and temperature T_{out} at along-hole distance s_{out} , for a given pressure p_{in} and temperature T_{in} at along-hole distance s_{in} , using numerical integration with the aid of the standard MATLAB function `ode45`. The distance s is measured from the separator towards the reservoir. The function `pipe_thermal.m` can be used for single-phase oil flow, single-phase gas flow, and multi-phase gas-oil-water flow analysis:

3.1.1 Single-phase Oil Flow (`oil_dpTds.m`)

After making sure that the input pressure (p_{in}) is above the atmospheric pressure, the bubble point pressure will be calculated using *Standing* or *Glaser* oil correlations (the inputs to these correlations are: GOR, $\rho_{g,sc}$, $\rho_{o,sc}$, T_{in}). Then, using the same correlations, local (in-situ) rates and density values at each T_{in} and p_{in} are calculated. Other fluid properties such as viscosity, Joule-Thomson coefficient, Reynold's number, and friction factor are also calculated at each T and p . If $C_{p,o}$ is known it is given as an input to the program (under `mixture_heat_propts.m`), and changes of $C_{p,o}$ versus temperature are neglected. Otherwise $C_{p,o}$ can be computed at each T and p using (Gambill, 1957); see Appendix D. The formation temperature T_e for each depth is calculated knowing the earth geothermal gradient.

```
s_tot = max(s_in,s_out); % total along-hole well depth, m

% Compute external (formation) temperature:
if s_in < s_out % top to bottom
    T_e = T_e_in + g_G * s * cos(alpha);
else % bottom to top
    T_e = T_e_in - g_G * (s_tot - s) * cos(alpha);
end
```

Total pressure gradient (`dpds_tot`) is calculated using Eq. (2.13). Then temperature losses due to pressure drop, gravity, and acceleration are computed based on Eq. (2.76). The heat loss

to the surroundings needs to be calculated using an iterative process that was explained in the ‘Overall Heat Transfer Coefficient’ section. The output of the `oil_dpTds.m` function consists of total and individual pressure and heat gradient terms:

```
dpTds =[dpds_tot;dpds_grav;dpds_fric;dpds_acc;dTds_tot;
        dTds_pres;dTds_grav;dTds_acc;dTds_loss];
```

The same procedure can be followed to compute and plot a traverse bottom-up (when wellhead pressure (p_{tf}) and temperature (T_{tf}) are known).

3.1.2 Single-phase Gas Flow (gas_dpTds.m)

The procedure is similar to single-phase oil flow, except that in single-phase gas, the fluid properties (Z_{factor} , dZ/dT and dZ/dp etc.) will be estimated using pseudo-critical pressure (p_{pr}) and pseudo-critical temperature (T_{pr}) of the gas mixture, with the aid of the *Sutton* (1985) correlation. In case of no available data for gas specific heat capacity, $C_{p,g}$, an estimation introduced by (Kareem Lateef and Omeke, 2011) can be used; see Appendix D.

3.1.3 Multi-phase Gas-Oil-Water (Muk_Brill_dpTds)

Local gas and liquid properties (flowrates, densities, viscosities, gas-liquid interfacial tension, and superficial velocities) at T_{in} and p_{in} will be first calculated. Afterwards, Duns and Ros dimensionless numbers (pipe diameter number, gas velocity number, liquid velocity number, and liquid viscosity number) are also calculated; see Appendix A. Using the Mukherjee and Brill correlation, the flow regime is detected; based on the flow regimes, flow direction, and dimensionless numbers, the hold ups (slip) and in-situ volume fractions (no-slip) can be determined. For each flow regime, Eq. (2.13) and Eq. (2.76) will be solved simultaneously to give T_{out} and p_{out} .

More details on the Mukherjee and Brill correlation are given in Appendix A.

3.2 Well Applications

In this section, examples to illustrate the application of the model in three-phase gas/oil/water, two-phase gas/oil-, and single-phase oil-flow situations are presented.

3.2.1 Case Study 1: Oil/Gas/Water Producer, Vertical Well

The first case study is based on the data reported by (Sagar et al., 1991) for a vertical flowing well that produced oil, water and gas. The well had been producing for 158 hours at 59 STB/D of 34 °API oil with 542 STB/D of water and 41 Mscf/D of gas through a 2.875-in ID tubing. Other well parameters are given in more detail in Appendix B. In this case, field data are only available for the temperature distribution in the wellbore. (Hassan and Kabir, 2002) also presented results for this data set. It can be seen that our model shows a good agreement with the field data. The Sagar et al. model differs from the actual data mainly because it ignores the natural convection heat mechanism in the annulus. One reason for neglecting convection in an annular fluid by many authors is probably the lack of any well-known correlation for

convective heat transfer in an annular geometry. The correlation used in this work, developed by (Dropkin and Somerscales, 1965) for a vertical space between parallel plates, appears quite reasonable and was recommended by (Willhite, 1967). In the program it is assumed that the annulus is filled with liquid (brine 20% NaCl) up to the wellhead (so that the natural convection factor is constant). The annulus fluid input data can be modified in the `Overall_heat_transfer_coeff.m` function file. Figures 3.1 through 3.6 show temperature profile, overall heat transfer coefficient, heat loss rate, pressure profile, and temperature gradient components versus along-hole depth.

In this case study, the flow regime changes from single-phase liquid to bubble flow around a depth of 4700 ft and from bubble flow to slug flow at around a depth of 107 ft. The change in the flow regime (from bubble to slug flow) at depth 107 ft, has a noticeable effect on the amount of heat loss to the formation per unit length of the well that can be seen in Figure 3.4; close to the surface (around a depth of 107 ft), the slope of the graph changes, resulting in a slightly higher heat loss per unit length of the well. This higher heat loss rate is a result of higher gas content in the wellbore, close to the surface. More investigation on the effect of gas bubbles in the wellbore is explained under “*Sensitivity Analysis*” section.

While Figure 3.1 shows good agreement between the field data and model computation, the data point nearest to the surface (at 0 ft) shows a lower fluid temperature than predicted. (Hasan & Kabir, 1994) suggested that the model can accurately predict this data point if a higher conductivity (68% higher) is used for the formation near the surface (k_e). This shows the utility of good temperature logs in estimating formation property values.

Some simulators assume a constant or a linear distribution in the wellbore or formation temperature. These assumptions cause the pressure, velocity or phase fraction profiles to be different from the profiles computed with simulated temperature. In order to compare these profiles, `example_traverse.m` file has been used. Unlike `example_traverse_thermal.m`, which accounts for temperature distribution calculations by solving the energy balance equation, `example_traverse.m` uses a linear interpolation based on a known T_{wf} and T_{tf} as follows:

$$T = T_{wf} + (T_{tf} - T_{wf}) * (s - s_{tot}) / (0 - s_{tot}); \quad \% \text{ temperature, } ^\circ\text{C}$$

Figure 3.2 shows the temperature profile obtained using `example_traverse.m`, ($T_{wf} = 108$ °F and $T_{tf} = 88$ °F), as well as measured field data versus along-hole depth. Although the resulting temperature profile is different between `example_traverse_thermal.m` and `example_traverse.m`, the pressure profiles hardly show any differences (the maximum difference is 0.22% and occurs at the well head, where $p = p_{tf}$). One reason for this is the use of known values for T_{tf} and T_{wf} in `example_traverse.m`. However, one should keep in mind that the bottom-hole temperature (T_{wf}) is not usually known. Thus, in case of inaccurate

input data of T_{wf} , the pressure profile will show a greater difference between the situation where the temperature profile is linear and when it is calculated using the energy balance.

Figure 3.5 shows that, in this case study, heat loss to the formation is the main factor in the fluid temperature decrease in the wellbore. This heat loss is not linear, because at the bottom of the well the fluid temperature (T_f) is closer to the formation temperature (T_e). However, as the fluid goes up along the well, the temperature difference ($T_f - T_e$) and hence the heat loss between the formation and the wellbore fluid increases. Furthermore, in this case, due to negative values of the mixture's Joule-Thomson coefficient, the pressure decrease along the wellbore results in an increase in the producing fluid temperature, thus a positive slope is obtained in Figure 3.5 for T_{pres} . The gravity component of the temperature loss is due to the change in density of the fluid, and contributes to a temperature decrease.

The measured field data, and the calculated data using `example_traverse_thermal.m` are given in Appendix B under *Case Study 1*.

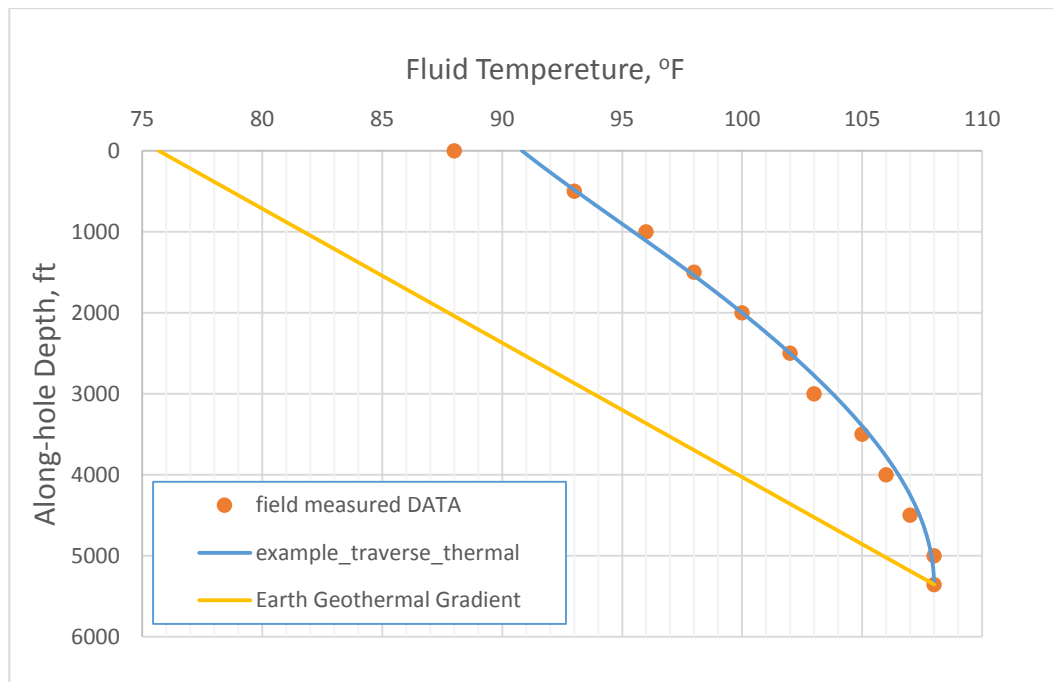


Figure 3-1. Comparison between computed fluid temperatures via `example_traverse_thermal.m` vs. along-hole depth, earth geothermal gradient, and field data. (Case study 1: A 5355 ft vertical well produces 59 STB/D oil, 41 Mscf/D gas and 542 STB/D water. Fluid enters the wellbore at 108 °F. The oil gravity is 34.3 °API, the gas gravity is 0.95)

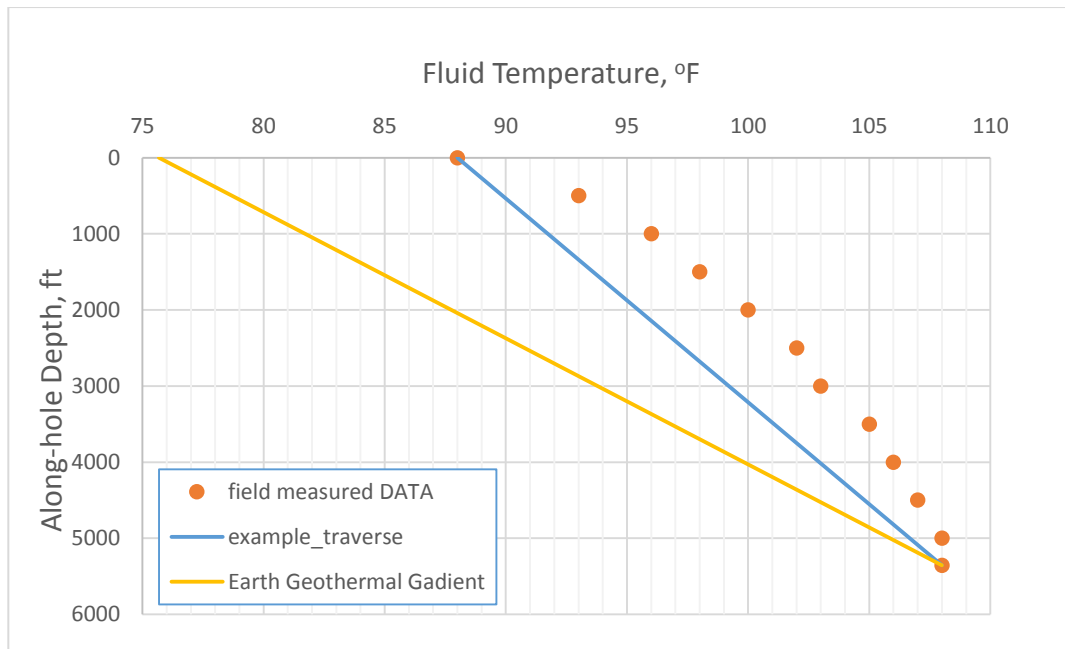


Figure 3-2. Temperature distribution prediction using linear interpolation (example_traverse.m), earth geothermal gradient, and field data (Case study 1: A 5355 ft vertical well produces 59 STB/D oil, 41 Mscf/D gas and 542 STB/D water. Fluid enters the wellbore at 108 °F. The oil gravity is 34.3 °API, the gas gravity is 0.95).

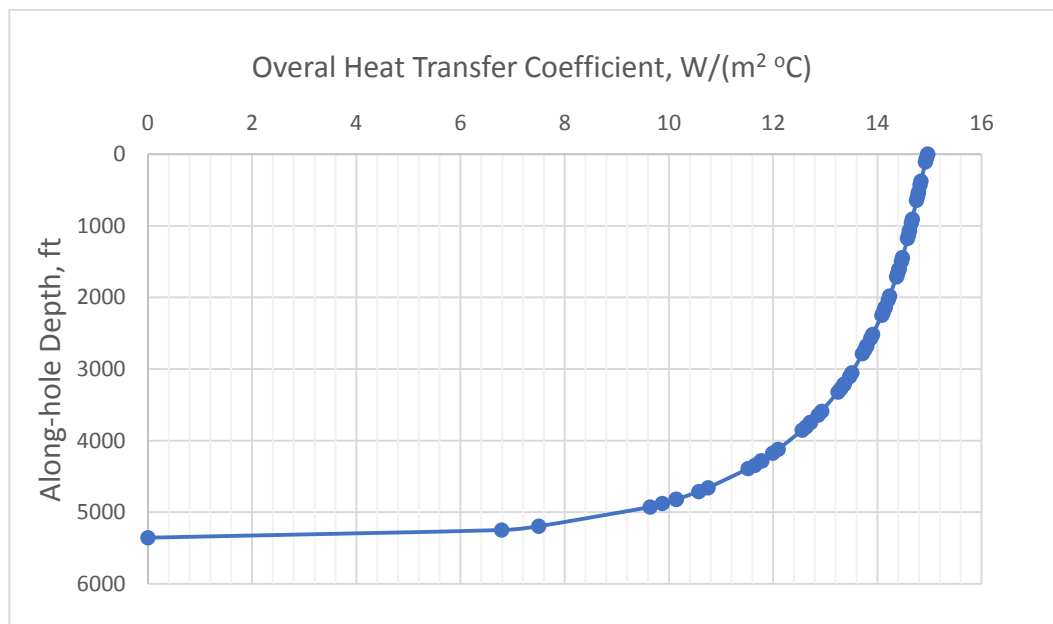


Figure 3-3. Overall heat transfer coefficient (U_{10}) as a function of depth. (Case study 1).

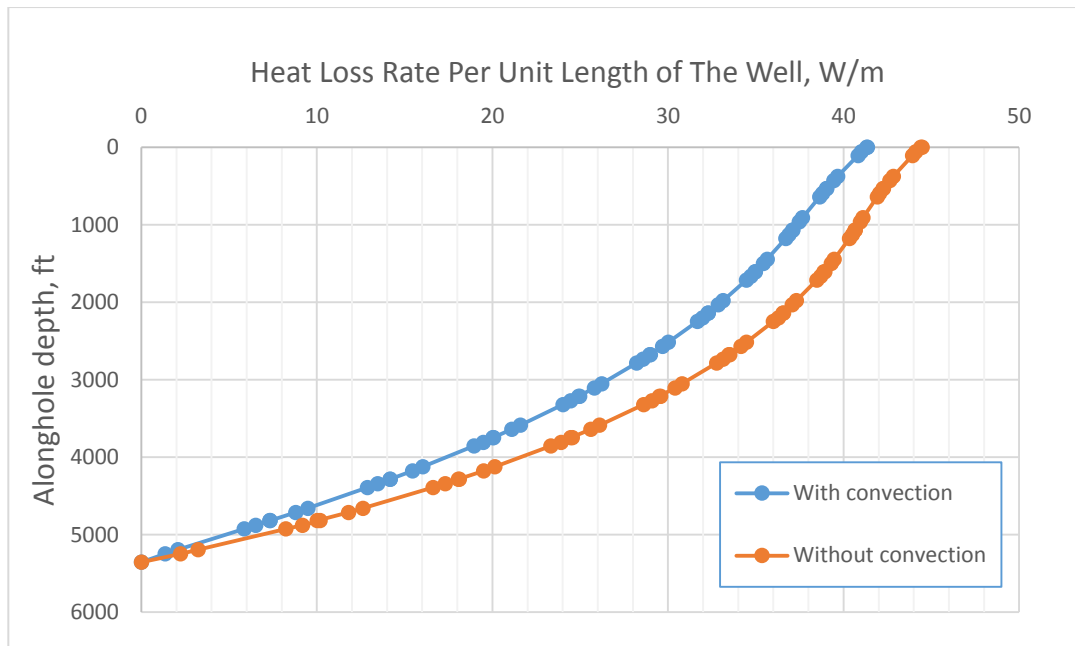


Figure 3-4. Radial heat loss rate per unit length of the well vs. along-hole depth with and without considering convective heat transfer in the annulus. (Case study 1: A 5355 ft vertical well produces 59 STB/D oil, 41 Mscf/D gas and 542 STB/D water. Fluid enters the wellbore at 108 °F. The oil gravity is 34.3 °API, the gas gravity is 0.95).

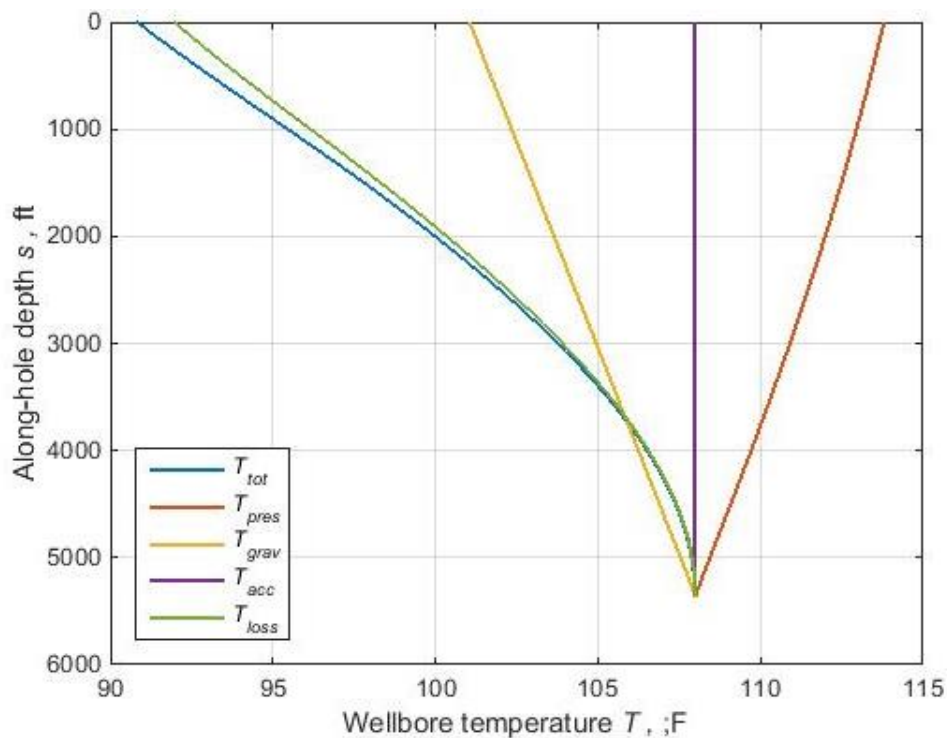


Figure 3-5. Temperature gradient different components; heat loss to formation, acceleration, gravity, Joule-Thomson effect (pressure effect), and total temperature gradient. (Case study 1: A 5355 ft vertical well produces 59 STB/D oil, 41 Mscf/D gas and 542 STB/D water. Fluid enters the wellbore at 108 °F. The oil gravity is 34.3 °API, the gas gravity is 0.95).

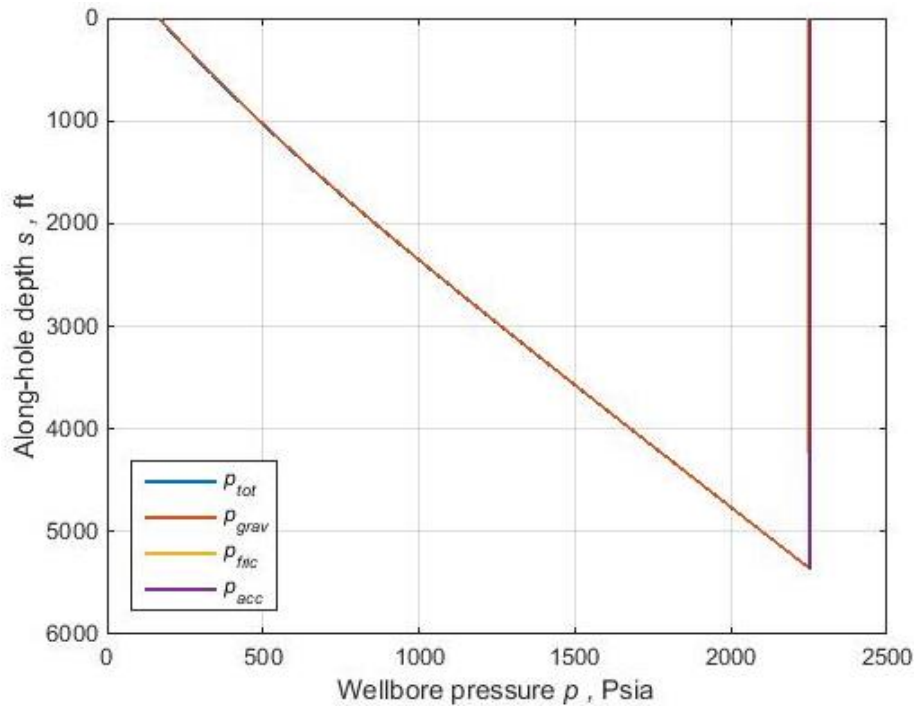


Figure 3-6. Pressure gradient different components; pressure loss due to gravity, friction, and acceleration forces. (Case study 1)

3.2.2 Case Study 2: Oil/Gas/Water Producer, Deviated Well

The second case study concerns a 4-in. ID tubing well that produces at 2,137 STB/D of oil with 49% water cut and a GOR of 1,100 scf/STB from 14,600-ft MD. The well is vertical down to a depth of 4,250 ft, after which the deviation quickly changes to approximately 39 degree from vertical, giving the well a true vertical depth (TVD) of approximately 13,000 ft. The well intercepts water at a depth of 2,800 ft (Hasan, Kabir, and Wang, 2009). More details are provided in Appendix B, under *Case Study 2*.

Figure 3.7 shows a schematic of the well configuration.

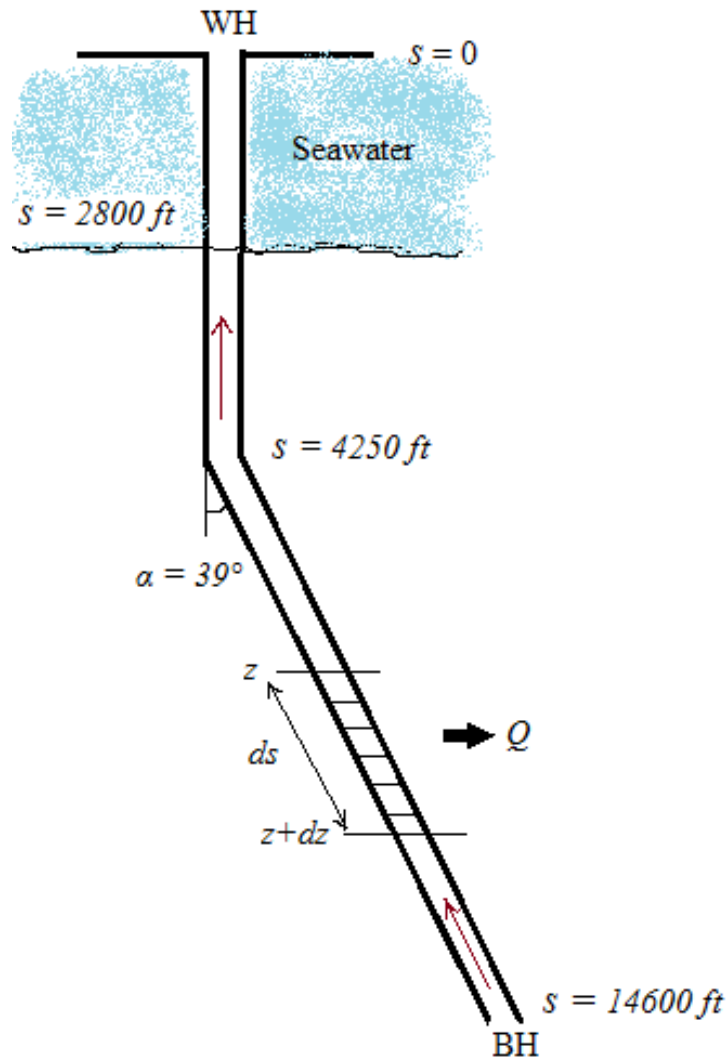


Figure 3-7. Well schematic for Case study 2: A 14600 ft (MD), partially deviated well, surrounded by sea water to depth 2800 ft, produces 2137 STB/D oil, 2.3507 MMscf/D gas and % 49 water-cut. The surface temperature of the water is 54°F, the temperature at the seabed is assumed to be 30°F. Formation BHT is 164°F. Picture after (Hasan, Kabir, and Wang, 2009).

A table of temperature data is not available, but the temperature profile is shown in Figure 3.8 together with the bottom-up computation as performed by (Hasan, Kabir, and Wang, 2009).

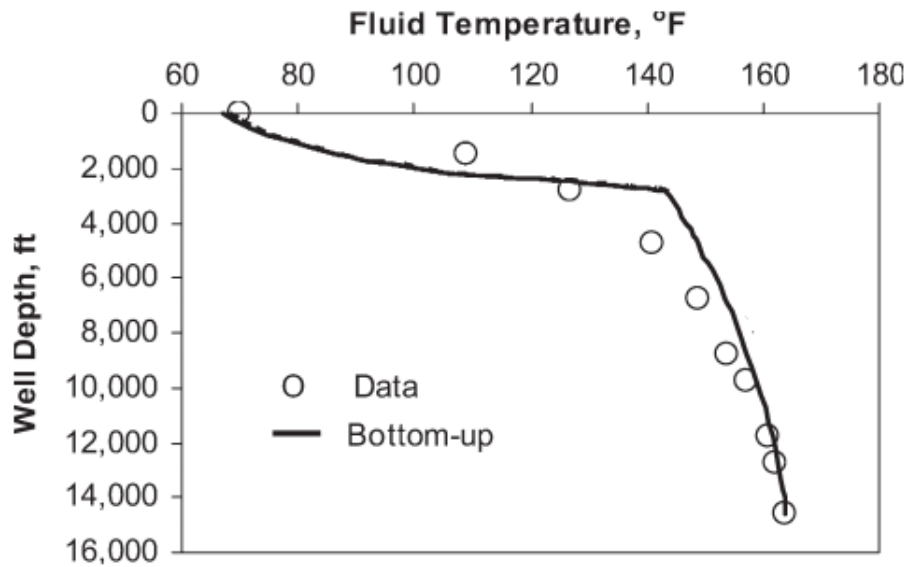


Figure 3-8. Temperature-traverse computation with bottom-up approach done by original writers, together with real field data, (Case study 2: A 14600 ft (MD), partially deviated well, surrounded by sea water to depth 2800 ft, produces 2137 STB/D oil, 2.3507 MMscf/D gas and % 49 water-cut. The surface temperature of the water is 54°F, the temperature at the seabed is assumed to be 30°F. Formation BHT is 164°F.), picture from (Hasan,Kabir, and Wang, 2009).

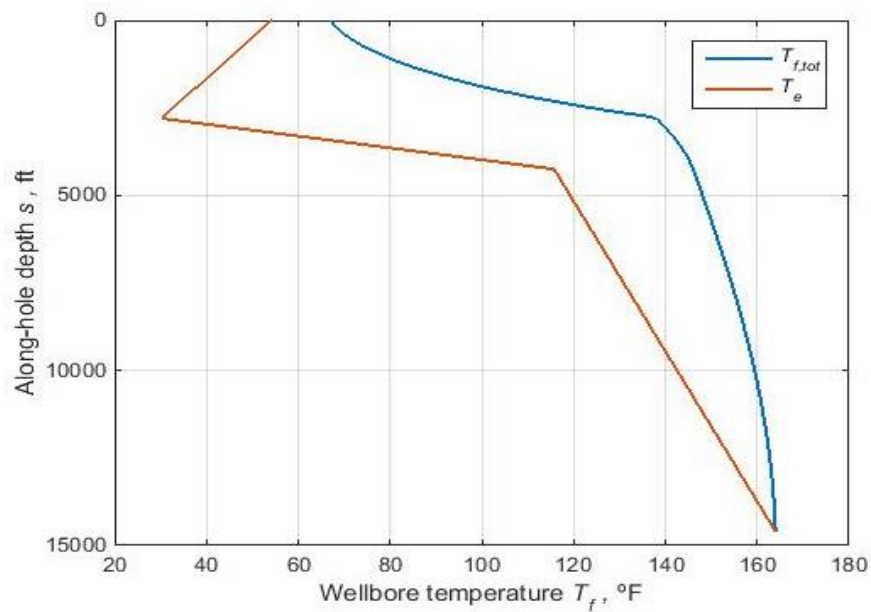


Figure 3-9. Computed fluid temperature vs. along-hole depth, and earth geothermal gradient using bottom-up integration, using example_traverse_thermal.m (Case study 2). There are three different segments for the geothermal gradient (shown by the red line).

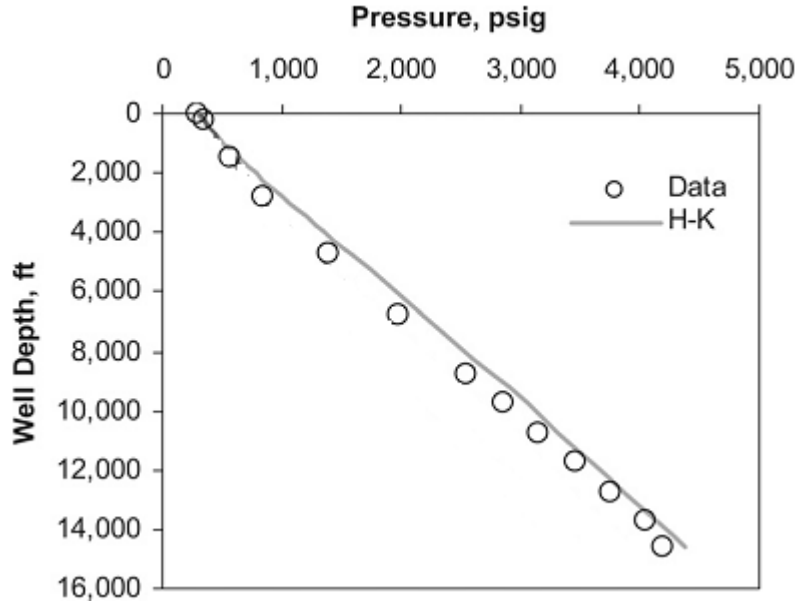


Figure 3-10. Comparison of pressure-traverse calculations between Hassan_kabir method, and the real field data.(Case study 2: A 14600 ft (MD), partially deviated well, surrounded by sea water to depth 2800 ft, produces 2137 STB/D oil, 2.3507 MMscf/D gas and % 49 water-cut. The surface temperature of the water is 54°F, the temperature at the seabed is assumed to be 30°F. Formation BHT is 164°F.), picture from (Hasan,Kabir, and Wang, 2009).

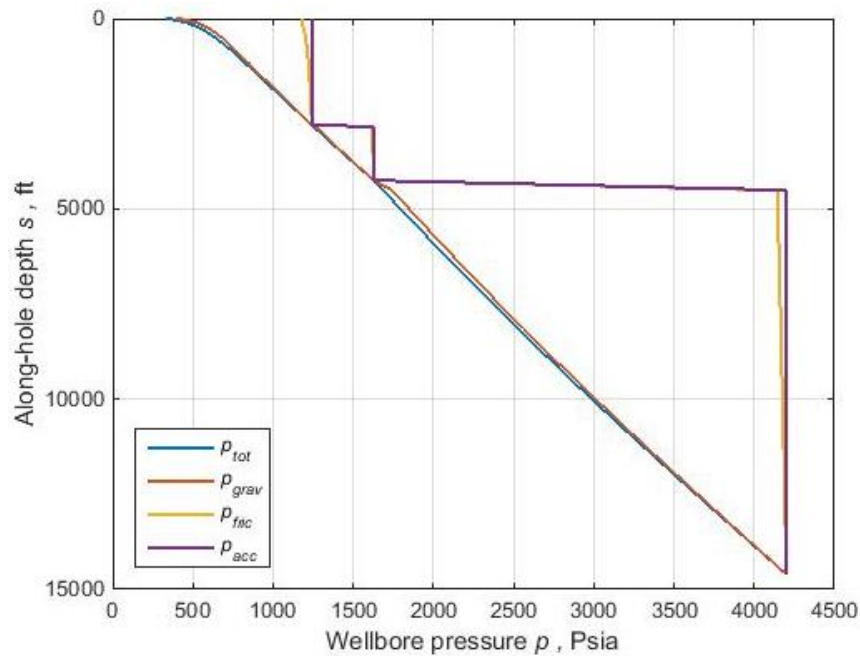


Figure 3-11. Pressure gradient equation components. (Case study 2: A 14600 ft (MD), partially deviated well, surrounded by sea water to depth 2800 ft, produces 2137 STB/D oil, 2.3507 MMscf/D gas and % 49 water-cut.)

Figure 3.11 shows the three different segments of the well (i.e. with different geothermal gradients and heat properties). This is the reason why the graph doesn't look continuous. The calculated wellhead pressure and fluid temperature are 328.3 psia and 67.3 °F, respectively. Despite the earth geothermal gradient, water thermal gradient is negative, because the surface water temperature is 54 °F, while the seabed temperature is 30 °F. This can be seen in figure, where T_e changes slope at a depth of 2800 ft.

3.2.3 Case Study 3: Oil Producer, Vertical Well

A vertical well producing single-phase oil at 5,866 STB/D from a 14,000-ft vertical well through a 4-in.-ID. The measured oil temperature at the wellhead is 200°F. More detail (including input and output data) is provided in Appendix B, under *Case Study 3*. Estimated pressure and temperature values along the wellbore are provided in Table B1. In Figure 3.12, a slight change in the slope of the fluid temperature gradient can be seen (around depth 2800 ft). This is due to using two different values for total heat transfer coefficient (U_{to}) along the wellbore (higher value is used closer to the surface). These values have been suggested and used by (Hasan,Kabir, and Wang, 2009). In their work, they have suggested using a *relaxation parameter*, L_R , of $L_R = 3.27 \times 10^{-5}$ (ft⁻¹) for depth lower than 2800 ft, and $L_R = 1.45 \times 10^{-5}$ (ft⁻¹) for higher depths. For more explanation and insights on relaxation parameter, L_R , see Appendix B.

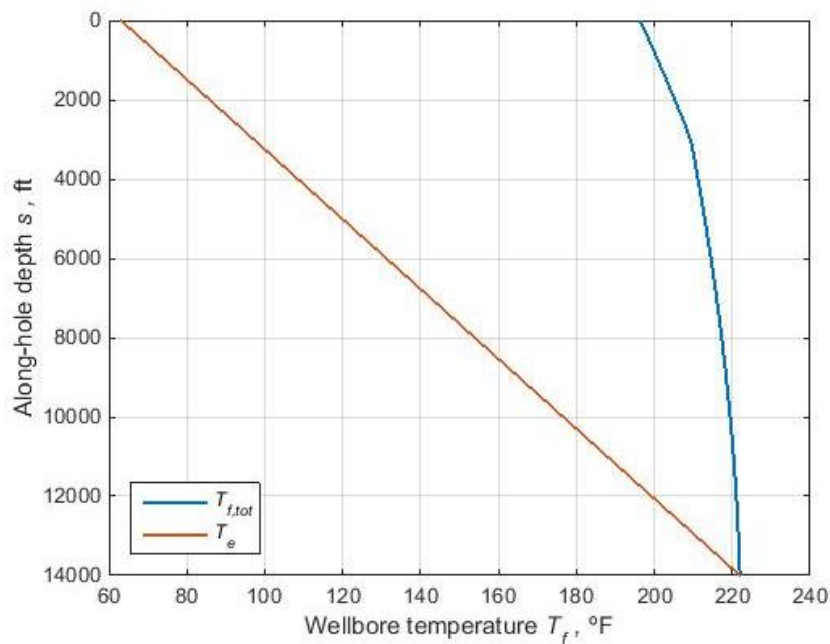


Figure 3-12. Computed fluid temperatures vs. along-hole depth, and earth geothermal gradient , calculations done Bottom-up (Case study 3: A 14000 ft vertical well, produces 5866 STB/D oil, with surface fluid temperature of 200 °F, and the surrounding earth temperature of 60 °F. Formation BHT is 222 °F, and at wellhead condition: $\rho_o = 40.209$ lbm ft⁻³).

Calculations for this case study has been done using `example_traverse_thermal.m` MATLAB file, with both Bottom-up and Top-down integrations. Bottom-up calculation seems to give a better match with available field data. (Hasan,Kabir, and Wang, 2009) came to a

similar conclusion as well. Comparison graph between the Bottom-up and Top-down calculations can be found in Appendix B, under Case Study 3.

The Joule-Thomson coefficient of the oil is calculated using Eq. (2.80). In this case values for η_{JT} are negative. Thus, as oil flows upward in the wellbore, the oil temperature increases (due to the decrease in the pressure). The red line in Figure 3.13 shows Joule-Thomson heating effect. Oil density does not vary significantly with depth, so the temperature decrease due to the gravitational force is linear. Also, pressure profile is linear because of the same reason. Pressure components profiles for this case study are displayed in Appendix B. In general, temperature decline along the wellbore in case of a single-phase oil flow is way less than the temperature decline in case of a single-phase gas flow. This is mainly due to the lower specific heat capacity and density of the gas.

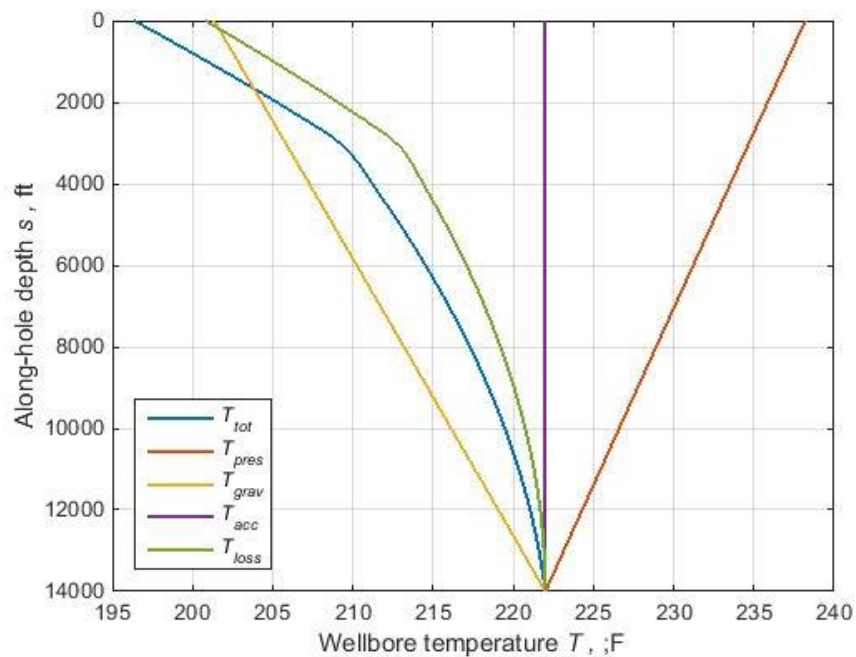


Figure 3-13. Temperature gradient equation components, calculations done Bottom-up (Case study 3: A 14000 ft vertical well, produces 5866 STB/D oil, with surface fluid temperature of 200 °F, and the surrounding earth temperature of 60 °F. Formation BHT is 222 °F, and at wellhead condition: $\rho_o = 40.209 \text{ lbm ft}^{-3}$).

In case of a single-oil flow, it is sometimes possible that the temperature of the fluid increase as it moves upward from the bottom-hole. This phenomenon can be justified by noting that friction converts pressure energy into heat, causing temperature rise. When frictional heat generation [related to $(dp/dz)_{fric}$] is greater than conductive heat loss to the formation (related to L_R), temperature will actually increase as the fluid moves up the wellbore. Of course, this temperature rise is most likely to occur near the bottom-hole because conductive heat loss to the formation increases as the fluid moves up and experiences greater temperature-difference driving force with the surroundings (Hasan, Kabir, and Wang, 2009).

3.2.4 Case Study 4: Oil/Gas Producer, Vertical Well

Case study 4 is based on the measurements presented by (Hassan and Kabir, 2002). A 5151 ft vertical well produces 23 °API dry oil at a flow rate equal to 1140 STB/D through a 2.99-in ID tubing. GOR is 450 scf/STB, and the gas gravity is 0.80. The simulated results are very close to the measured data. The measured wellhead pressure is 505 psig. In this case, only the pressure data measurements versus depth are available (field temperature data were only available for 2 points; bottom-hole and well-head). Figure 3.14 through Figure 3.18 show the pressure profile, temperature profile, pressure and temperature gradient components, and the Joule-Thomson coefficient versus along-hole depth. Figure 3.14 shows computed fluid pressure using `example_traverse_thermal.m` and the real field data.

More details can be found in Appendix B, under *Case study 4*.

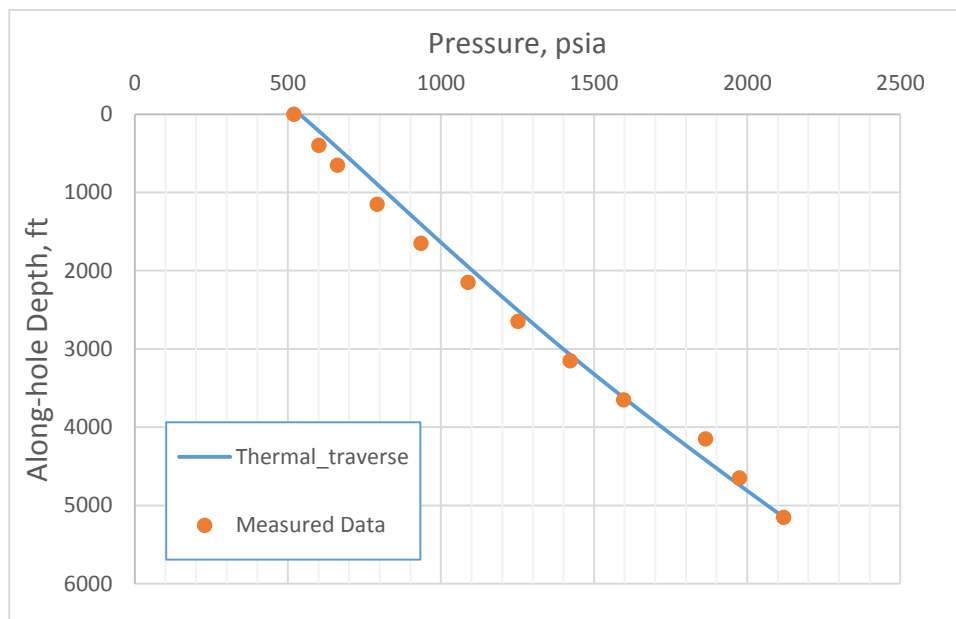


Figure 3-14. Computed pressure profile vs. real field data. (Case study 4: A 5151 ft vertical well produces 23 °API dry oil at flow rate equal to 1140 STB/D through a 2.99-in ID tubing. The gas/oil ratio is 450 scf/STB, and the gas gravity is 0.80)

Figure 3.15 represents the Joule-Thomson coefficient values of the oil/gas mixture versus depth. Here, a negative η_{JT} means that the temperature of the fluids will increase as fluid pressure decreases along the wellbore. From the bottom of the well (depth of 5151 ft) to almost half of the well, the flow is in a bubble flow regime, and around a depth of 2678 ft it changes to a slug flow, meaning that there is more free gas in the upper part of the wellbore (from 0 to 2678 ft). Changing from a bubble flow to a slug flow regime at this depth, results in a change in the slope of η_{JT} vs. depth (η_{JT} values increase again). Consequently, a change in the slope of T_{press} (temperature change due to pressure loss, in other word, Joule-Thomson effect) in Figure 3.17 is seen.

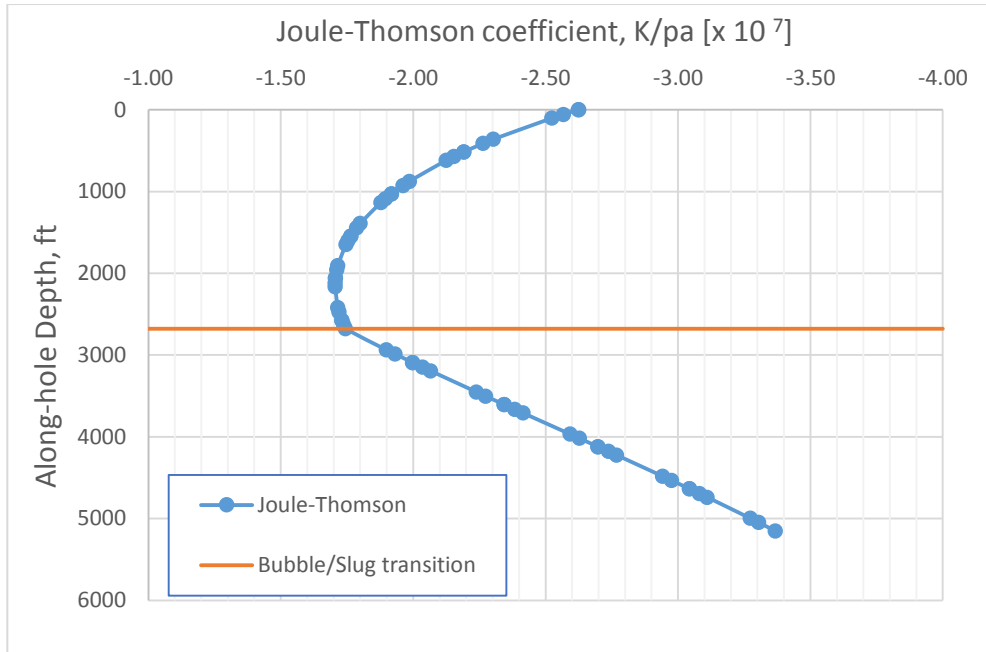


Figure 3-15. Joule-Thomson coefficient vs. depth and flow regime, $\eta_{JT} \in [-1.5E-7 \text{ to } -3.5E-7]$. Around the depth of 2678 ft, flow regime changes from bubble flow to slug flow, resulting in an increase in mixture η_{JT} . (Case study 4: A 5151 ft vertical well produces 23 °API dry oil at flow rate equal to 1140 STB/D through a 2.99-in ID tubing. The gas/oil ratio is 450 scf/STB, and the gas gravity is 0.80)

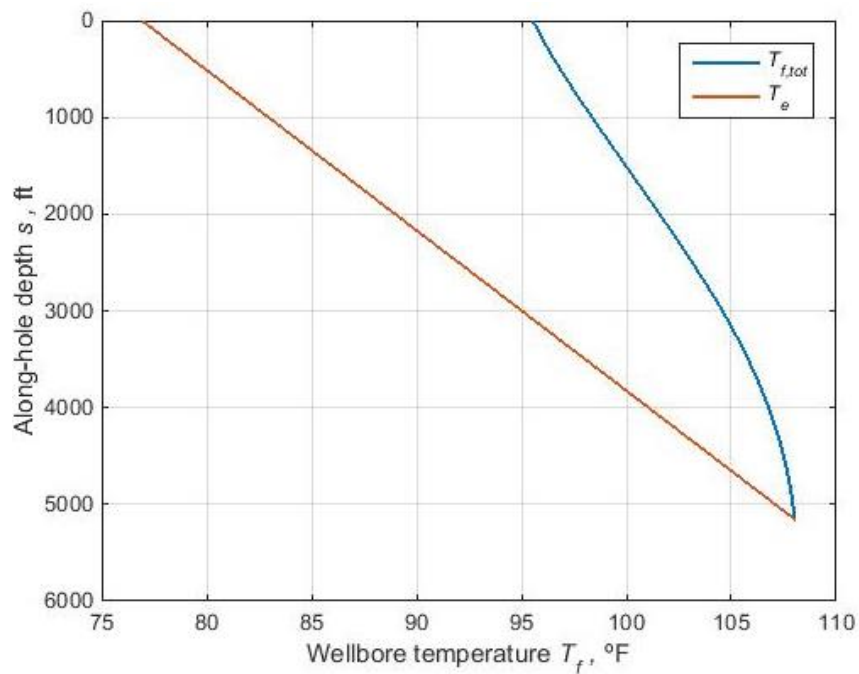


Figure 3-16. Computed temperature profile (Case study 4)

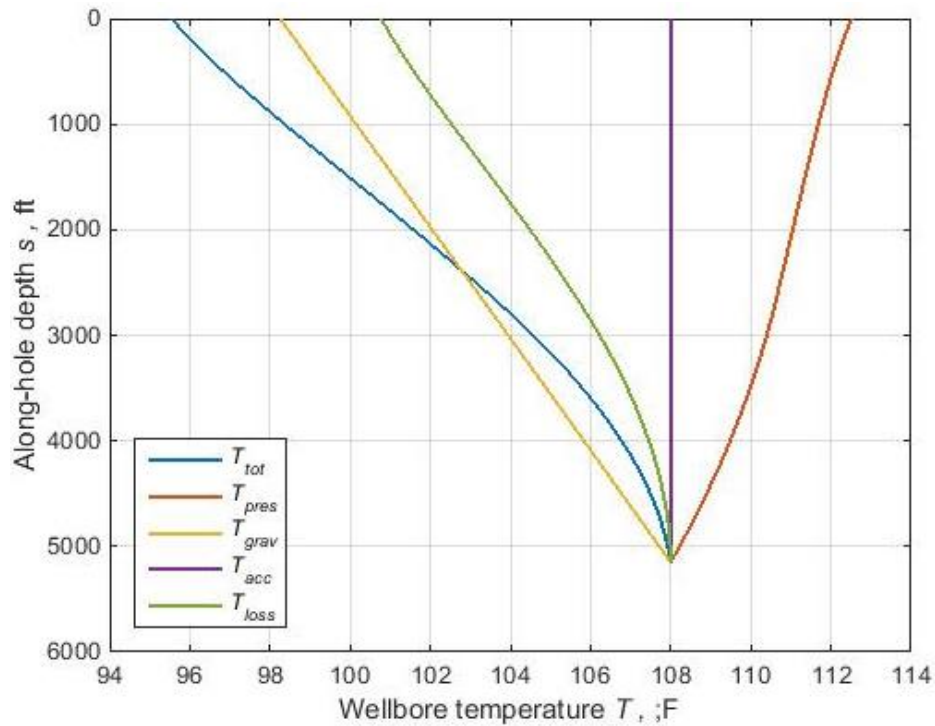


Figure 3-17. Temperature profile components, flow regime changes around 2678 ft and this results in a change in the slope of this graph at that depth (Case study 4: A 5151 ft vertical well produces 23 °API dry oil at flow rate equal to 1140 STB/D through a 2.99-in ID tubing. The gas/oil ratio is 450 scf/STB, and the gas gravity is 0.80)

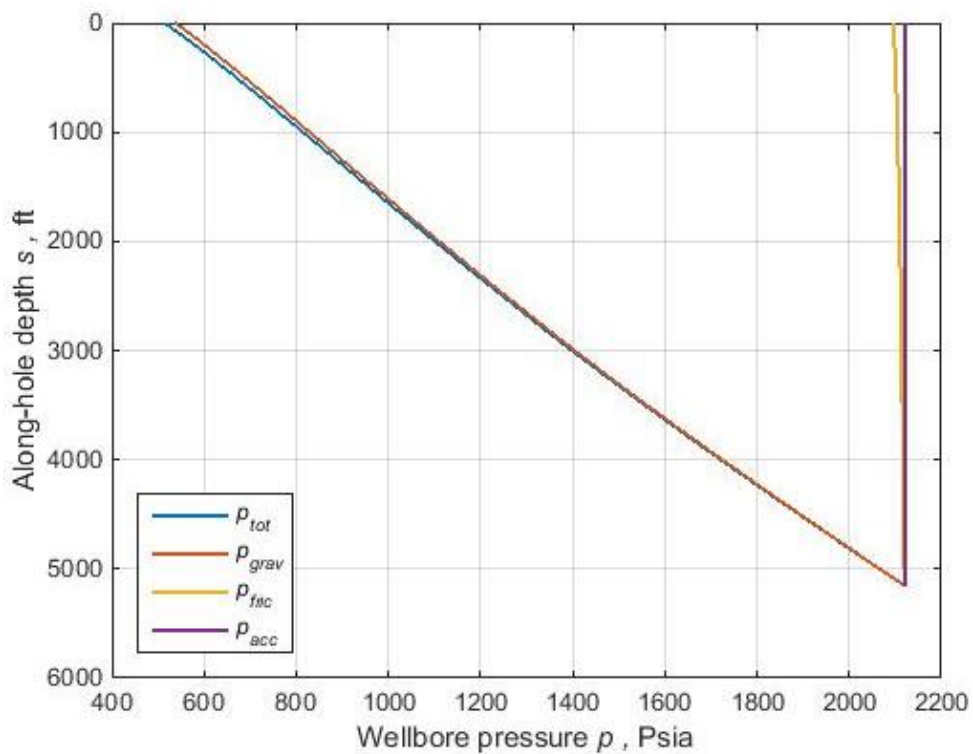


Figure 3-18. Computed pressure profile (Case study 4)

3.3 Sensitivity Analysis

In the following section the sensitivity of the temperature distribution in the wellbore to tubing diameter, GOR, WOR, earth thermal conductivity, and production time is discussed. The sensitivity analysis can be justified with two main formulations; temperature and pressure gradient equations:

$$\frac{dp}{ds} = -\frac{\rho}{2d} f \times v|v| + \rho g \cos \alpha - \rho v \frac{dv}{ds}, \quad (2.11)$$

$$\frac{dT}{ds} = \eta_{JT} \frac{dp}{ds} + \frac{1}{C_p} \left(-\frac{U\pi d (T_f - T_e)}{w} + g \cos \alpha - v \frac{dv}{ds} \right). \quad (2.76)$$

The Base-case uses Case Study1 data (reported in Appendix B).

3.3.1 Effect of Tubing Diameter

In this section, the wellbore geometry is changed by changing the tubing diameter (annulus and casing diameters are kept constant). Figure 3.19 shows the effect of tubing diameter on the temperature distribution. In this case, as the tubing diameter increases, considering constant flow rates, there will be a very small decrease in dp/ds . In the case of a negative Joule-Thomson coefficient, this will lead to an increase in dT/ds . Furthermore, as can be seen in Figure 3-20, the heat loss to the formation, $Q = U\pi d (T_f - T_e)$, increases with increasing tubing diameter. Thus, in total, as the tubing inside diameter increases, the temperature gradient increases too. In other words, for a fixed bottom-hole temperature, a lower wellhead temperature is obtained for a bigger tubing size.

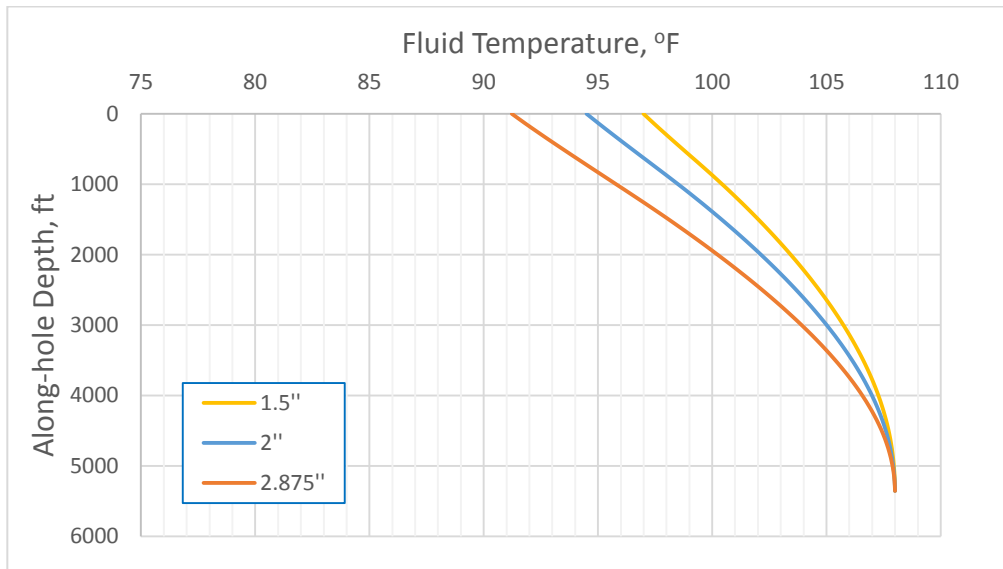


Figure 3-19. Effect of tubing diameter on temperature profile in the wellbore (A 5355 ft vertical well produces 59 STB/D oil, 41 Mscf/D gas and 542 STB/D water; flow rates are kept constant for different tubing diameters)

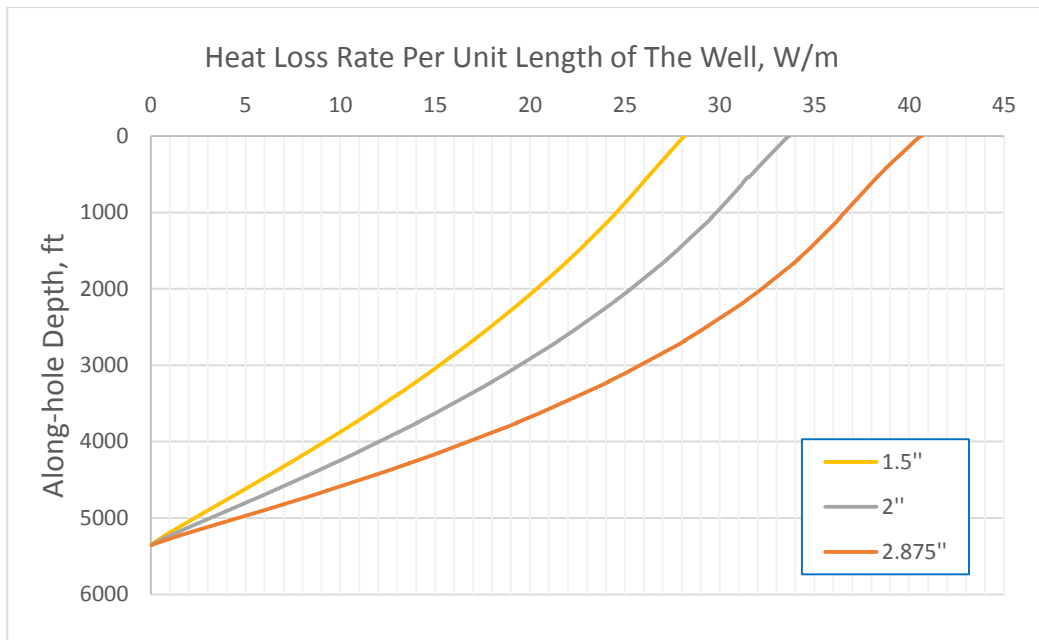


Figure 3-20. Effect of tubing diameter on wellbore heat-loss to the formation (A 5355 ft vertical well produces 59 STB/D oil, 41 Mscf/D gas and 542 STB/D water; flow rates are kept constant for different tubing diameters)

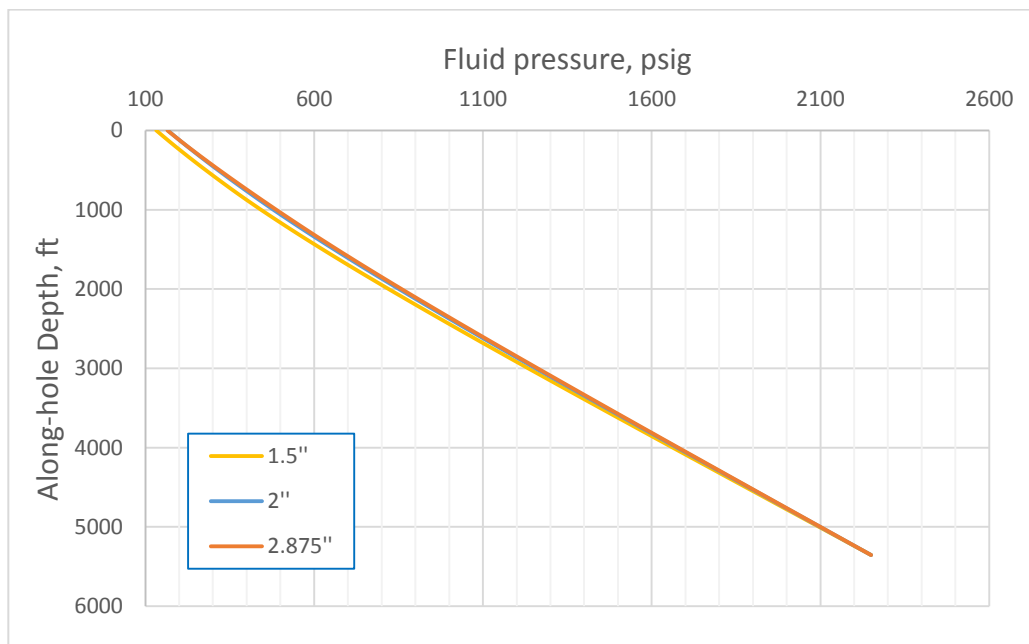


Figure 3-21. Effect of tubing diameter on pressure profile (A 5355 ft vertical well produces 59 STB/D oil, 41 Mscf/D gas and 542 STB/D water; flow rates are kept constant for different tubing diameters)

3.3.2 Effect of Gas-Liquid Ratio

Determining the effect of the gas oil ratio (GOR) on temperature gradient is tricky, because gas properties and flow rate have various (usually opposite) impacts on different temperature loss components. In this section, to investigate the gas effect, four cases have been tested; in the Base-Case, water has been replaced by oil, so in all cases $q_o = 600 \text{ STB/D}$, $q_w = 0$, and GOR values changes as 50, 695, 1000, and 1400 Scf/STB , respectively. With constant oil rate, as GOR increases, the density of the wellbore fluid (ρ_m) decreases. Consequently, the total pressure gradient along the wellbore decreases. This can be seen in Figure 3.22. Note that when variation in two-phase mixture density (ρ_m) along the well is small, the pressure profile is almost linear (as can be seen for the case of $\text{GOR} = 50 \text{ scf/STB}$). A higher GOR will produce a more concave upward curve (due to gas expansion, especially closer to the surface). Plots of pressure profile components for each case can be seen under Appendix C.

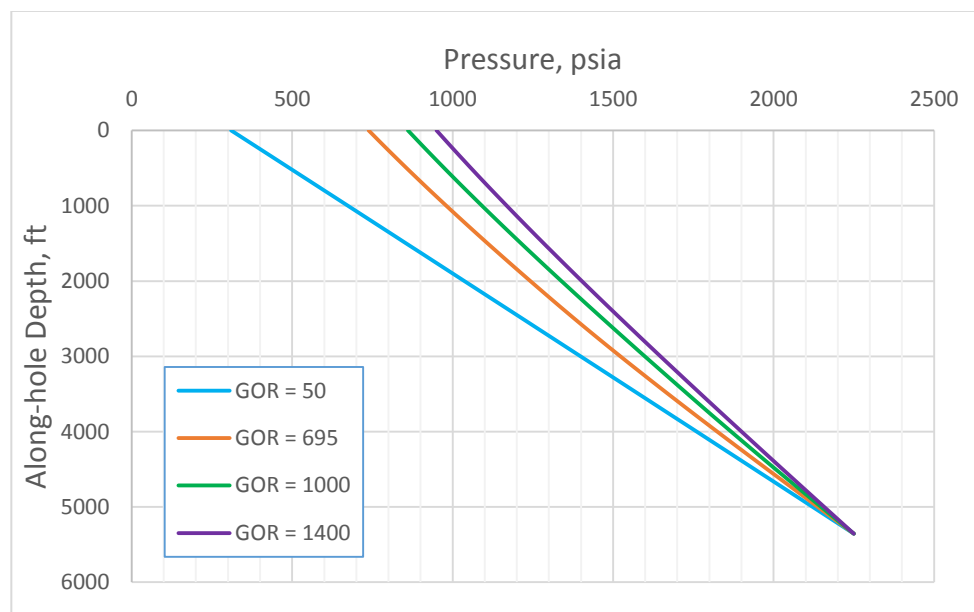


Figure 3-22. Effect of GOR on pressure profile (A 5355 ft vertical well produces 600 STB/D oil, with zero water production), GOR units are in scf/STB.

With a negative Joule-Thomson coefficient, a decrease in pressure gradient results in an increase in temperature gradient. Gas has a lower C_p , in comparison with oil and water. Thus a higher GOR will lead to a lower averaged mixture C_p . A lower C_p and a lower mixture density will result in a higher temperature loss due to heat exchange between the wellbore fluids and surrounding formation. However, an opposite effect takes place at the same time; the temperature loss due to heat exchange decreases with higher GOR as a result of higher flow rate. As these effects nearly cancel each other out, in general, as the GOR increases we will see a very small increase in the temperature gradient. Thus for a fixed T_{wf} , a lower T_{tf} is expected. The effect of GOR on different temperature losses can be seen in Figure 3.23.

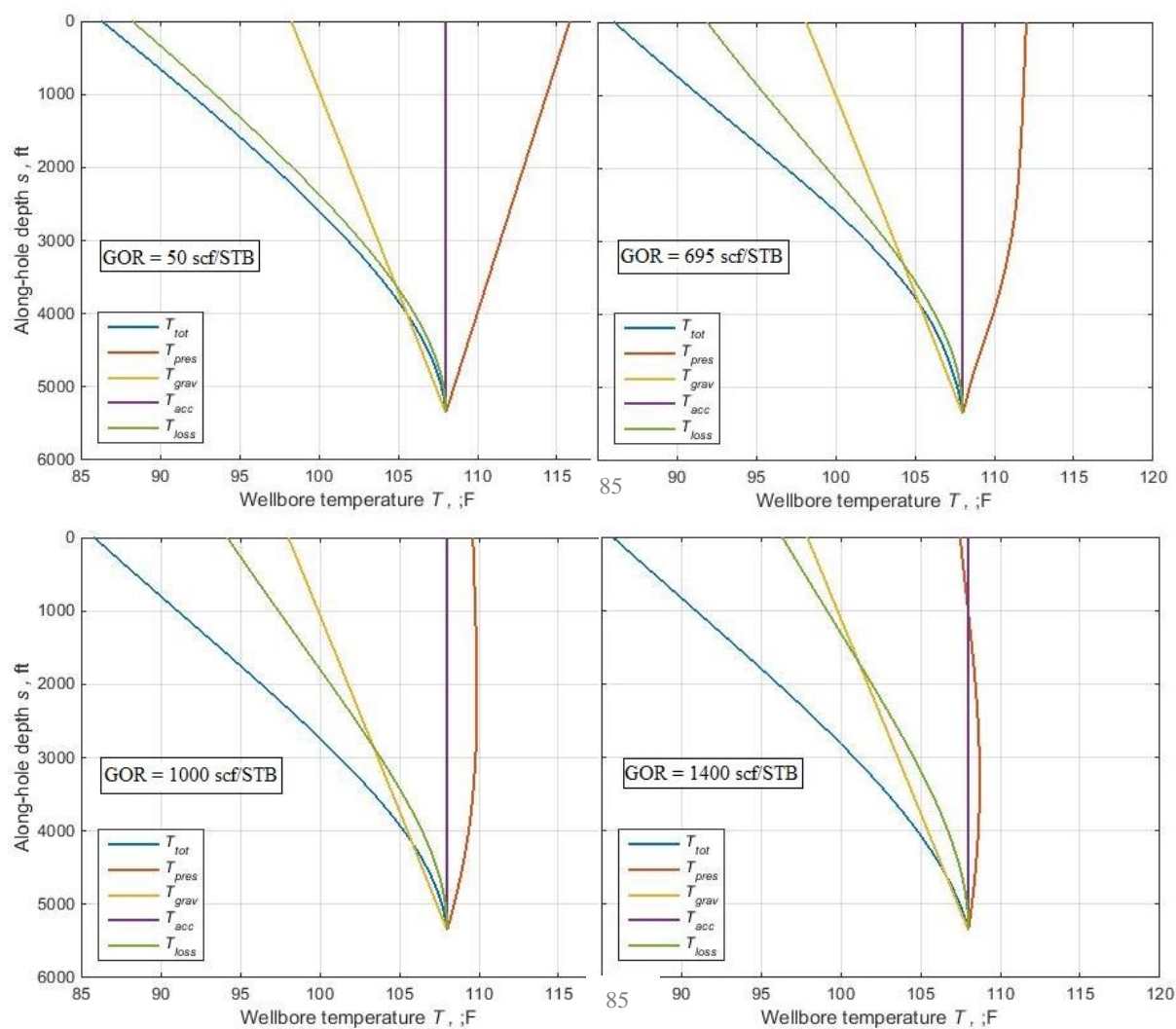


Figure 3-23. Effect of GOR on temperature gradient components (A 5355 ft vertical well produces 600 STB/D oil, with zero water production).

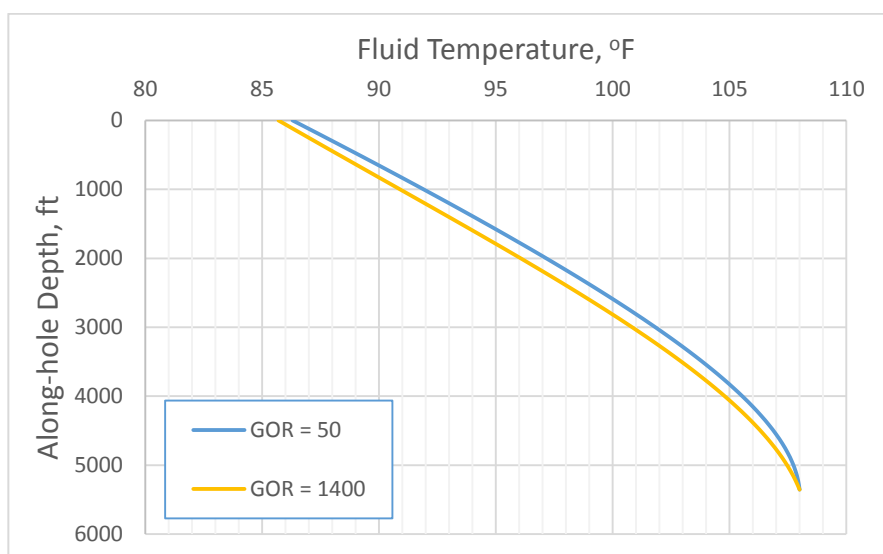


Figure 3-24. Effect of GOR on temperature gradient (A 5355 ft vertical well produces 600 STB/D oil, with zero water production, GOR units are in scf/STB).

3.3.3 Effect of Water-Oil Ratio

In this section temperature and pressure profiles have been modeled for four different water fraction values (f_w): 0, 0.3, 0.7, and the Base-Case which has a water fraction of 0.9018. As the water fraction increases, by keeping the oil rate (q_o) constant, the liquid rate increases. In general, under identical conditions a higher liquid flow rate results in a smaller temperature drop along the wellbore. According to Eq. (2.17) a higher water fraction means a higher mixture density (ρ_m), and a higher ρ_m leads to a higher dp/ds . Also, a higher liquid flow rate results in a higher pressure loss due to friction. An increase in density and velocity, together, result in a higher dp/ds . With a negative Joule-Thomson coefficient, a higher dp/ds means a lower dT/ds . Furthermore, water has a higher specific heat capacity (C_p). Hence, by increasing the water fraction, the overall heat capacity increases. With the same heat exchange between the fluid and formation (Q), cooling down a system with higher heat capacity is more difficult; hence a higher value of WOR causes a lower dT/ds , as shown in Figure 3.25. Figure 3.26 shows temperature gradient components (due to heat loss, Joule-Thomson effect, gravity, and acceleration). The effect of a higher C_p in case of a higher f_w is evident; a more concave downward shape means cooling is more difficult (especially at the bottom of the well where the surrounding temperature is close to the temperature of the wellbore fluid).

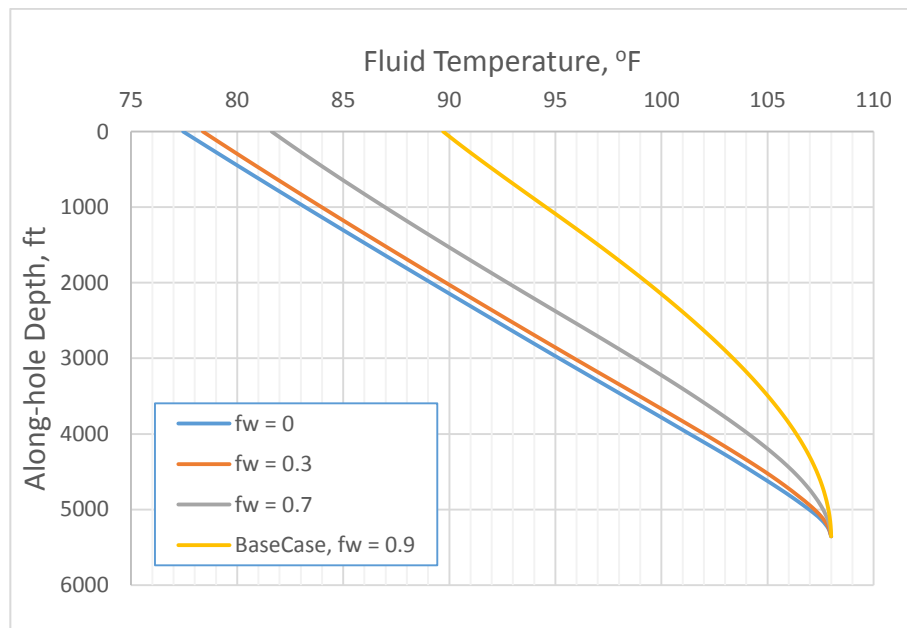


Figure 3-25. Effect of water fraction on temperature profile in the wellbore (A 5355 ft vertical well produces 59 STB/D oil, 41 Mscf/D gas and 542 STB/D water; oil and gas flow rates are kept constant)

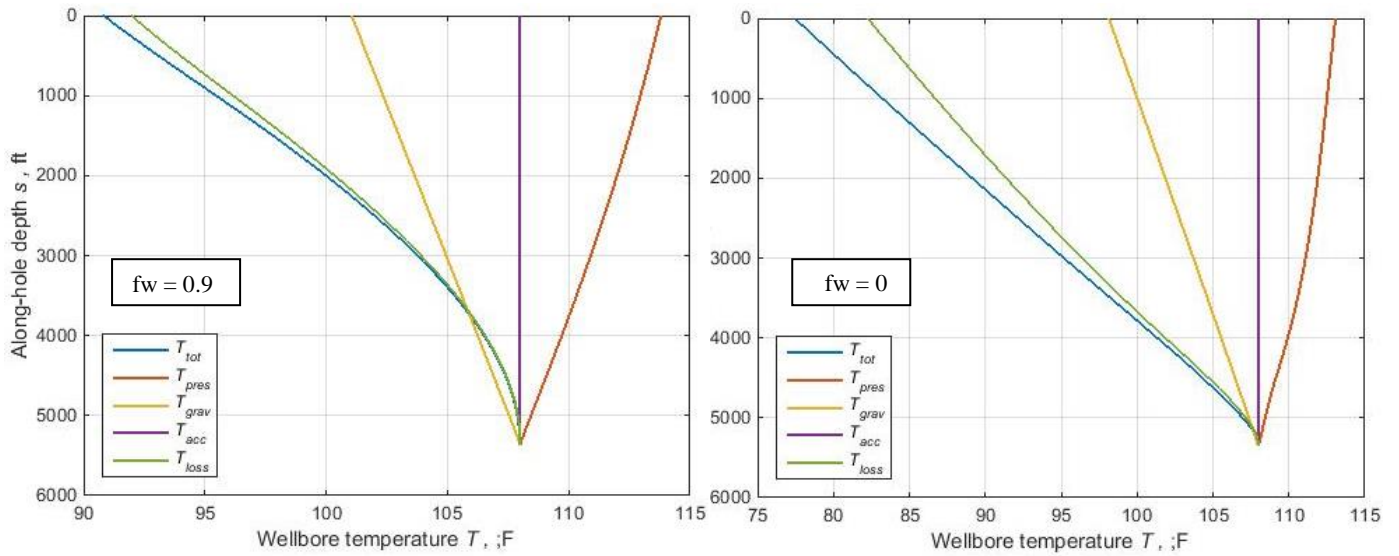


Figure 3-26. Effect of water fraction on temperature gradient components, left graph shows the BaseCase ($q_w = 542$ STB/D), and right graph is when $q_w = 0$

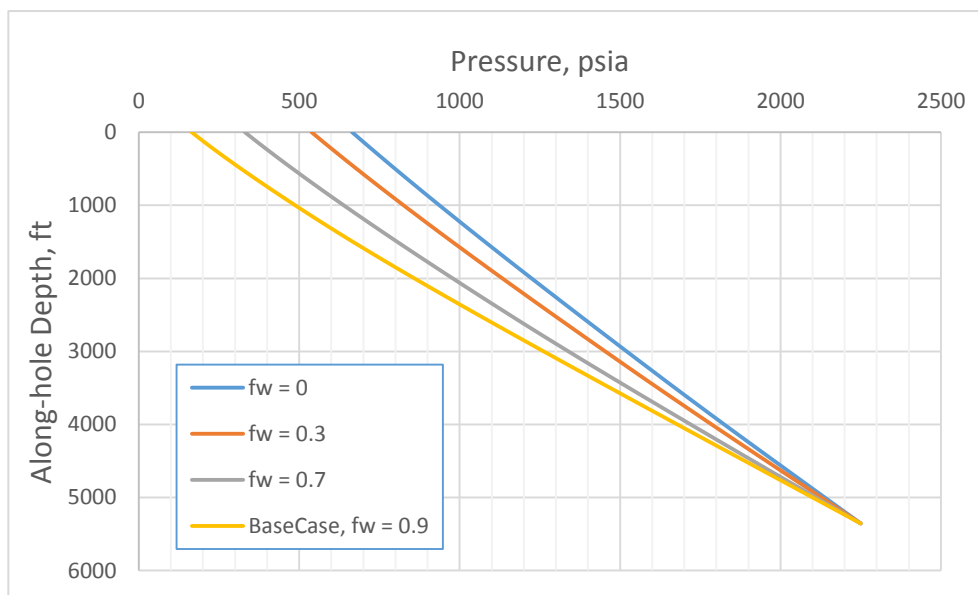


Figure 3-27. Effect of water fraction on pressure profile in the wellbore (A 5355 ft vertical well produces 59 STB/D oil, 41 Mscf/D gas and 542 STB/D water; oil and gas flow rates are kept constant)

3.3.4 Effect of Formation Thermal Conductivity

Thermal conductivity (k) is the capacity of a material to conduct or transmit heat, whilst thermal diffusivity (α) describes the rate at which heat is conducted through a medium. The thermal conductivity of deposits and soils will depend on the nature of the deposit, the bulk porosity of the soil and the degree of saturation. Deposits containing silt or clay portions will have higher thermal conductivities than those of unsaturated clean granular sand. Clean sands have a low thermal conductivity when dry but a higher value when saturated. For sedimentary rocks the primary control on thermal conductivity is the lithology of the sedimentary rock, porosity, and the extent of saturation. Mudstones have thermal conductivities in the range $1.2\text{--}2.3 \text{ W m}^{-1}\text{K}^{-1}$. As a reference, water has a thermal conductivity of $0.6 \text{ W m}^{-1}\text{K}^{-1}$ and air a thermal conductivity of $0.0252 \text{ W m}^{-1}\text{K}^{-1}$. More details on rocks thermal conductivities can be found in (British Geological Survey, 2011).

In this section, three different values for k_e have been tested; 0.83, 1.4 (Base-Case), and 2.3 $\text{Btu hr}^{-1}\text{ft}^{-1} \text{ } ^\circ\text{F}^{-1}$. Figure 3.28 shows the fluid temperature gradients for these three cases. A higher thermal conductivity results in a higher overall heat transfer coefficient (U_{to}), and Hence a higher heat exchange rate between the wellbore fluid and the earth, and finally a higher temperature gradient. Thus, for the same T_{wf} , a higher k_e results in a lower T_{tf} .

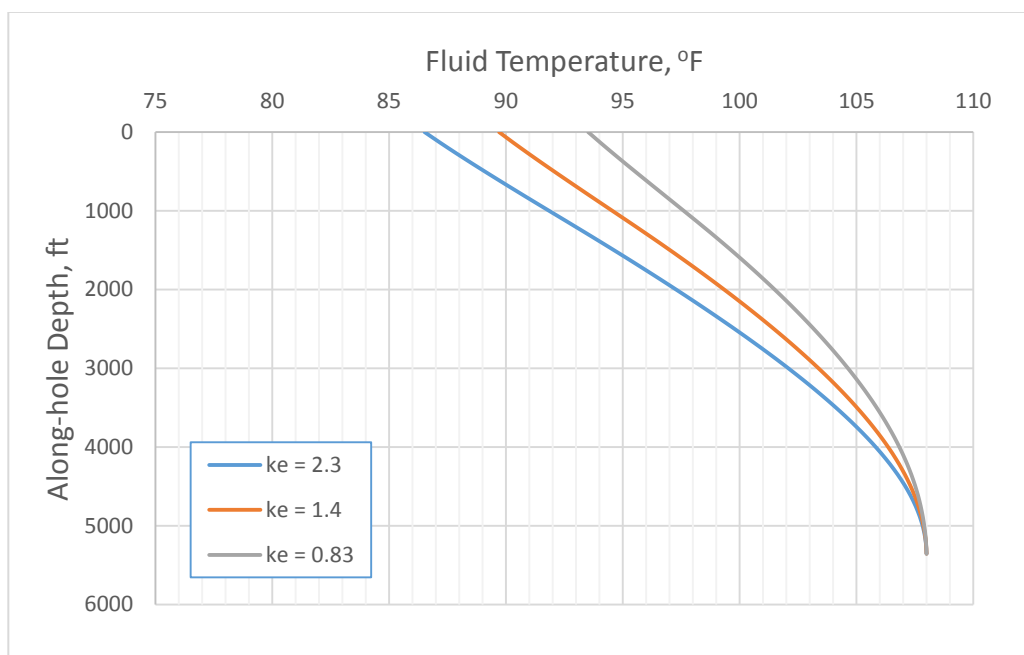


Figure 3-28. Effect of the earth thermal conductivity on temperature profile (A 5355 ft vertical well produces 59 STB/D oil, 41 Mscf/D gas and 542 STB/D water, earth thermal diffusivity is assumed to be constant and equal to $0.04 \text{ ft}^2/\text{hr}$).

3.3.5 Effect of Production Time

Although this work assumes a steady state condition where all properties stay constant with time, there is a time parameter in the program that has an effect on the dimensionless time (t_{Dw}) and the dimensionless temperature (T_D); production time (t_p). Later on, production affects earth thermal properties, and so on. To see this effect, the program has been tested for $t_p = 1$ week, 1 month, 6 months, 3 years, and 10 years[§]. As can be seen in Figure 3.29, higher t_p values result in higher values of t_{Dw} and T_D , a lower U_{to} , and finally a lower dT/ds . Also, the surrounding formation gradually heats up due to the production, which is another reason why the heat transfer rate decreases as the production time increases. As production goes on, after a while a balance will be reached, which is why the temperature gradient in Figure 3.29 is different from 1 week to 1 month, but this difference decreases between 3 years and 10 years.

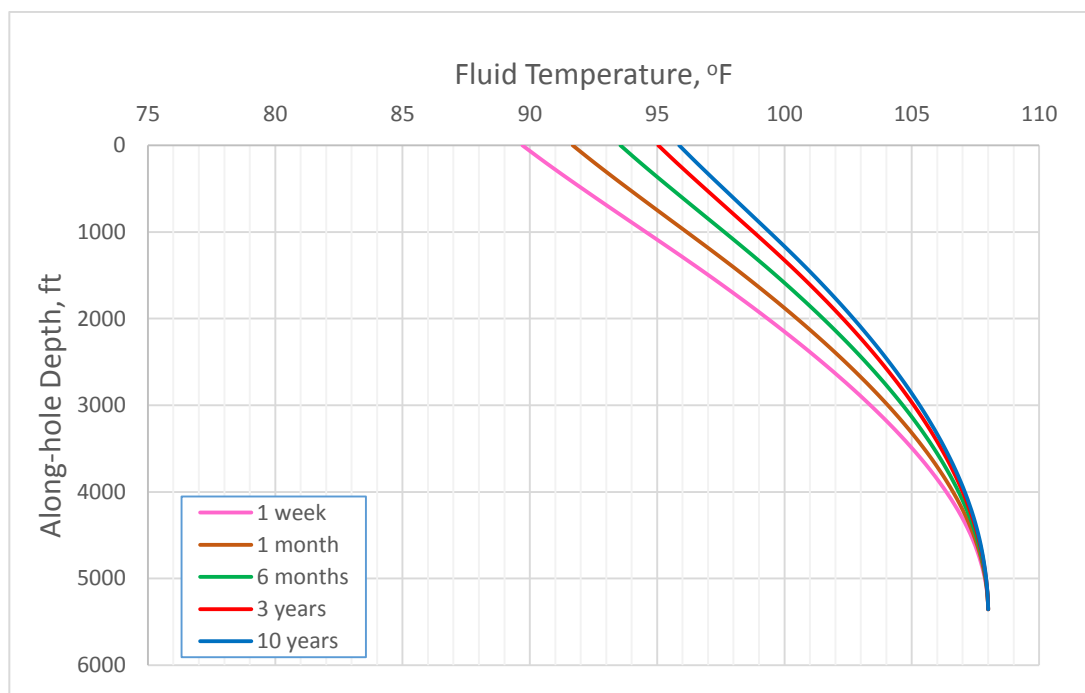


Figure 3-29. Effect of production time on temperature profile (A 5355 ft vertical well produces 59 STB/D oil, 41 Mscf/D gas and 542 STB/D water)

[§] Each month is considered to be 30 days and each year 365 days.

4 SUMMARY, CONCLUSION, AND FUTURE WORK

4.1 Summary and Conclusion

In this work, a temperature prediction model for predicting flowing temperatures in wellbores is developed. The model is general and can be applied to producing (and injecting) wells over the inclination angle range from, vertical to deviated, with black-oil models. It uses MATLAB software to solve pressure and temperature equations simultaneously. The model is usable for single-phase oil, single-phase gas, and multiphase flow systems. The utilized multiphase flow model is from Brill and Mukherjee; an extended description of their method is presented in Appendix A. Previous works on temperature predictions use empirical correlations to account for Joule-Thomson and friction effect. However, in this work, approximate methods for determining the three-phase heat capacity and the Joule-Thomson coefficient have been used. These approximations are useful when the generation of enthalpy tables is impossible or inconvenient. An accurate estimation of the Joule-Thomson effect is an important aspect of flowing-fluid-temperature. Modern wells often produce fluids at very high rates with consequent large pressure gradients, thereby accentuating the Joule-Thomson effect. A well producing multiphase fluid could experience an increase or decrease in temperature with reduction in pressure, depending on the fraction of each phase present. The use of empirical expressions in such cases, similar to the one used by (Sagar et al., 1991), may result in a significant inaccuracy in the estimated temperature. In the method presented in this work, the Joule-Thomson coefficient is calculated based on an analytical approximation suggested by (Alves et al., 1992). This method requires only pressure/volume/temperature data for the produced fluids, and is applicable to single-phase and multiphase flow systems, without any additional limiting assumptions. Instead of using restrictive approximate analytical expressions that assume constant variables such as dp/ds , U_{to} , C_p , η_{JT} , α , v , dv/ds , and g_G over the entire wellbore section, this program is improved with a numerical differentiation scheme. To solve this differential equation in each interval of the well, a fourth order Runge-Kutta method is used with the standard MATLAB 'ode45' function which integrates the pressure and temperature gradient equations simultaneously. Temperature and pressure of each depth interval are used as inputs to obtain fluid properties for the next depth interval. The proposed temperature model and approximations show a good performance over a broad range of flow conditions compared with previous simplified methods.

Different well configuration setups are available, such as a production scheme with one tubing and one casing, as well as a well completion design with three casings (one surface and two intermediates) and one tubing.

The validity of the program has been tested using four different real field data sets, and a good match with the data has been obtained. Furthermore, a sensitivity analysis has been conducted to analyze the effect of some of the main parameters, such as tubing inside diameter, GOR, WOR, earth thermal conductivity, and production time. In general, in a three phase flow system

through a vertical well (Base-Case), the temperature gradient decreases due to water entry resulting from, e.g., water coning or higher water-cut values (WOR), leading to a higher wellhead temperature for a fixed bottom-hole temperature. Conversely, a higher gas content (i.e. a higher GOR) causes the temperature gradient to increase, leading to a lower wellhead temperature for a fixed bottom-hole temperature. However, the effect of WOR on the temperature profile is more significant than effect of GOR. An increase in the earth thermal conductivity (k_e), and an increase in the tubing inside diameter both will increase the temperature gradient.

4.2 Future Work

Possible extensions to the present work include:

- A temperature model to account for flow through restrictions, such as choke flow.
- A temperature prediction model for a transient flow process (drawdown or build-up processes).
- The program uses *Standing* and *Glaser* correlations, to estimate oil properties. These correlations are only valid for a certain range of input data, limiting the application of the program. To be able to account for more cases, other correlations or table of properties should be used.
- Extending the ability of the developed simulator to model fluid flow in horizontal wells. Moreover, a coupled reservoir/wellbore model can be used to model fluid exchange between reservoir layers and different types of wells. It can also be modified to model temperature distribution during hot or cold fluid injection into deviated or horizontal wells.
- Using a variable-formation-temperature scheme vs. production time, to improve estimation of temperature by accounting for the changes in heat-transfer rate between the wellbore fluids and formation, which in turn, improves the pressure calculations.
- Hydrocarbon may be produced from different layers in the reservoir through wellbores. The simulator can be extended to account for multiple production zone. Then it can be used further as a tool to estimate near wellbore reservoir properties such as permeability and porosity.
- Extending the program to consider production through multiple tubing strings, instead of only one.
- Using a compositional approach to simulate wellbore fluid flow (instead of black-oil approximation).
- Testing the program validity versus industrial software such as HYSYS or PipeSim.

NOMENCLATURE

A = pipe cross-sectional area, m^2 , in^2
 C_p = specific-heat capacity of fluid at constant pressure, $\text{J}/(\text{kg}\cdot^\circ\text{C})$, $\text{Btu}/(\text{lbm}\cdot^\circ\text{F})$
 $C_{p,avg}$ = average specific-heat capacity of fluid at constant pressure, $\text{J}/(\text{kg}\cdot^\circ\text{C})$, $\text{Btu}/(\text{lbm}\cdot^\circ\text{F})$
 d = pipe diameter, m , in
 e = intrinsic specific energy, J/kg , Btu/lbm
 f = Moody friction factor
 f_w = water fraction
 g = gravitational acceleration, m/sec^2 , ft/sec^2
 g_G = geothermal temperature gradient, $^\circ\text{C}/\text{m}$, $^\circ\text{F}/\text{ft}$
 GOR = gas oil ratio, m^3/m^3 , scf/STB
 h = fluid specific enthalpy, J/kg , Btu/lbm
 h = convective film coefficient, $\text{W}/(\text{m}^2\cdot^\circ\text{C})$, $\text{Btu}/(\text{hr}\cdot\text{ft}^2\cdot^\circ\text{F})$
 H_g = gas holdup parameter
 H_l = liquid holdup parameter
 k = thermal conductivity, $\text{W}/(\text{m}\cdot^\circ\text{C})$, $\text{Btu}/(\text{hr}\cdot\text{ft}\cdot^\circ\text{F})$
 L_R = relaxation parameter defined by Eq. (B-1), m^{-1} , ft^{-1}
 L_{RC} = relaxation parameter for submerged section of a well, defined by Eq. (B-2), m^{-1} , ft^{-1}
 M = molar mass, kg/mol , lbm/lbmol
 N_{Gr} = Grashof number, dimensionless
 N_{Nu} = Nusselt number, dimensionless
 N_{Pr} = Prandtl number, dimensionless
 N_{Re} = Reynolds number, dimensionless
 p = pressure, pa , psi
 p_r = pseudo-reduced pressure ($= p/p_c$), dimensionless
 q = volumetric flow rate, m^3/sec , bbl/day
 q = heat flow rate (amount of heat flowing radially), W , Btu/hr
 Q = heat flow rate from the wellbore fluid to the formation, per unit length of wellbore, W/m , $\text{Btu}/(\text{hr}\cdot\text{ft})$
 Q'' = heat flux, W/m^2 , $\text{Btu}/(\text{hr}\cdot\text{ft}^2)$
 r = radius, m , ft
 r_w = well radius, m , ft
 R = universal gas constant, $\text{J}/(\text{mol}\cdot\text{K})$
 s = along-hole distance measured from the separator towards the reservoir, m , ft
 t = time, sec , hr
 t_D = dimensionless time
 T_f = fluid temperature, $^\circ\text{C}$, $^\circ\text{F}$
 T_D = dimensionless temperature
 T_e = earth, or formation, temperature, $^\circ\text{C}$, $^\circ\text{F}$
 T_{ei} = undisturbed earth, or formation, temperature, $^\circ\text{C}$, $^\circ\text{F}$

T_r = pseudo-reduced temperature ($= T/T_c$), dimensionless
 T_{wb} = wellbore/Earth-interface temperature, °C, °F
 u = specific internal energy, J/kg, Btu/lbm
 U_{to} = overall-heat-transfer coefficient, W/(m²-°C), Btu/(hr-ft²-°F)
 v = velocity, m/sec, ft/sec
 v_{sg} = superficial gas velocity, m/sec, ft/sec
 v_{sl} = superficial liquid velocity, m/sec, ft/sec
 V = fluid specific volume, m³/kg, ft³/lbm
 WOR = water oil ratio, m³/m³, bbl/STB
 w = mass flow rate, kg/sec, lbm/hr
 x = gas mass fraction (quality), dimensionless
 z = Well vertical depth from surface, m, ft
 Z = gas compressibility factor, dimensionless
 α = thermal diffusivity, m²/sec, ft²/hr
 α = well inclination angle, degrees
 β = thermal expansion coefficient, °C⁻¹, °F⁻¹
 γ_o = oil gravity, °API
 γ_g = gas gravity, dimensionless
 ε = pipe roughness, m, ft
 η_{JT} = Joule-Thomson coefficient, °C /pa, °F/(lbf/ft²)
 λ = no slip gas/liquid volume fraction
 μ = fluid viscosity, pa.sec, cp
 ρ = fluid density, kg/m³, lbm/ft³
 τ = shear stress, pa, psi
 ϕ = Joule-Thomson and friction factor lumped parameter, °C/m, °F/ft

Subscripts

ann = annulus
 acc = acceleration
 c = casing
 ci = inside casing
 co = outside casing
 Dw = dimensionless at wellbore
 e = earth
 el = elevation
 f = fluid
 $fric$ = friction
 g = gas
 HT = heat transfer terms in temperature gradient equation

L = liquid
 m = mixture
 mn = mixture no-slip
 ms = mixture slip
 o = oil
 sc = standard condition
 tf = wellhead flowing
 ti = inside tubing
 to = outside tubing
 w = water
 wf = bottom-hole flowing
 wh = wellhead

REFERENCES

- Alves, I.N., Alhanti, F.J.S. and Shoham, O., (1992): “*A unified model for predicting flowing temperature distribution in wellbores and pipelines*”. SPE Production Engineering Vol. 7, NO.04, pp.363-367. DOI: 10.2118/20632-PA.
- Ameen, M.M., (1992): “*Unified Model for Two- Phase Flow and Heat Transfer in Wellbores*”, MS thesis, U. of North Dakota, Grand Forks, North Dakota. (Quoted in Hassan and Kabir (2002); not consulted because of unavailability).
- Bird, R.B., Stewart, W.E. and Lightfoot, E.N., (1960): “*Transport Phenomena*”. Wiley, New York.
- Brill, J.P. and Mukherjee, H., (1999): “*Multi-phase flow in wells*”. SPE Monograph Series, Vol. 17, SPE, Richardson.
- British Geological Survey., (2011): “*Temperature and Thermal Properties*”, NATURAL ENVIRONMENT RESEARCH COUNCIL, BGS Report No: GR_999999/1.
- Coulter, D. M., Bardon, M. F., (1979): “*Revised Equation Improves Flowing Gas Temperature Prediction*”, Oil & Gas J, Vol. 2, NO.26, pp.107-108.
- Dake, L.P., (1978): “*Fundamentals of Reservoir Engineering*”. Elsevier Science.
- Dropkin, D and Somerscales, E., (1965): “*Heat Transfer by Natural Convection in Liquids Confined by Two Parallel Plates Which Are Inclined at Various Angles With Respect to the Horizontal*”. J. Heat Transfer, Trans. ASME, Series C. Vol. 87, NO.1, pp. 77-82, DOI:10.1115/1.3689057.
- Duns, H. and Ros, N.C.J., (1963): “*Vertical flow of gas and liquid mixtures in wells*”. Proc. 6th World Petroleum Congress, section II, 451-465, paper 22-PD6.
- Edwardson, M. J., Girner, H. M., Parkison, H. R., Williams, C. D., & Matthews, C. S., (1962): “*Calculation of Formation Temperature Disturbances Caused by Mud Circulation*”. Journal of Petroleum Technology. Vol. 14, NO.04, pp.416-426, DOI: 10.2118/124-PA.
- Gambill, W.R., (1957): “*You Can Predict Heat Capacities*”. Chemical Engineering Journal, pp. 243-248.
- Hagoort, J., (2004): “*Ramey’s Wellbore Heat Transmission Revisited*”. SPE Journal. Vol. 9, NO.04, pp. 465 - 474, DOI:10.2118/87305-PA.
- Hasan, A. R., & Kabir, C. S., (1994): “*Aspects of Wellbore Heat Transfer During Two-Phase Flow*”. SPE Production & Facilities. Vol. 9, NO.3, pp.211-216, DOI:10.2118/22948-PA.

Hasan, A. R., Kabir, C. S., & Wang, X., (2007): “*A Robust Steady-State Model for Flowing-Fluid Temperature in Complex Wells*”. SPE Annual Technical Conference and Exhibition, 11-14 November, Anaheim, California, U.S.A. DOI:10.2118/109765-MS.

Hasan, A. R., Kabir, C. S., (2002): “*Fluid Flow and Heat Transfer in Wellbores*”. SPE Richardson.

J. P. Holman., (1958): *Heat transfer (4th edition)*. New York: McGraw-Hill Book Co.

Jansen, J.D., (2016): “*Nodal analysis of oil and gas wells – system modeling and numerical implementation*”. SPE Textbook Series. SPE, Richardson. In production.

Lateef, A. K., & Omeke, J., (2011): “*Specific Heat Capacity of Natural Gas; Expressed as a Function of Its Specific Gravity and Temperature*”. SPE. Presented at the Nigeria Annual International Conference and Exhibition, 30 July - 3 August, Abuja, Nigeria, DOI:10.2118/150808-MS.

Kirkpatrick, C. V., (1959): “*Advances in Gas-lift Technology*”. American Petroleum Institute. Drilling and Production Practice, 1 January, New York.

James G. Knudsen and Donald L. Katz., (1958): “*Fluid Dynamics and Heat Transfer*”. New York, McGraw-Hill Book Co., Inc.

Lesem, L. B., Greytok, F., Marotta, F., & McKetta, J. J., (1957): “*A Method of Calculating the Distribution of Temperature in Flowing Gas Wells*”. SPE. Published in Petroleum Transactions, AIME, Volume 210, pages 169-176.

Livescu, S., Durlofsky, L.J., and Aziz, K., (2008): “*A Semi-analytical Thermal Multiphase Wellbore Flow Model for Use in Reservoir Simulation*”. Paper SPE 115796 presented at the SPE Annual Technical Conference and Exhibition, Denver, 21-24 September. DOI: 10.2118/115796-MS.

Livescu, S., Durlofsky, L. J., Aziz, K., & Ginestra, J.-C., (2008): “*Application of a New Fully-Coupled Thermal Multiphase Wellbore Flow Model*”. SPE. Presented at the SPE Symposium on Improved Oil Recovery, 20-23 April, Tulsa, Oklahoma, USA. DOI:10.2118/113215-MS.

Livescu, S., Aziz, K., & Durlofsky, L. J., (2009): “*Development and Application of a Compositional Wellbore Model for Thermal Recovery Processes*”. SPE. Presented at the SPE Western Regional Meeting, 24-26 March, San Jose, California. DOI :10.2118/121306-MS.

Livescu, S., Durlofsky, L.J., Aziz, K., and Ginestra, J.C., (2010): “*A Fully Coupled Thermal Multiphase Wellbore Flow Model for Use in Reservoir Simulation*”. J. Pet. Sci. Eng. 71: 138-146. DOI: 10.1016/j.petrol.2009.11.022.

Maric., (2005): “*The Joule–Thomson Effect in Natural Gas Flow Rate Measurements*”. Flow Measurement and Instrumentation. Volume 16, Issue 6, pp.387–395, ELSEVIER. DOI:10.1016/j.flowmeasinst.2005.04.006.

Moss and White., (1959): “*How to Calculate Temperature Profiles in a Water-Injection Well*”. *Oil & Gas*, 174.

Mukherjee H. and Brill, J.P., (1983): “*Liquid holdup correlations for inclined two-phase flow*”. *Journal of Petroleum Technology*. Vol.35, NO.05, pp. 1003-1008. DOI: 10.2118/10923-PA.

Mukherjee H. and Brill, J.P., (1985a): “*Pressure drop correlations for inclined two-phase flow*”. *ASME Journal of Energy Resources Technology*. Vol.107, NO.04, pp. 549-554. DOI: 10.1115/1.3231233.

Mukherjee H. and Brill, J.P., (1985b): “*Empirical equations to predict flow patterns in two phase inclined flow*”. *International Journal of Multi-phase Flow*. Vol.11, NO.03, pp. 299-315. DOI: 10.1016/0301-9322(85)90060-6.

Pourafshary, P., Varavei, A., Sepehrnoori, K., & Podio, A., (2008): “*A Compositional Wellbore/Reservoir Simulator to Model Multiphase Flow and Temperature Distribution*”. *International Petroleum Technology Conference*, 3-5 December, Kuala Lumpur, Malaysia. DOI: 10.2523/IPTC-12115-MS.

Ramey, H. J., (1962): “*Wellbore Heat Transmission*”. *SPE. Journal of Petroleum Technology*. Vol. 14, NO.04, pp.427-435, DOI: 10.2118/96-PA.

Ros, N.C.J., (1961): “*Simultaneous flow of gas and liquid as encountered in well tubing*”. *Journal of Petroleum Technology* Vol. 13, NO.10, pp.1037-1049. DOI: 10.2118/18-PA.

Sagar, R., Doty, D. R., & Schmidt, Z., (1991): “*Predicting Temperature Profiles in a Flowing Well*”. *SPE Production Engineering*. Vol. 06, NO.04, pp. 441-448, DOI: 10.2118/19702-PA.

Satter, A., (1965): “*Heat Losses During Flow of Steam Down a Wellbore*”. *Journal of Petroleum Technology*. Vol. 17, NO.07, pp. 845 - 851, DOI: 10.2118/1071-PA.

Semenova, A., Livescu, S., Durlofsky, L. J., and Aziz, K., (2010): “*Modeling of Multisegmented Thermal Wells in Reservoir Simulation*”. Paper SPE 130371 presented at the SPE/EUROPEC/EAGE Annual Conference and Exhibition, Barcelona, Spain, 14–17 June.

Shirdel, M. and Sepehrnoori, K., (2011). “*Development of a Transient Mechanistic Two-Phase Flow Model for Wellbores*”. Paper presented at the SPE Reservoir Simulation Symposium, The Woodlands, Texas, USA, 21–23 February. DOI:10.2118/142224-MS.

K. C. Shiu and H. D. Beggs., (1980): “*Predicting Temperatures in Flowing Oil Wells*”. *J. Energy Res. Tech.* Vol. 102, NO.01, DOI: 10.1115/1.3227845.

Stone, T. W., Bennett, J., Law, D. H.-S., & Holmes, J. A., (2002): “*Thermal Simulation With Multi-segment Wells*”. *SPE Reservoir Evaluation & Engineering*. Vol. 5, NO.03, pp. 206 – 218, DOI: 10.2118/78131-PA.

Stone, T. W., Edmunds, N. R., & Kristoff, B. J., (1989): “*A Comprehensive Wellbore/Reservoir Simulator*”. Conference Paper presented at SPE Symposium on Reservoir Simulation, 6-8 February, Houston, Texas. DOI: 10.2118/18419-MS.

Wang, (1996): “*Modeling Coupled Transient Transport of Mass, Momentum and Energy in Wellbore/Reservoir Systems*”. Ph.D. dissertation, The University of North Dakota.

Willhite, G. P., (1967): “*Over-all Heat Transfer Coefficients in Steam And Hot Water Injection Wells*”. Journal of Petroleum Technology. Vol. 19, NO.05, pp. 607-615, DOI: 10.2118/1449-PA.

APPENDIX A

In this appendix some insights on the multiphase flow system is described, such as dimensionless numbers suggested by (Ros, 1961), as well as Mukherjee and Brill model that is used in this work.

Hold-up and Friction Correlations

Many empirical correlations and semi-empirical models have been developed for multi-phase flow in pipes. (Brill and Mukherjee, 1999) distinguish three types of correlations of increasing complexity, in addition to even more complex *mechanistic models*:

- First (simplest) group of correlations consists of empirical expressions for the friction factor in terms of no-slip mixture properties.
- Second category takes slip into account and consists of empirical expressions for hold-up and friction.
- Thirds category also considers different flow regimes.

The latter two categories typically use a set of dimensionless groups defined in terms of the essential variables^{**} to describe the physics of multi-phase flow. In this section, four (out of nine) of the most important dimensionless groups to study the dimensionless pressure gradient $(dp/ds)/(\rho_l g)$ are described. For more information on dimensional analysis see (Ros, 1961).

the liquid velocity number:
$$N_{lv} = |v_{sl}|^4 \sqrt{\frac{\rho_l}{g \sigma_{gl}}}, \quad (\text{A.1})$$

the gas velocity number:
$$N_{gv} = |v_{sg}|^4 \sqrt{\frac{\rho_l}{g \sigma_{gl}}}, \quad (\text{A.2})$$

the pipe diameter number:
$$N_d = d \sqrt{\frac{g \rho_l}{\sigma_{gl}}}, \quad (\text{A.3})$$

the liquid viscosity number:
$$N_\mu = \mu_l^4 \sqrt{\frac{g}{\rho_l \sigma_{gl}^3}}. \quad (\text{A.4})$$

Mukherjee and Brill

Mukherjee and Brill model is a correlation of the third category, i.e. it takes into account flow regimes, and it is valid for vertical, deviated or horizontal wells or pipes. The models is defined in terms of the dimensionless groups (A.1) – (A.4), plus the wellbore inclination (α). After performing a large number of experimental tests and through curve fitting of the measurements, Mukherjee and Brill developed a set of numerical expressions for the flow pattern boundaries

^{**} Such as pipe diameter, pipe roughness, pressure, fluid velocities, fluid viscosities, fluid densities etc.

in terms of dimensionless numbers (A.1) – (A.4) and a pipeline inclination angle θ_{MB} that can be related to the definition for the well bore inclination α according to

$$\theta_{MB} = d \left| \alpha - \frac{\pi}{2} \right|, \quad (\text{A.5})$$

where d is the flow direction. For a flow from bottom-hole to wellhead (production well), $d = 1, -1$, and 0 when $\alpha < \pi/2$, $\alpha > \pi/2$, and $\alpha = \pi/2$, respectively. After defining the flow direction, flow regimes can be determined by comparing the flow regimes transition boundaries and dimensionless numbers. Table A.1 summarizes the boundaries between different flow regimes. The boundary between bubble flow and slug flow depends on the flow direction; there are two boundaries, one for up-flow and one for down-flow and horizontal flow direction

<i>Boundary between annular-mist flow - bubble or slug flow</i>	$N_{gv,sm} = 10^{A_1} \quad (\text{A.6})$
<i>Boundary between bubble flow - slug flow (depends on the flow direction)</i>	upflow boundary $N_{lv,bs} = 10^{A_2} \quad (\text{A.7})$
	downflow and horizontal slug $N_{gv,bs} = 10^{A_3} \quad (\text{A.8})$
<i>Boundary between slug flow and stratified flow</i>	$N_{lv,st} = 10^{A_4} \quad (\text{A.9})$

Table A.1. Summary of the boundaries recognition between different flow regimes, using Mukherjee and Brill numerical expressions

where

$$A_1 = 1.401 - 2.694 N_\mu + 0.521 N_{lv}^{0.329}, \quad (\text{A.10})$$

$$A_2 = \log N_{gv} + 0.940 + 0.074 \sin \theta_{MB} - 0.855 \sin^2 \theta_{MB} + 3.695 N_\mu, \quad (\text{A.11})$$

$$A_3 = 0.431 - 3.003 N_\mu - [1.138 \log N_{lv} + 0.429 (\log N_{lv})^2 - 1.132] \sin \theta_{MB}, \quad (\text{A.12})$$

$$A_4 = 0.321 - 0.017 N_{gv} - 4.267 \sin \theta_{MB} - 2.972 N_\mu - 0.033 (\log N_{gv})^2 - 3.925 \sin^2 \theta_{MB} \quad (\text{A.13})$$

Once the flow regime has been determined, the liquid hold-up can be computed. Mukherjee and Brill determined a single hold-up correlation for all flow regimes given

$$H_l = \exp \left[\left(C_1 + C_2 \sin \theta_{MB} + C_3 \sin^2 \theta_{MB} + C_4 N_\mu^2 \right) \left(\frac{N_{gv}^{C_5}}{N_{lv}^{C_6}} \right) \right], \quad (\text{A.14})$$

where the coefficients C_1 to C_6 depend on the flow regime and are given in Table A.2.

<u>Coefficient</u>	<u>Uphill or horizontal flow</u>	<u>Downhill stratified flow</u>	<u>Other downhill flow</u>
C_1	-0.380113	-1.330282	-0.516644
C_2	0.129875	4.808139	0.789805
C_3	-0.119788	4.171584	0.551627
C_4	2.343227	56.262268	15.519214
C_5	0.475686	0.079951	0.371771
C_6	0.288657	0.504887	0.393952

Table A.2. Coefficients C_1 to C_6 used to calculate liquid hold-up in Mukherjee and Brill single hold-up correlation Eq. (A.14). (Jansen, 2016)

Pressure drop analysis

The pressure drop equation used by Mukherjee and Brill is flow regime dependent. For slug and bubble flow it can be written as

$$\frac{dp}{ds} = \frac{1}{1 - E_{K,D}} \left(\rho_{ms} g \cos\alpha - \frac{\rho_{ms}}{2d} f_{ms} v_{ms} |v_{ms}| \right), \quad (\text{A.15})$$

where $E_{K,D}$ is dimensionless mixture kinetic energy term defined by (Beggs and Brill, 1973)

$$E_{K,D} = \frac{\rho_{ms} v_{ms} v_{sg}}{p}. \quad (\text{A.16})$$

The friction coefficient f_{ms} is determined from the Moody diagram. For stratified flow the friction factor is computed with the aid of a mechanistic model that explicitly accounts for the velocities in the liquid and gas layers, and for the shear forces between the layers and between the fluids and the wall. See (Mukherjee and Brill, 1985a) or (Brill and Mukherjee, 1999) for further details.

APPENDIX B

Input data for 4 case studies, introduced under well application section, is summarized in Appendix B.

Case Study 1: Oil/Gas/Water Producer, Vertical Well

$Depth, ft$	5355
$q_o, STB/D$	59
$q_w, STB/D$	542
$q_g, MScf/D$	41
$\gamma_o, ^\circ API$	34.3
γ_w	1.01
γ_g	1.04 ^{††}
d_{ti}, in	2.875
d_{to}, in	3
d_{ci}, in	6.46
d_{co}, in	7
d_{wb}, in	9
$P_{wh}, psig$	113
$T_{ewh}, ^\circ F$	76
$T_{eibh} = T_{fbh}, ^\circ F$	108
t_p, hr	158

Table B.1. Input data for Vertical oil/gas/water producer well, Case study 1.

Since actual conductivity data, needed for estimating the overall heat transfer coefficient, were unavailable; typical values assumed by Sagar et al. were used. The following typical values for the thermal properties of the various elements were used:

$k_e, BTU/(hr-ft-^\circ F)$	1.4
$k_{cem}, BTU/(hr-ft-^\circ F)$	4.021
$k_c, BTU/(hr-ft-^\circ F)$	16
$k_t, BTU/(hr-ft-^\circ F)$	25
$k_a, BTU/(hr-ft-^\circ F)$	0.383
$C_{p,water}, BTU/(lbm-^\circ F)$	1
$C_{p,oil}, BTU/(lbm-^\circ F)$	0.947
μ_a, cp	1.5
$\alpha, ft^2/hr$	0.04
$g_G, ^\circ C/m$	0.011

Table B.2. Thermal properties input data for Vertical oil/gas/water producer well, Case study 1.

†† Due to Standing correlation range the value for γ_g , was set equal to 0.95 instead of 1.04 in the m.file. However, the obtained results do not show a huge difference with the original value.

<i>Depth</i>	<i>Measured data</i>
<i>S (ft)</i>	<i>T_{fluid} (°F)</i>
0	88
500	93
1000	96
1500	98
2000	100
2500	102
3000	103
3500	105
4000	106
4500	107
5000	108
5355	108

*Table B.3. Measured field temperature data, Vertical oil/gas/water producer well, Case study 1
Reported from (Hassan and Kabir, 2002), page 71.*

<i>s(ft)</i>	<i>T_{fluid} (°F)</i>	<i>T_{earth} (°F)</i>	<i>P_{psig}</i>
5355	108	108	2250
4953.375	107.856	105.5762	2080.323
4551.75	107.4607	103.1524	1910.724
4150.125	106.8136	100.7285	1741.484
3748.5	105.9356	98.30471	1572.856
3346.875	104.8512	95.88089	1405.158
2677.5	102.6464	91.84118	1129.115
2275.875	101.1186	89.41736	966.8269
1874.25	99.4585	86.99353	808.4248
1472.625	97.6806	84.56971	655.5397
1071	95.79763	82.14589	510.2719
669.375	93.87898	79.72207	372.4677
401.625	92.61913	78.10618	284.8637
267.75	92.00312	77.29824	242.7039
133.875	91.40163	76.4903	201.8902
0	90.81989	75.68236	162.6935

*Table B.4. Calculated fluid temperature, pressure and surrounding formation temperature using
example_traverse_thermal.m, Vertical oil/gas/water producer well, Case study 1.*

Case Study 2: Oil/Gas/Water Producer, Deviated Well

The surface temperature of the water is approximately 54 °F, while the temperature at the seabed is assumed to be 30 °F. Formation BHT is 164 °F, and the geothermal gradient is 0.006 °F /ft. The gauge reports a BHP of 4,186 psig and WHP of 290 psig. There is no data reported on well configuration and thermal conductivities, so overall heat transfer coefficient, U_{to} , cannot be calculated using `Overall_heat_transfer_coeff.m` function file. However, (Hasan, Kabir, and Wang, 2009) calculated and used the *relaxation parameter*, L_R , ft^{-1} as follow:

- For a wellbore section surrounded by earth, L_R is given by

$$L_R \equiv \frac{2\pi}{C_p w} \left[\frac{r_{to} U_{to} k_e}{k_e + (r_{to} U_{to} T_D)} \right], \quad (\text{B.1})$$

- Whereas L_R for a section submerged in water is

$$L_{RC} \equiv \frac{2\pi r_{to} U_{to}}{C_p w}. \quad (\text{B.2})$$

Heat flux from the wellbore fluid to the formation per unit length of wellbore, is then given by

$$Q \equiv L_R w C_p (T_f - T_e). \quad (\text{B.3})$$

Although for the part of the well adjacent to the sea water (Hasan, Kabir, and Wang, 2009) used $L_R = 4.129\text{e-}5 \text{ ft}^{-1}$, in this work, a much higher value of L_R is needed to get a good match with the measured data. Thus, in the MATLAB file, $L_R = 50\text{e-}5 \text{ ft}^{-1}$ is used when $s < 2800 \text{ ft}$. Table B.5 summerises input data used in the program:

Depth interval, ft	Geothermal gradient, °F/ft
0-2800 (seawater)	-0.00857
2800-4250	0.059
4250-14600	0.006

Table B.5. Input data for partially deviated oil/gas/water producer well, Case study 2.

$\rho_{g,sc}$, lbm/ft	0.05 ^{††}
$\rho_{o,sc}$, lbm/ft	57
$\rho_{w,sc}$, lbm/ft	62.8
$C_{p,g}$	Computed using (Kareem Lateef and Omeke, 2011) at each T & p
$C_{p,o}$	Computed using (Gambill, 1957) at each T & p
$C_{p,w}$	Computed using (Holman, 1958) at each T & p

Table B.6. Input data for partially deviated oil/gas/water producer well, Case study 2.

^{††} In the original work, $\rho_g = 1.05 \text{ lbm ft}^{-3}$ is reported. However, this is far above Standing correlation range and leads to wrong results if used. To solve this, in the m.file, $\rho_g = 0.05 \text{ lbm ft}^{-3}$ is used instead. Value of ρ_g does not have a large impact on the final result. Thus this modification doesn't decrease the accuracy of the model.

As it can be seen in Figure (3.9) and Table B.5, there are 3 different segments in this case. The approach taken in this study entails dividing the wellbore into many sections of uniform thermal properties and deviation angle. The governing differential equation is solved for each section, with fluid temperature from the prior section as the boundary condition. This piecewise approach makes the model versatile, allowing step-by-step calculation of fluid temperature for the entire wellbore. This is done as follow:

```
s_tot = from_ft_to_m(14600); % total along-hole well depth, m
s_mid1 = from_ft_to_m(4250); % start of deviation depth, m
s_seabed = from_ft_to_m(2800); % seabed, m

alpha1 = from_deg_to_rad(39); % wellbore inclination, rad
alpha2 = from_deg_to_rad(0); % wellbore inclination, rad

% geothermal gradient
g_G_1 = from_deg_F_per_ft_to_K_per_m(0.006);
g_G_2 = from_deg_F_per_ft_to_K_per_m(0.059);
g_G_sea = from_deg_F_per_ft_to_K_per_m((30-54)/2800);

% Compute and plot traverse bottom-up:

[p_mid1, s1, T_mid1, pT1] =
pipe_thermal(alpha1, Delta_T_ann_guess, d_ti, e, fluid, g_G_1, oil, p_wf, q_sc, Rel_Tol_itt, rho_sc, s_tot, s_mid1, t_p, T_wf, T_wf);

% external (formation) temperature 1, :C
T_e1 = T_wf - g_G_1 * (s_tot - s1) * cos(alpha1);
-----
T_e_in = T_e1(end);

[p_mid2, s2, T_mid2, pT2] =
pipe_thermal(alpha2, Delta_T_ann_guess, d_ti, e, fluid, g_G_2, oil, p_mid1, q_sc, Rel_Tol_itt, rho_sc, s_mid1, s_seabed, t_p, T_mid1, T_e_in);

% external (formation) temperature 2, :C
T_e2 = T_e_in - g_G_2 * (s_mid1 - s2) * cos(alpha2);
-----
T_e_in_sea = T_e2(end);

[p_tf, s3, T_tf, pT3] =
pipe_thermal(alpha2, Delta_T_ann_guess, d_ti, e, fluid, g_G_sea, oil, p_mid2, q_sc, ...
Rel_Tol_itt, rho_sc, s_seabed, 0, t_p, T_mid2, T_e_in_sea);

% external (formation) temperature 3, :C
T_e3 = T_e_in_sea - g_G_sea * (s_seabed - s3) * cos(alpha2);
```

Table B.7 shows the results for Bottom-up integration

$s(ft)$	$T_{fluid} (^{\circ}F)$	$T_{earth} (^{\circ}F)$	P_{psig}
14600	164	164	4200.5
10718.75	160.5592	145.9022	3171.506
6837.5	152.8236	127.8044	2215.687
4068.75	145.4286	105.0455	1578.506
3525	142.8978	72.96423	1431.794
2981.25	139.4159	40.88297	1288.668
2100	107.2996	36.18922	1062.461
1400	86.52309	42.18922	884.8595
1050	79.27222	45.18922	795.374
700	73.69865	48.18923	700.9988
350	69.60767	51.18923	586.7588
135.3906	67.84985	53.02873	480.9733
35.7591	67.32999	53.88272	394.9667
11.9197	67.2876	54.08706	357.5633
0	67.31124	54.18923	328.296

Table B.7. Calculated fluid temperature, pressure and surrounding formation temperature using example_traverse_thermal.m, for a partially deviated oil/gas/water producer well, Case study 2.

Case Study 3: Oil Producer, Vertical Well

The producing-oil temperature at surface is approximately 200 °F, and the surrounding earth temperature is 60 °F. Formation BHT is 222 °F, and the geothermal gradient is 0.01135 °F /ft. The gauges report a BHP of 7,254 psig and WHP of 3,380 psig. Density of the oil at well-head is $\rho_o = 40.209 \text{ lbm ft}^{-3}$. Since for single-phase oil well changes of density with depth is very small, in example_traverse_thermal.m file $\rho_{o,sc}$ is set to be 40.87 lbm ft⁻³.

In this work the two values suggested by (Hasan,Kabir, and Wang, 2009) for L_R is used:

```

if s < from_ft_to_m(2800)
    L_R = (3.27e-5) * (0.3048)^-1;
else
    L_R = (1.45e-5) * (0.3048)^-1;
end

dTds_loss = L_R*(T_tot-T_e); % heat loss to the surrounding, :C/m

```

Oil specific heat capacity, $C_{p,o}$ is estimated using (Gambill, 1957).

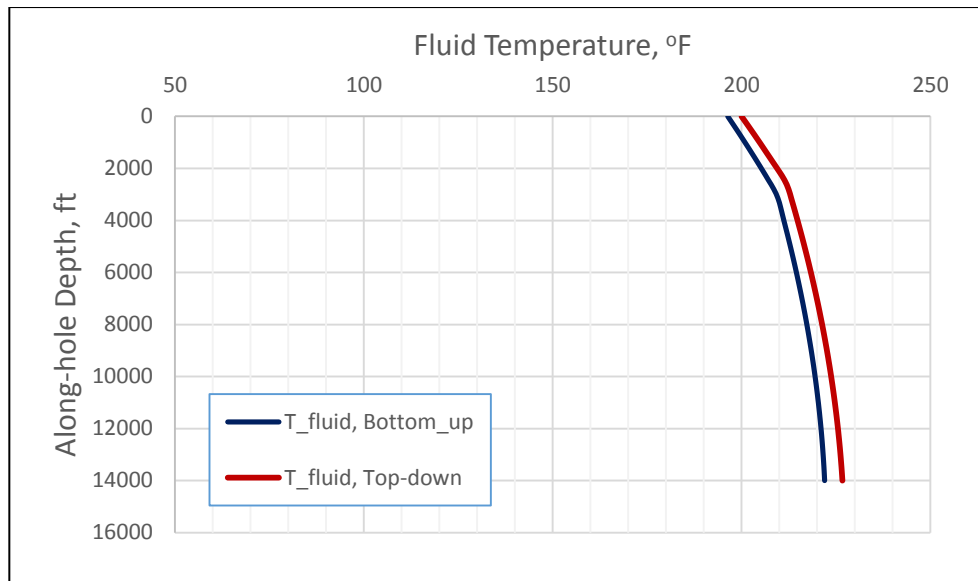


Figure B-1. Comparison between computed fluid temperatures bottom-up and top down using `example_traverse_thermal.m` file, for a vertical oil producer well, Case study 3. Bottom-up calculation appears to be slightly more accurate than Top-down integration.

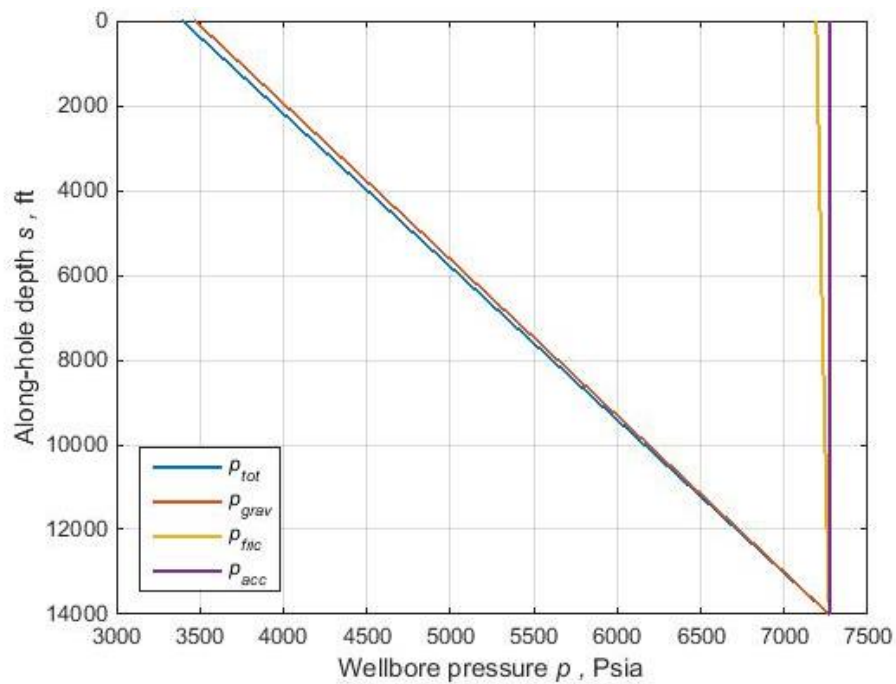


Figure B-2. Pressure gradient equation components, Vertical oil producer well, Case study 3.

Bottom_up				Top_down			
p_{psia}	$s(ft)$	$T_{fluid} (^{\circ}F)$	$T_{earth} (^{\circ}F)$	p_{psia}	$s(ft)$	$T_{fluid} (^{\circ}F)$	$T_{earth} (^{\circ}F)$
7268.5	14000	222	222	3394.5	0	200	60
6977.949	12950	221.5783	210.0825	3685.567	1050	205.019	71.9175
6687.465	11900	220.9827	198.165	3976.251	2100	209.8794	83.835
6397.031	10850	220.2158	186.2475	4266.599	3150	213.161	95.7525
6106.631	9800	219.2804	174.33	4556.82	4200	215.2083	107.67
5816.247	8750	218.1791	162.4125	4846.955	5250	217.1047	119.5875
5525.863	7700	216.9144	150.495	5137.021	6300	218.8479	131.505
5235.463	6650	215.489	138.5775	5427.035	7350	220.4354	143.4225
4945.029	5600	213.9053	126.66	5717.015	8400	221.8646	155.34
4654.543	4550	212.1659	114.7425	6006.976	9450	223.1331	167.2575
4363.987	3500	210.3493	102.825	6296.937	10500	224.2384	179.175
4073.323	2450	207.1206	90.90749	6586.912	11550	225.1778	191.0925
3782.356	1400	202.6709	78.98999	6876.92	12600	225.9487	203.01
3491.039	350	197.9712	67.07249	7166.975	13650	226.5485	214.9275
3393.851	0	196.3506	63.09999	7263.673	14000	226.7099	218.9

Table B-8. Comparison between bottom-up and top down calculation results, using example_traverse_thermal.m file, for a vertical oil producer well, Case study 3. Bottom_up calculation appears to be slightly more accurate than Top_down integration.

Case Study 4: Oil/Gas Producer, Vertical Well

Case study 4 is based on the measurements presented by (Hassan and Kabir, 2002). A 5151 ft vertical well produces 23 °API dry oil at a flow rate equal to 1140 STB/D through a 2.99-in ID tubing. GOR is 450 scf/STB, and the gas gravity is 0.80. The simulated results are very close to the measured data. Wellhead measured pressure is 505 psig. In this case, only the filed pressure data measurements are available. To run the program a constant overall heat transfer coefficient of $U_{to} = 13 \text{ W/(m}^2 \text{ }^{\circ}\text{C)}$ ($U_{to} = 2.2894 \text{ Btu/(hr ft}^2 \text{ }^{\circ}\text{F)}$) is considered.

Depth, ft	5151
q_o , STB/D	1140
γ_o , °API	23
d_{ti} , in	2.99
GOR, scf/STB	450
γ_g	0.80
p_{wh} , psig	505
T_{wf} , °F	108
P_{wf} , psig	2105
g_G , Kelvin/m	0.011
C_{p_o} , Btu lbm ⁻¹ °F ⁻¹	Calculated using Gambill correlation
K_e , Btu hr ⁻¹ ft ⁻¹ °F ⁻¹	1.4

Table B-9. Input data file for a vertical oil/gas producer well, case study 4.

<i>Depth</i>	<i>Field data</i>	<i>Hassan & Kabir results</i>
<i>s(ft)</i>	<i>P (psig)</i>	
0	505	505
400	587	593
650	647	654
1150	777	781
1650	920	918
2150	1074	1063
2650	1237	1212
3150	1407	1369
3650	1582	1530
4150	1850	1695
4650	1960	1864
5151	2105	2034

Table B-10. Measured field data and Hasan & Kabir results for a vertical oil/gas producer well, Case study 4, Table from (Hassan and Kabir, 2002), page 33.

<i>s(ft)</i>	<i>T_{fluid} (°F)</i>	<i>P (psia)</i>
5151	108	2119.5
4764.675	107.7592	1983.417
4378.35	107.3441	1849.628
3992.025	106.7627	1718.585
3605.7	106.0237	1590.785
3219.375	105.137	1466.76
2833.05	104.1132	1347.045
2446.725	102.9728	1231.641
2060.4	101.7723	1118.302
1674.075	100.5347	1006.706
1287.75	99.28462	896.3725
901.425	98.05298	786.3249
515.1	96.88281	674.5572
128.775	95.84248	556.5177
0	95.544	514.0389

Table B.11. Calculated fluid temperature and pressure temperature, using example_traverse_thermal.m file, for a vertical oil/gas producer well, Case study 4.

APPENDIX C

GOR sensitivity analysis on a 5355 ft vertical well that produces 600 STB/D oil, 0 water.

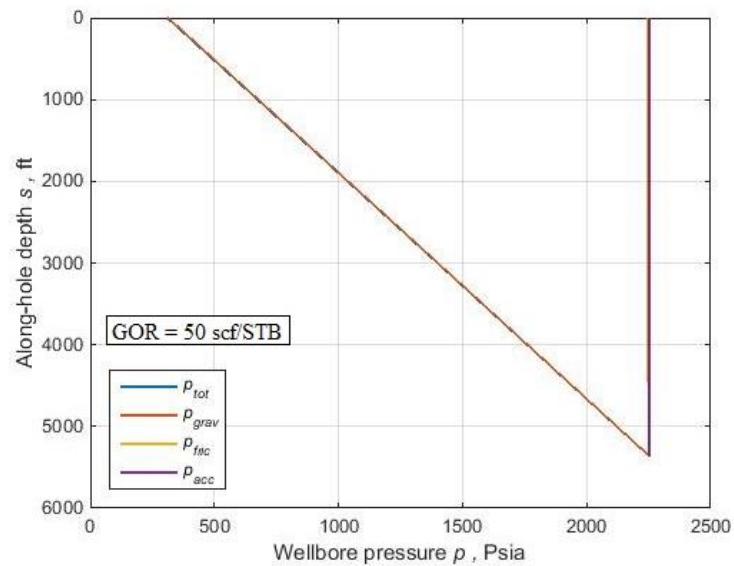
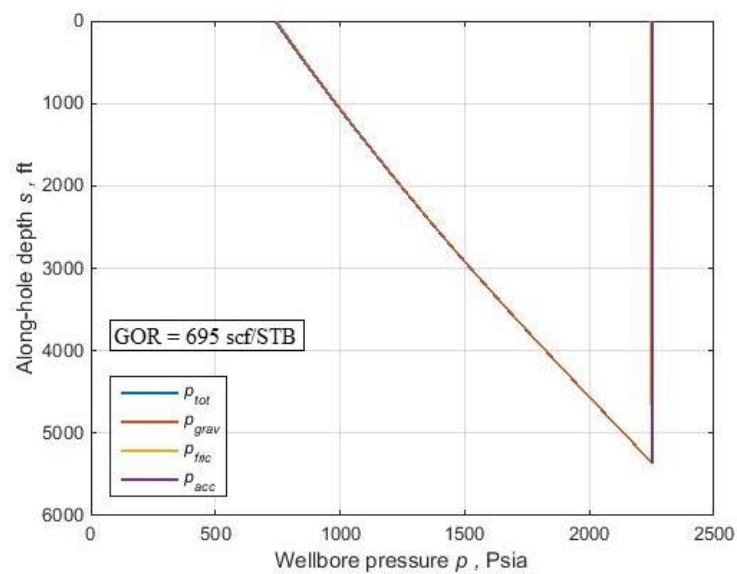


Figure C-1. Effect of GOR on pressure profile components in the wellbore (A 5355 ft vertical well produces 600 STB/D oil, 0 water).



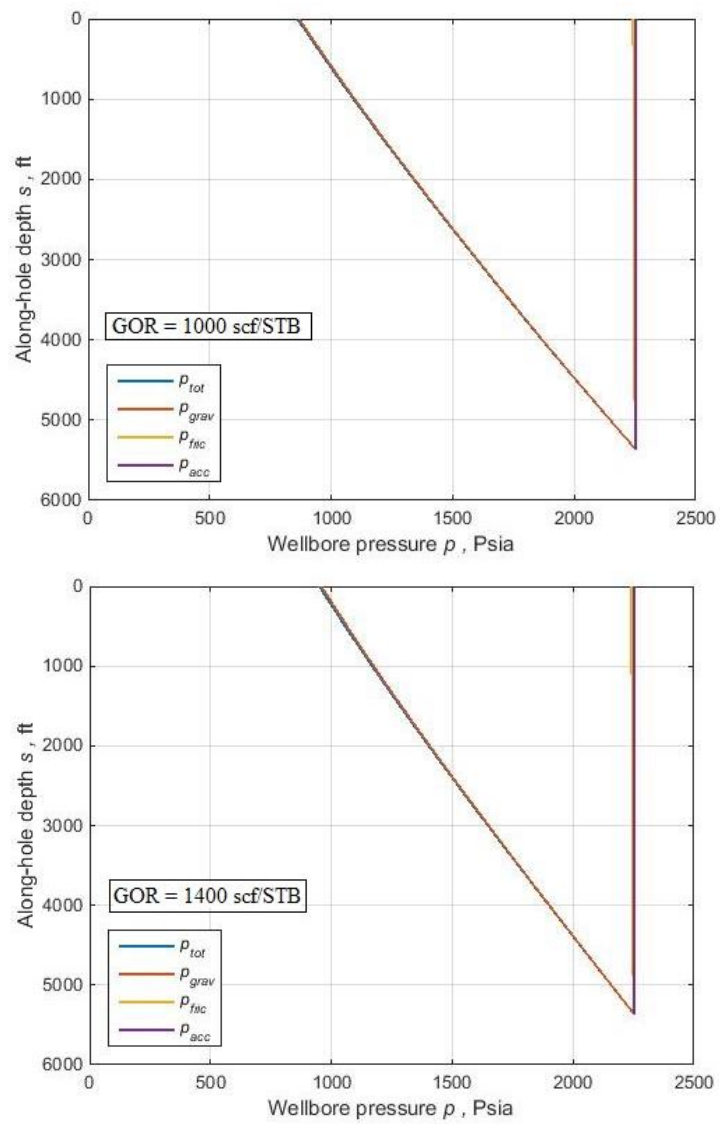


Figure C-1. Effect of GOR on pressure profile components in the wellbore (A 5355 ft vertical well produces 600 STB/D oil, 0 water).

APPENDIX D

Joule-Thomson derivation

According to the first law of thermodynamics which is a statement of the conservation of energy:

$$dh = Tds + Vdp, \quad (D.1)$$

$$\left(\frac{dh}{dp}\right)_T = T \left(\frac{ds}{dp}\right)_T + V, \quad (D.2)$$

where

h is the specific enthalpy, $J\ kg^{-1}$, and

s is the specific entropy of the system, $J\ kg^{-1}\ ^\circ C^{-1}$, and

V is the specific volume, $m^3\ kg^{-1}$.

From Maxwell relations, it is known that

$$\left(\frac{\partial s}{\partial p}\right)_T = -\left(\frac{\partial V}{\partial T}\right)_p. \quad (D.3)$$

By rearranging Eq. (D.2), using Eq. (2.76), and substitution of $\left(\frac{ds}{dp}\right)_T$ using Maxwell relation, a general expression for Joule-Thomson coefficient can be obtained as follow

$$\eta_{JT} = \left(\frac{dT}{dp}\right)_h = -\frac{1}{C_p} \left(\frac{\partial h}{\partial p}\right)_T = -\frac{1}{C_p} \left[T \left(\frac{ds}{dp}\right)_T + V \right] = -\frac{1}{C_p} \left[-T \left(\frac{dV}{dT}\right)_p + V \right]. \quad (D.4)$$

Oil Heat Capacity

Oil specific heat capacity can be calculated using the following formula as a function of absolute temperature and oil-specific gravity (Gambill, 1957):

$$C_{p,oil} \left(\frac{J}{kg.K}\right) = \frac{1684 + 3.389T_{(K)}}{\sqrt{\gamma_{oil}}}. \quad (D.5)$$

Water Heat Capacity

The specific heat capacity of water is well known for a wide range of temperature and pressure based on the data measured by (Holman, 1958). For temperatures between 20°C and 290°C specific heat capacity is given by

$$C_{p,water} \left(\frac{J}{kg.K}\right) = \frac{4245 - 1.841T_{(K)}}{\rho_{water} \left(\frac{kg}{m^3}\right)}. \quad (D.6)$$

Gas Heat Capacity

(Kareem Lateef and Omeke, 2011) suggested that the specific heat capacity of a gas at constant pressure is also expressed as a degree 3 function of absolute temperature:

$$C_{p,g} \left(\frac{J}{mol.K}\right) = a + bT_{(K)} + cT_{(K)}^2 + dT_{(K)}^3, \quad (D.7)$$

where

$$a = 59.55\gamma_g^2 - 97.86\gamma_g + 56.46, \quad (\text{D.8})$$

$$b = -0.17084\gamma_g^2 + 0.46755\gamma_g - 0.15883, \quad (\text{D.9})$$

$$c = 1.52903 \times 10^{-4}\gamma_g^2 - 3.57387 \times 10^{-4}\gamma_g + 1.65604 \times 10^{-4}, \quad (\text{D.10})$$

$$d = -4.5789 \times 10^{-8}\gamma_g^2 + 9.8468 \times 10^{-8}\gamma_g - 5.2019 \times 10^{-8}. \quad (\text{D.11})$$